STRUCTURAL SYSTEMS
RESEARCH PROJECT

Report No.
SSRP - 91/06

FLEXURAL RETROFIT OF CIRCULAR REINFORCED CONCRETE BRIDGE COLUMNS BY STEEL JACKETING

– Experimental Studies –

by

Yuk Hon Chai
M.J. Nigel Priestley
Frieder Seible

Final Report on a Research Project funded through
Caltrans under Contract Number F88SD06 and
Agency Grant Number RTA-59G267

October 1991

Department of Applied Mechanics
and Engineering Sciences
University of California, San Diego
La Jolla, California

University of California, San Diego
Structural Systems Research Project

Report No. SSRP-91/06

FLEXURAL RETROFIT OF CIRCULAR REINFORCE CONCRETE BRIDGE COLUMNS BY STEEL JACKETING

– Experimental Studies –

by

Y. H. Chai
Graduate Research Assistant

M.J. NIGEL PRIESTLEY
Professor of Structural Engineering

F. SEIBLE
Professor of Structural Engineering

Final Report on a Research Project funded through
Caltrans under Contract Number F88SD06 and
Agency Grant Number RTA-59G267

October 1991

Department of Applied Mechanics and Engineering Sciences
University of California, San Diego
La Jolla, California 92093-0411

Technical Report Documentation Page

1. Report No.	2. Government Accession No. PB95-239950	3. Recipient's Catalog No.
4. Title and Subtitle FLEXURAL RETROFIT OF CIRCULAR REINFORCED CONCRETE BRIDGE COLUMNS BY STEEL JACKETING – EXPERIMENTAL STUDIES		5. Report Date October 1991
		6. Performing Organization Code
7. Author(s) Yuk Hon Chai, M.J. Nigel Priestley, Frieder Seible		8. Performing Organization Report No. UCSD/SSRP-91/06
9. Performing Organization Name and Address Structural Systems Research Project, Department of Applied Mechanics and Engineering Sciences, University of California, San Diego, La Jolla, CA 92093-0411		10. Work Unit No. (TRAIS)
		11. Contract or Grant No. RTA -59G267
12. Sponsoring Agency Name and Address California Department of Transportation, Office of Structures Design, 1801 30th Street, Sacramento, CA 94272-0001		13. Type of Report and Period Covered Preliminary Report June 1, 1988 - June 01, 1991
		14. Sponsoring Agency Code F88 SD06

15. Supplementary Notes

Prepared in cooperation with the State of California, Business and Transportation Agency, the U.S. Department of Transportation, Federal Highway Administration and the National Science Foundation

16. Abstract

Collapse or severe damage of a number of California Bridges in recent moderate earthquakes has emphasized the need to develop effective retrofit measures to enhance the flexural strength and ductility, as well as the shear strength, of bridge columns designed before current seismic design provisions were implemented. This report presents the results of an experimental study in which the potential plastic hinge region of circular bridge columns is encased with a steel jacket for enhanced flexural performance.

Results from large-scale column tests showed that the steel jacket acts efficiently as confinement reinforcement, enabling column ductilities exceeding those designed with current codes to be achieved. The jacket also inhibits bond failure in the lap-splices of the longitudinal reinforcement by restraining the dilation and spalling of the cover concrete which would otherwise precipitate rapidly degrading bond failures. Steel jacketing is also effective for post-earthquake repair of columns which have suffered bond failure at the lap-splices of the longitudinal reinforcement. The tests identified brittle shear failure at the footing/column joint as a potential failure mechanism for old footing designs.

17. Key Words Earthquake Engineering, Seismic Retrofit, Steel Jacketing, Bridges, Columns, Footings, Flexural Strength, Ductility, Confined Concrete, Plastic Hinge Length.	18. Distribution Statement Unlimited

19. Security Classif. (of this report)	20. Security Classif. (of this page)	21. No. of Pages	22. Price
Unclassified	Unclassified	151	

Form DOT F 1700.7 (8-72) Reproduction of completed page authorized

Acknowledgements

The research described in this report has been funded by the California Department of Transportation and the Federal Highway Administration under Grants RTA599267 and F885D06. The comments and conclusions made in this report are solely those of the authors and do not necessarily reflect the views of Caltrans or the FHA.

The helpful comments of the bridge engineers of Caltrans, especially those of Mr. Guy Mancarti, James Gates, Ray Zelinski and Brian Maroney are gratefully appreciated.

The generous contribution of concrete for the project by Nelson & Sloan Transit Mixed Concrete, and grout admixture by Atlas Construction Supply, both of San Diego, are also acknowledged.

Table of Contents

List of Figures

List of Tables

Chapter 1

Introduction

1.1 Background

The San Fernando earthquake of February 9, 1971 caused extensive damage to a large number of highway bridges in the vicinity of fault rupture. More than forty bridges were affected including total collapse of five newly constructed bridges [1,2,3]. The earthquake was rated at a Richter magnitude of 6.6 which most seismologists would consider a moderate event. The widespread damage, however, demonstrated the vulnerability of bridge structures to earthquakes and forced bridge engineers to reassess their design philosophy. Substantial modifications to bridge design criteria were soon adopted in California. Design factors were introduced to include regional seismicity, dynamic characteristics of bridges, influence of underlying site soils on bridge response, and the possible reduction of elastic forces for ductile structural systems [4,5].

Research interest in seismic performance of bridge structures was heightened after the earthquake. International efforts were made to improve analytical techniques for predicting the inelastic response of bridges when subjected to strong ground shaking, and to gather basic data on the strength and deformation characteristics of the load resisting mechanisms in bridges. In the United States, research emphasis was primarily directed towards the development of sophisticated time-history analysis techniques. Experimental research was mainly pursued as a mean of verifying the analytical techniques.

Parallel to the analytical development in the United States, a comprehensive research program pertaining to the strength and ductility of bridge columns was carried out at the University of Canterbury, New Zealand, under the sponsorship of the New Zealand Roads Board. The research program, spanning over fifteen years, produced detailed information on the flexural strength and ductility, and on the shear strength, of both reinforced concrete columns and steel-encased concrete piles [6]. Particular emphasis was placed on quantifying the influence and effectiveness of lateral confining steel in the plastic hinge regions of the columns for increasing ductility. Well confined columns were shown to develop stable hysteretic response up to displacement ductility factors of $\mu \geq 6$. The findings were supported by recent tests on full-scale bridge columns [7].

While the new design guidelines are considered adequate, there is an urgent need for mitigating the seismic risk associated with the older bridges still in service. Although column failure was recognized as a major problem after the 1971 San Fernando earthquake, the greatest risk was assessed to be due to inadequate connection between adjacent spans of the superstructure across movement joints. Consequently, a major retrofit program was undertaken by Caltrans to install restraining devices across movement joints to reduce the risk of span collapse when excessive relative movement occurs [8,9,10]. A total of 1250 bridges were retrofitted in California and the program was recently completed in 1988 [11].

The recent shear failure in the columns of the I-5/I-605 Separator (a major freeway overpass) during the Whittier Narrows earthquake of October 1, 1987 [12,13] and the tragic collapse of the Cypress Viaduct, and other bridge failures, during the Loma Prieta earthquake of October 17, 1989 [14] re-emphasized the inadequacies of the pre-1971 design and the urgent need to upgrade the seismic resistance of older bridge substructures.

The structural deficiencies inherent in many of the older bridge substructures can be categorized as follows:

Inadequate Flexural Strength: Lateral force coefficients for seismic design were typically about 6% in pre-1971 design and are comparatively low by the current standard. Although the use of elastic design generally resulted in the actual flexural strength being significantly higher than that required by the assumed lateral force, low lateral flexural design strength results in high potential ductility demand in many cases.

Undependable Flexural Strength: In many of the tall bridges designed using the pre-1971 guideline, the column longitudinal reinforcement was spliced with starter bars extending from the footing with a lap length of 20 times the bar diameter. This lap length is insufficient for developing the yield strength of the longitudinal bars especially when large diameter bars are involved. As a consequence, the flexural strength degrades rapidly under cyclic loads. Occasionally, the column longitudinal reinforcement was extended straight into the footing or pile cap without 90 degree hooks. Such details allow pulling out of column reinforcement when subjected to large intensity seismic load reversals [1].

Inadequate Flexural Ductility: Bridge columns designed before the 1971 San Fernando earthquake typically contain insufficient transverse reinforcement. A common provision for both circular and rectangular columns involved the use of #4 transverse peripheral hoops placed at 12 inches centers regardless of the column section dimensions. These hoops were often closed by lap-splices in the cover concrete, instead of being lap-welded or anchored by bending back into the core concrete. As a result, the ultimate curvature developed within the potential plastic hinge region is limited by the strain at which the cover concrete begins to spall which is typically in the range of 0.005 strain. At higher longitudinal strains the hoop steel unravels and the meager amount of confinement provided by the hoops becomes ineffective.

Inadequate Column Shear Strength: Conservative flexural design, using elastic methods coupled with less conservative shear strength provisions of the 1950's and 1960's, typically results in the actual flexural strength of short columns exceeding their actual shear strength. Inadequate anchorage of the transverse reinforcement in the cover concrete compounds the problem. As a consequence, the probable failure mode for shorter columns involves brittle shear failure with low ductility and energy absorption characteristics.

Footing Failures: Pile caps and footing in older bridges are often provided with only a horizontal layer of reinforcement in the bottom region of the member. Top steel and shear reinforcement were considered unnecessary and were routinely omitted. Such practice may be attributed to the use of elastic design which assumes full gravity load during the seismic event while concurrently prescribing unrealistically low values of lateral seismic forces, corresponding to specified working stress levels.

Joint Failures: Joint regions either between column and footing or between column and bent-cap beams are subjected to very high shear stresses during a severe seismic attack. These regions traditionally have not been designed to resist this high level of seismic shear stresses.

Abutment Failures: The transverse response of the bridge structure may cause severe pounding of the superstructure on the side-walls of bridge abutments. The lateral restraint and shear keys provided in the abutment were often ineffective against the superstructure span from sliding off the abutment. Damage resulting from bridge pounding on the abutment under longitudinal seismic response is also common.

Although most of the above design deficiencies have been rectified in current seismic codes and should no longer affect new bridge design, the conditions of many old bridge columns built before the 1970's is a cause for major concern. The experimental work described herein is the basis for the second phase of the Caltrans retrofit program in which retrofit of deficient circular flexural columns by steel jacket are implemented.

1.2 Confinement of Columns by Steel Jackets

Current seismic design philosophy requires the provision of a minimum lateral strength in the structure so that the structure can remain essentially elastic in cases of moderate earthquakes of frequent occurrence, and an assurance of a ductile behavior so that large deformations into the inelastic range can occur without collapse of the structure during the maximum credible earthquake [15]. The requirement for ductile behavior during a severe earthquake arises from the fact that the maximum response acceleration of an elastic system may be several times the maximum ground acceleration, depending on such factors as the stiffness and damping of the structure. For economic reasons, structures are not designed to resist the full elastic inertial force induced by the maximum credible earthquake, but are designed to a reduced force level and detailed for ductility in the critical members to ensure adequate inelastic displacement capacity in the structure without significant degradation of strength [16]. For bridge structures, preferred locations of inelastic deformations are in the pier regions because of the difficulty associated with providing ductility in the superstructure. The current seismic design of bridge columns relies on proper confinement of the potential plastic hinge regions by closely-spaced transverse hoops and spirals. Such provisions allow the ultimate compressive strain to be increased from a value of about 0.005 in unconfined concrete to a value which may be 0.03 or higher in confined concrete. The increase in ultimate compressive strain significantly enhances the ductility capacity of the concrete section.

Various retrofit methods have been advanced to enhance the flexural strength and ductility of deficient bridge columns [17]. Ordinary reinforcing hoops of 0.5 inch diameter placed at 3.5 inches centers and tightened at two ends using specially designed turnbuckles was an early suggestion as a possible mean of increasing the transverse confinement reinforcement. A similar approach, but using 0.25 inch diameter prestressing wire wrapped under tension appeared to be a feasible alternative, although problems were foreseen with secure anchorage of the prestressing wire in order to maintain effective confinement to the existing concrete.

An alternative, and potentially more cost-effective method of retrofit could be achieved by encasing the deficient columns at the critical regions using site-welded cylindrical steel sleeves or jackets. The jacket is introduced slightly oversize for ease of construction and the gap between the column and jacket is pressure-injected with a cement-based grout. The jacket is terminated slightly above the critical section at the column base to avoid additional strength enhancement resulting from end-bearing of the sleeve on the footing when in compression. Figure 1.1 shows conceptually the application of steel jacket as retrofit

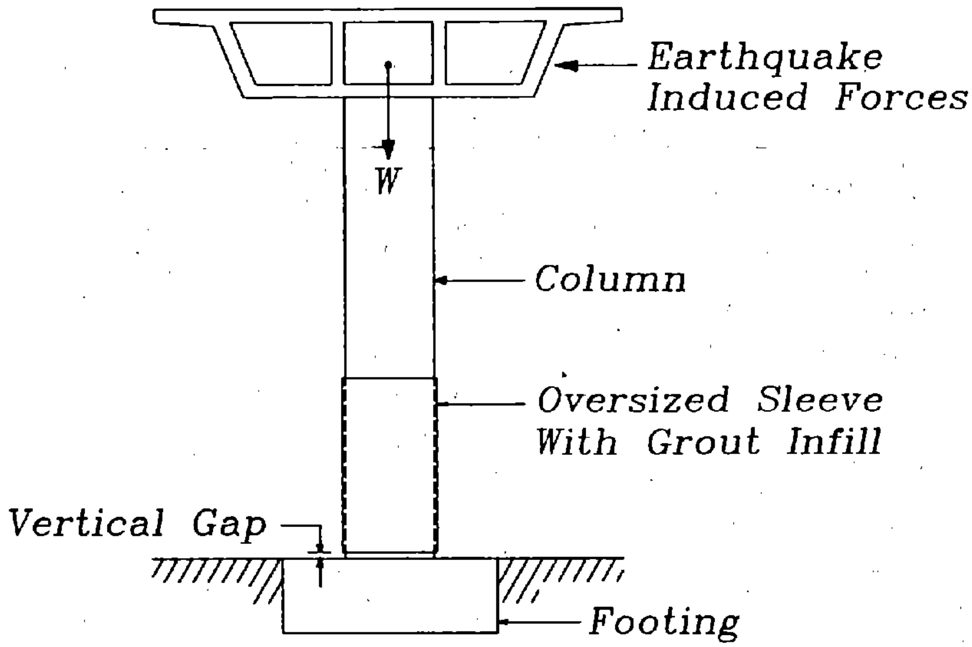

Figure 1.1: **Steel Jacketing of Circular Bridge Column**

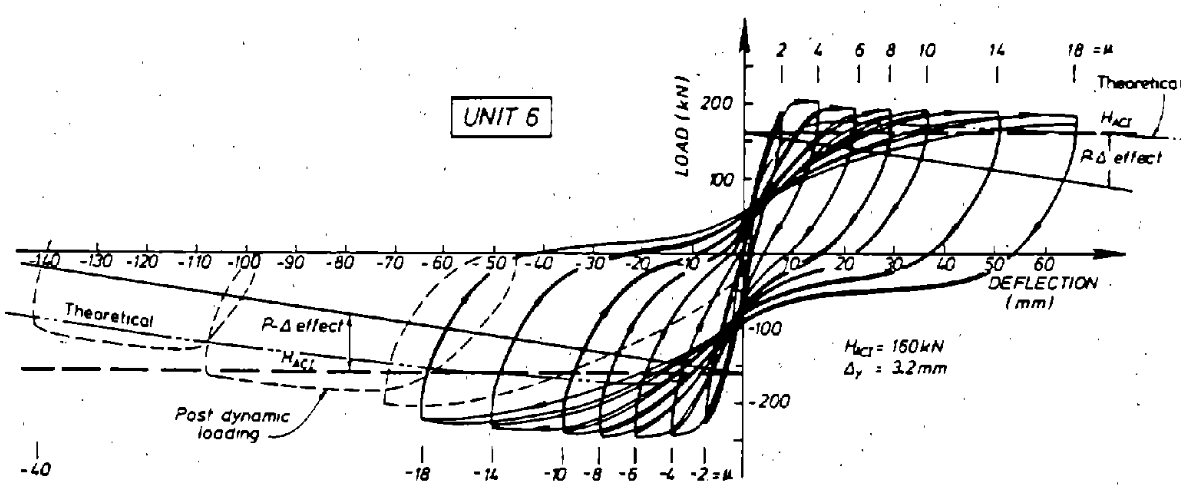

Figure 1.2: **Ductile Response of Steel Encased Concrete Pile (Park et al - Ref. 18)**

in a circular bridge column. Although not shown in Figure 1.1, consideration of the longitudinal response might necessitate the use of a steel jacket in the upper region of the column. The basis for the development of this approach was the excellent ductile response of steel-encased concrete piles tested by Park et al [18,19,20], as illustrated by the example in Figure 1.2.

An enhancement in the flexural strength of the column can be expected since an increase in the concrete compressive strength will result from the confining action of the steel jacket. Mander et al [21] recently proposed that the increase in concrete compressive strength in the presence of lateral pressure may be written as:

$$f'_{cc} = f'_{co}(2.254\sqrt{1 + \frac{7.94 f'_l}{f'_{co}}} - \frac{2 f'_l}{f'_{co}} - 1.254) \tag{1.1}$$

where f'_{cc}, f'_{co} are the confined and unconfined compressive strengths of concrete, respectively, and f'_l is the effective lateral confining pressure exerted on the core concrete by the confining steel at yield. More importantly, a substantial increase in the ductility of confined concrete can be achieved with moderate amounts of transverse reinforcement. An ultimate compressive strain exceeding 0.03 can be developed in well confined concrete. The enhancement of compressive strength and ductility of concrete under confined condition is illustrated in Figure 1.3.

Even though Eqn. 1.1 was proposed for sections confined by internal reinforcement, its application to steel jacket retrofit can be made by rewriting the expression for the lateral pressure. The lateral pressures can be obtained from the equilibrium of internal forces acting the dissected sections shown in Figure 1.4. For the cover concrete and grout, the equilibrium of forces at yield of the

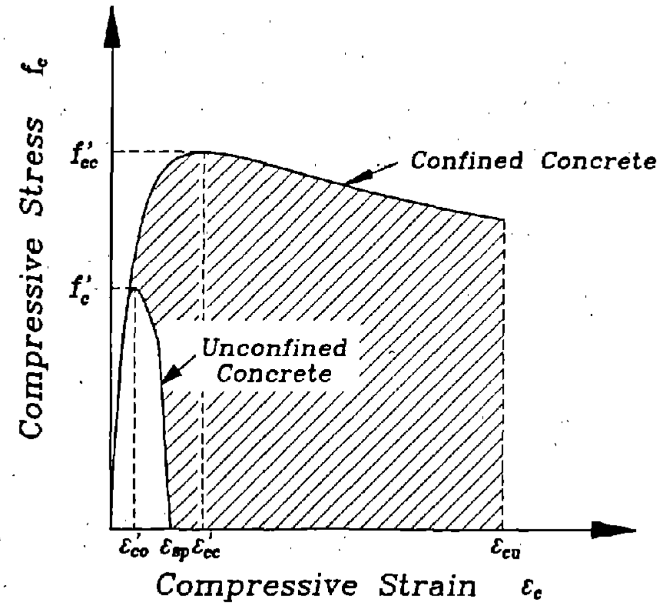

Figure 1.3: **Confining Effect on Compressive Response of Concrete**

jacket requires:

$$f'_{lj} = \frac{2f_{yj}t_j}{(D_j - 2t_j)} \tag{1.2}$$

where f'_{lj} is the lateral pressure acting on the cover concrete; D_j and t_j are the outside diameter and thickness of the jacket, respectively; and f_{yj} is the yield strength of the steel jacket. By defining a confining ratio for the steel jacket as:

$$\rho_{sj} \equiv \frac{4t_j}{D_j - 2t_j} \tag{1.3}$$

Eqn. 1.2 may be written as

$$f'_{lj} = \frac{1}{2}\rho_{sj}f_{yj} \tag{1.4}$$

By substituting $f'_l = f'_{lj}$ into Eqn. 1.1, the enhanced compressive strength of cover concrete can be determined.

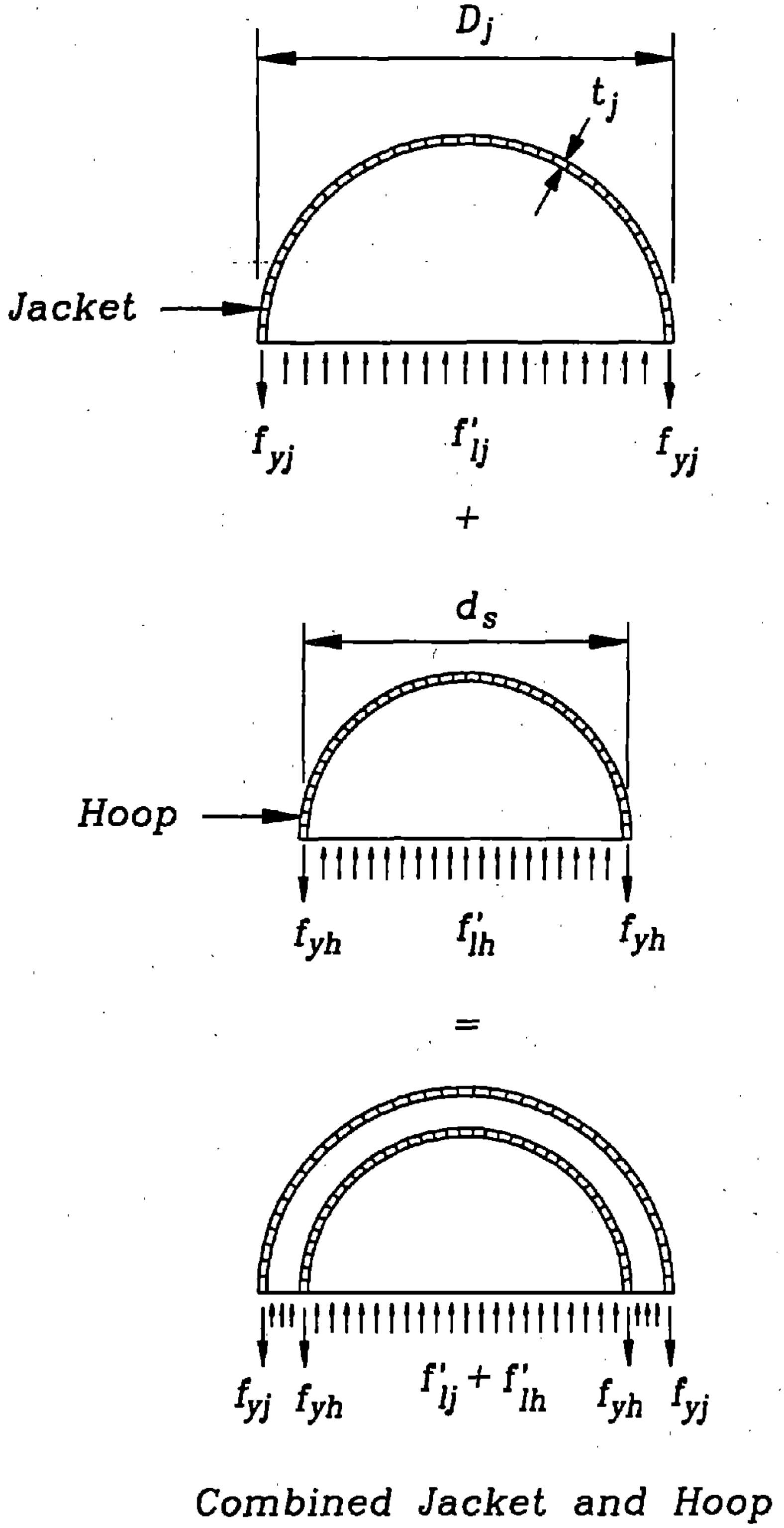

Figure 1.4: **Confining Actions of Steel Jacket and Internal Hoops**

For the concrete core, additional confinement is provided by the transverse steel. The additional lateral pressure, f'_{lh}, may also be determined from the equilibrium of forces, assuming yield of the transverse steel i.e.

$$f'_{lh} = 2k_e \frac{f_{yh}A_{sh}}{d_s s} \tag{1.5}$$

where d_s is the diameter of concrete core defined along the center line of transverse steel; s is the vertical spacing of the transverse steel; f_{yh} is the yield strength of the transverse reinforcement; A_{sh} is the cross-sectional area of transverse steel. The parameter k_e is termed as the confinement effectiveness coefficient and is defined as:

$$k_e \equiv \frac{A_e}{A_{cc}} \tag{1.6}$$

where A_e = area of an effectively confined concrete core (see Figure 1.5) and $A_{cc} = A_c(1 - \rho_{cc})$; ρ_{cc} = ratio of area of longitudinal reinforcement to core area of the section A_c. The substitution of $f'_l = f'_{lj} + f'_{lh}$ into Eqn. 1.1 will allow the enhanced compressive strength of the core concrete to be determined.

In assessing the inelastic displacement capacity of ductile columns, a realistic estimation of the ultimate compressive strain, ϵ_{cu}, must be made. It has been proposed [21] that ϵ_{cu} be defined as the longitudinal compressive strain when first fracture of the transverse steel occurs. The additional ductility in confined concrete is provided by the strain energy capacity of the transverse reinforcement. By equating the work done on the confined concrete and longitudinal reinforcement when in compression to the available strain energy capacity of the transverse reinforcement, a value for ϵ_{cu} may be estimated. The approach has resulted in the reasonably accurate prediction of ϵ_{cu} [22].

The steel jacket is expected to enhance the ultimate concrete compres-

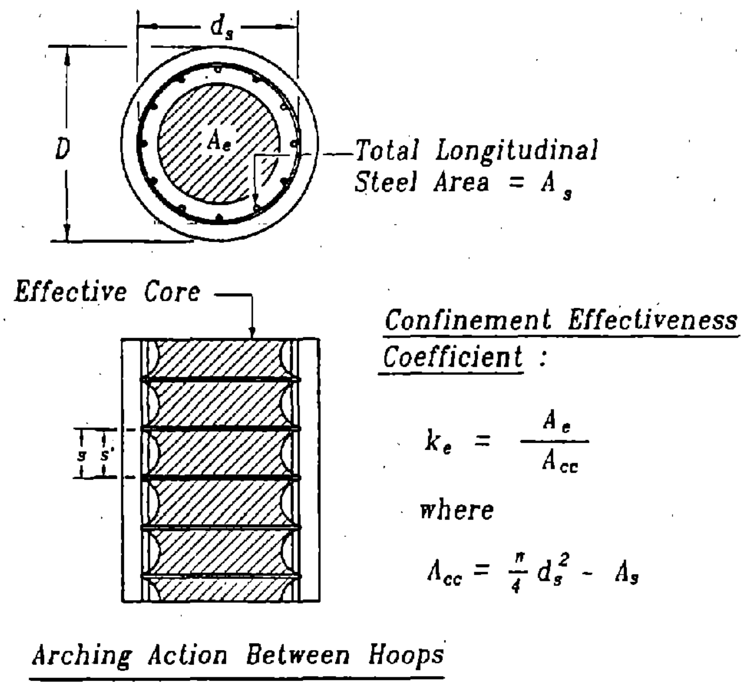

Figure 1.5: **Definition of Confinement Effectiveness Coefficient**

sive strain in a manner similar to that of the confinement provided by internal transverse reinforcement to the core concrete. The energy balance method may therefore be extended for the prediction of ϵ_{cu} for concrete confined by a steel jacket.

For simplicity, let us consider the enhancement of ultimate compressive strain in a column of concrete encased by a steel jacket. The energy density required to change the concrete from an unconfined to a confined state is given by the shaded area between the stress-strain curves of the unconfined and confined concrete, as shown in Figure 1.3. The shaded area may be written as:

$$A_1 = \gamma_1 f'_{cc}(\epsilon_{cu} - \epsilon_{sp}) \tag{1.7}$$

where ϵ_{sp} = the spalling strain of the unconfined concrete; f'_{cc} = the compressive

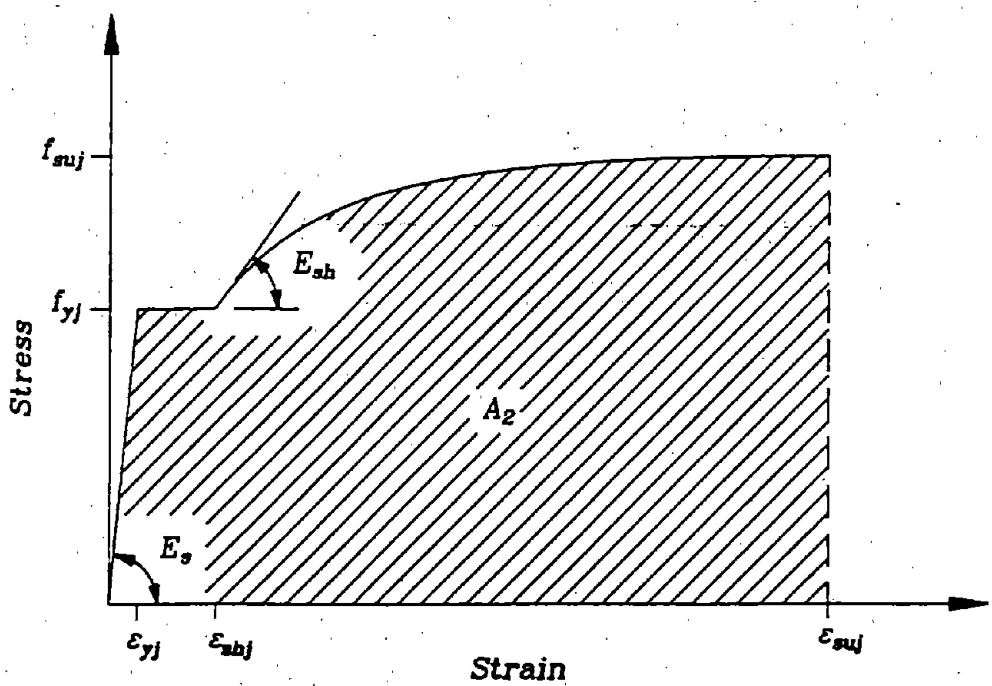

Figure 1.6: **Stress-Strain Curve for Steel Jacket**

strength of confined concrete defined by Eqn. 1.1; and γ_1 denotes the coefficient of integration which depends on the shape of the stress-strain curves of both confined and unconfined concrete.

The strain energy capacity of the steel jacket, as given by the area under the stress-strain curve in Figure 1.6, may be written as:

$$A_2 = \gamma_2 f_{yj} \epsilon_{suj} \tag{1.8}$$

where f_{yj}, ϵ_{suj} are the yield stress and ultimate strain for the steel jacket, respectively; and γ_2 is the coefficient of integration which also depends on the shape of the stress-strain curve for the steel jacket.

The balance of strain energies between concrete and steel jacket requires:

$$\gamma_1 f'_{cc}(\epsilon_{cu} - \epsilon_{sp})\frac{\pi}{4}(D_j - 2t_j)^2 = \gamma_2 f_{yj}\epsilon_{suj}(D_j - t_j)t_j\pi \tag{1.9}$$

which reduces to

$$\epsilon_{cu} = \epsilon_{sp} + \frac{\gamma_2}{\gamma_1}\frac{f_{yj}}{f'_{cc}}\epsilon_{suj}\frac{4t_j(D_j - t_j)}{(D_j - 2t_j)^2} \tag{1.10}$$

For practical application, since the thickness of the jacket will be small compared with the diameter i.e. $t_j \ll D_j$, we may write:

$$\frac{4t_j(D_j - t_j)}{(D_j - 2t_j)^2} \approx \frac{4t_j}{D_j - 2t_j} = \rho_{sj} \tag{1.11}$$

where ρ_{sj} denotes the confining ratio of steel jacket defined in Eqn. 1.3. Thus the limiting concrete compressive strain ϵ_{cu} for encased concrete may be written as:

$$\epsilon_{cu} = \epsilon_{sp} + \frac{\gamma_2}{\gamma_1}\frac{f_{yj}}{f'_{cc}}\epsilon_{suj}\rho_{sj} \tag{1.12}$$

For example, the retrofit of a 60 inch diameter column with a 1/2 inch thick jacket ($D_j \approx 62$ inches and $f_{yj} = 36$ ksi) would provide a confining ratio of $\rho_{sj} = 0.033$. The available lateral pressure from the jacket from Eqn. 1.4 is $f'_{lj} = 590$ psi. If a concrete strength of $f'_{co} = 5000$ psi is used, the corresponding confined compressive strength f'_{cc} from Eqn. 1.1 would be 8230 psi. Numerical integration of the stress-strain curves for concrete and typical steel for the jacket (A36) would provide a ratio of γ_2/γ_1 of about 1.4. Assuming the ultimate tensile strain of the steel jacket as $\epsilon_{suj} = 0.20$ and the spalling strain of unconfined concrete as $\epsilon_{sp} = 0.005$, the ultimate compressive strain would be $\epsilon_{cu} = 0.045$ which is nine times larger than the spalling strain of unconfined concrete.

It should however be noted that in order to develop the increased ultimate concrete compressive strain, a corresponding increase in the extreme tension steel strain must occur. A possible limit state then exists in which the behavior of retrofitted column may be governed by fracturing of the longitudinal steel. Large inelastic load reversals can cause serious reduction of the fracturing strain;

a phenomenon associated with low-cycle fatigue of metal. The reduction in fracturing strain may result in a smaller cyclic displacement ductility factor than that implied by the ultimate compressive strain.

In addition to providing confinement to the concrete, the steel jacket was expected to be effective in resisting a portion of the total column shear force in the potential plastic hinge region. Figure 1.7 shows the shear resistance of a steel jacket assuming a 45^0 failure plane. The failure plane will expose a tension resultant $f_{yj}t_j$ tangential to the steel jacket. For an infinitesimal jacket height dz, the shear force resisted by the steel jacket is:

$$dV_{sj} = 2f_{yj}t_j \sin\alpha \, dz \tag{1.13}$$

In the coordinate system shown, the shear failure plane is given by $z = -y$. Since $y = r' \cos\alpha$ where $r' = (D_j - t_j)/2$, the infinitesimal height dz may be written as:

$$dz = r' \sin\alpha \, d\alpha \tag{1.14}$$

Substituting back into Eqn. 1.13 gives:

$$V_{sj} = \int_0^{\pi} 2f_{yj}t_j r' \sin^2\alpha \, d\alpha \tag{1.15}$$

Noting that

$$\int_0^{\pi} \sin^2\alpha d\alpha = \frac{\pi}{2} \tag{1.16}$$

the shear force resisted by the steel jacket is:

$$V_{sj} = \frac{\pi}{2} f_{yj}t_j(D_j - t_j) \tag{1.17}$$

In multistory buildings where it is often desirable to splice the column main reinforcement at the story level, the lap-splices can be designed to assure satisfactory performance in the member provided that extensive yielding of spliced bars is carefully avoided [23]. Such conditions in multistory building can be achieved by adopting capacity design principles [24] in which the columns are designed for reserve strength to resist the maximum moment input expected from plastic hinging in the adjoining beams. However, the need to form plastic hinges in the columns instead of the superstructure means that the lap-splices of the longitudinal reinforcement in the plastic hinge region of bridge columns are subjected to more severe stresses and deformations under the design earthquake than are building columns. The current Caltrans approach [25] has been to avoid lap-splicing of the main reinforcement in the potential plastic hinge region of bridge columns even though experimental testing have shown that lap-splices can be safely designed to sustain high-intensity cyclic loads with at least 15 or 20 excursions into the inelastic range [26]. The primary consideration for a satisfactory performance in the lap-splices in the plastic hinge region under seismic loads is the provision of closely-spaced, uniformly distributed transverse steel.

Figure 1.8 shows the potential splitting cracks associated with overlapping parallel bars. The transverse steel is seen to provide a clamping force across the crack, thereby enabling a shear friction mechanism to transfer forces from one spliced bar to another. By assuming that the clamping force required is equal to the yield force in the longitudinal steel, the transverse steel spacing, s, can be shown to be [23]:

$$s = \frac{A_{sh} f_{yh} l_s}{f_y A_b} \tag{1.18}$$

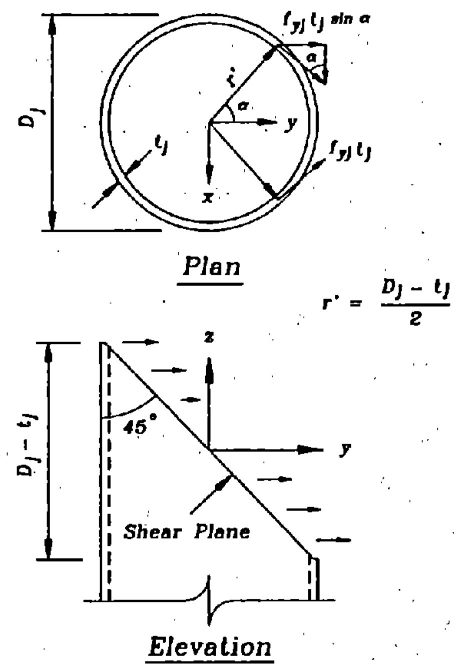

Figure 1.7: **Shear Strength Contribution from Steel Jacket**

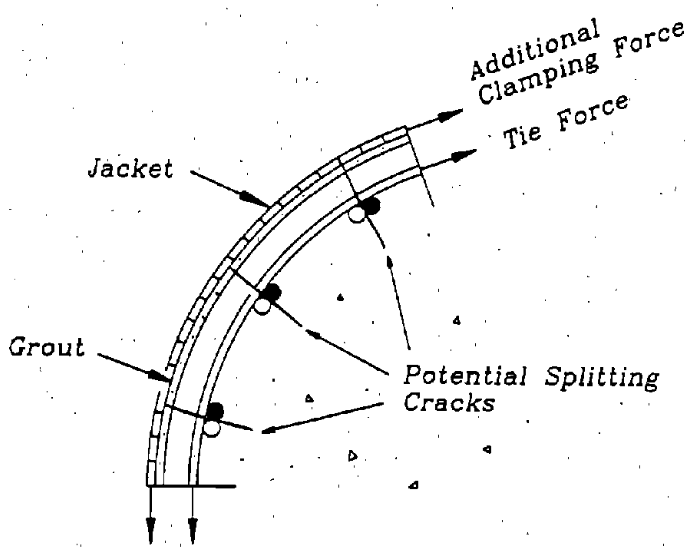

Figure 1.8: **Shear Friction Mechanism for Force Transfer at Lap-splices**

where A_{sh} = transverse steel area; A_b = longitudinal steel area; f_{yh} = yield strength of transverse steel; f_y = yield strength of longitudinal steel; and l_s = length of lap-splice. For example, consider the splicing of #14 bars in prototype bridge columns with a lap length of $l_s = 20d_b$. If #4 bars are used for the transverse steel and have the same yield strength as the longitudinal steel, the transverse tie spacing required by Eqn. 1.18 is 3 inches. The pre-1971 provision of #4 bars at 12 inches centers for transverse steel is therefore unlikely to be adequate for development of the yield strength in the longitudinal reinforcement. It should also be noted that the approach described above may be non-conservative as a result of overestimating the confining force transmitted across the potential splitting crack. The presence of a steel jacket, however, would increase the clamping force, thereby improving the bond transfer and possibly inhibit the bond failure at the lap-splices. A more detailed assessment of the mechanism of splice failure has recently been proposed by Priestley and Seible [27].

Although steel encasement of concrete columns has not been previously utilized for new or retrofitted bridge columns in the United States, there is some relevant application elsewhere [28,29]. Recent Japanese earthquakes (Miyagi-ken-oki earthquake in 1978 and Urakawa-oki earthquake in 1982) caused brittle failures in a number of bridge piers with 50% termination of the main reinforcement at mid-height. Fully epoxy grouted steel jackets were introduced to increase the effective longitudinal reinforcement area and to improve shear resistance in the cut-off regions. In circular columns, the jackets were of relatively large diameter to thickness ratio ($410 \geq D_j/t_j \geq 580$). Even though experimental testing had verified the adequacy of steel jacket encasement only in the zone of termination of longitudinal reinforcement, field application has tended to use full height jackets to provide uniformity of appearance to the column.

Research on steel encased concrete columns in multistory buildings is also relevant for the application of steel jacket. A steel tube filled with concrete is often used to reduce the column dimensions in the bottom stories. While early efforts concentrated on the axial load carrying capacity of concrete-filled steel tubes [30,31], recent research carried out in Japan examined the behavior of these members under simulated seismic loads [32]. Test columns were of the low shear span to width ratio typical of building construction, with the encasing steel tube terminated slightly short of the adjoining beams. The casing was successful in inhibiting brittle shear failure and produced a ductile flexural mode of inelastic displacement with stable hysteretic loops even in columns subjected to high axial loads.

Even though test results showed successful inhibition of brittle failures in the region of main reinforcement cut-off at mid-height [33], the use of steel jacket for flexural ductility enhancement and prevention of bond failure at the lap-splice region is less certain. The injection of epoxy resin as grout infill assures full composite action of the jacket with the column causing a possibly undesirable increase in the lateral stiffness of the column, especially when associated with a lower diameter to jacket thickness ratio.

This report summaries the results of an initial phase of a research program funded by Caltrans and the Federal Highway Administration on flexural retrofit of circular bridge column using steel jacket. Experimental testing was carried out at the Large-Scale Structural Testing Facility at the University of California, San Diego. Theoretical aspects related to the development of a computer program for assessment and retrofit design of circular bridge columns are covered in a separate report [34]. Subsequent phases of the research project deal with flexural retrofit of rectangular columns, with shear retrofit of circular and rectangular columns, with shear strength of knee joint, and with footing retrofit. These research will be separately reported.

Chapter 2

Column Design and Testing

2.1 Preliminary

This chapter describes the design and test setup for the experimental program. Only salient features will be discussed. Material properties and construction processes are included in Appendix A of this report.

In order to minimize the extrapolation of results, the test columns were designed to as large a scale as could be tested with the available equipment. This was achieved at a geometric scale of 0.4. Non-ductile details typical of the pre-1971 design, together with materials representative of the actual bridge construction, were incorporated in the design of the test column. The test columns were constructed with a footing (66 inches square by 18 inches high) to include foundation influence or interaction on the column behavior.

2.2 Test Matrix

Table 2.1 shows the test matrix for the circular flexural retrofit program. A total of six columns were constructed; two of which were tested 'as-built' while the remaining four were tested after retrofitting with steel jackets. The program also investigated the possible use of steel jacket for post-earthquake repair of damaged bridge columns by testing one of the damaged 'as-built' columns after subsequent jacketing. Other design variations include:

1. **Anchorage of Longitudinal Reinforcement:** As noted earlier, the col-

umn longitudinal reinforcement in the pre-1971 design was often lap-spliced with starter bars from the footing at a lap length of 20 times the bar diameter. Such a lap length is insufficient to develop yield of the reinforcement especially under large inelastic load reversals. Consequently, the column behavior is characterized by an undependable flexural strength with very rapid strength degradation. This deficiency was duplicated in four of the columns. In addition, reinforcement extending without laps into the footing and anchored with 90^0 hooks was also investigated in two columns; shown as column 3 and 4 in Table 2.1.

2. Strength of Footing: Uncertainties arise with regard to whether pre-1971 footings will have sufficient strength to resist the column plastic moment, particularly when the moment enhancement expected of the column after retrofit with a steel jacket is considered. The initial pair of the columns were constructed with footings representative of the pre-1971 design, referred to as 'weak footing' in the test matrix. The test on the retrofitted column of this pair confirmed the anticipated weakness, and footings for the remaining columns were redesigned to resist the full moment and shear input. The strengthened footing will be referred to as the 'strong footing' hereinafter.

3. Partial Column Retrofit: A partial retrofit approach was undertaken in column 5 to investigate the possibility of containing the base of the column and to maintain the axial load carrying capacity without attempting to improve the flexural strength or ductility of the column. This could be adopted in design where the dependable lateral strength of a column would not be needed to ensure satisfactory response of the bridge as a whole and where full retrofit might place excessive moment demand on the footing. To this end, a thin sheet of styrofoam (1/4 inch thick at the model scale) was added between the column and the grout infill to allow a controlled dilation of the cover concrete at large lateral displacement. Bond failure was expected at the lap-splice but complete loss of cover concrete should not occur as a result of restraint by the steel jacket.

4. **Repair of Column With Steel Jacket:** After the initial test of the lapped column in the 'as-built' condition, the column was repaired with a steel jacket, indicated as 1-R in the test matrix, and retested using the same force and deformation history. Loose cover concrete around the splice region of the main reinforcement was removed before installing the steel jacket. Instead of providing a vertical gap, the jacket was extended down to the top of the footing to ensure good seal against the grouting pressure. The same cement-based grout was used to fill the gap between the jacket and column. The weak footing was strengthened by external prestressing to a total of 300 kips at mid-height of the footing in the direction of lateral load.

2.3 Design Considerations and Details

This section describes the design of the test columns. Comparisons between the prototype and test columns are summarized in Table 2.2.

2.3.1 Column Height

The column aspect ratio (height to diameter) was chosen to ensure a flexural response. The criterion used was to limit the nominal shear stress to below the level expected to cause diagonal tension cracking. In this case, by adopting a column height of six times the diameter, the shear stress, corresponding to nominal flexural strength, using an effective shear area of $0.8A_g$ [35] was 128 psi. This value is less than the ACI's expression of $2\sqrt{f'_{co}} = 141$ psi. Note

Table 2.1: **Test Matrix**

Test Units	Column & Footing Details		Remarks
1	20 d_b Lap For Long. Bars Without Steel Jacket	Weak Footing	Reference
2	20 d_b Lap For Long. Bars With Steel Jacket	Weak Footing	Full Retrofit
3	Continuous Column Bars Without Steel Jacket	Strong Footing	Reference
4	Continuous Column Bars With Steel Jacket	Strong Footing	Full Retrofit
5	20 d_b Lap For Long. Bars 1/4" Styrofoam and Jacket	Strong Footing	Partial Retrofit
6	20 d_b Lap For Long. Bars With Steel Jacket	Strong Footing	Full Retrofit
1-R	20 d_b Lap For Long. Bars Repaired By Steel Jacket	Weak Footing 300 kips Prestress	Full Retrofit

Table 2.2: **Design of Test Columns**

Parameters	Prototype	Test Column
Diameter	60"	24"
Height	360"	144"
Cover to Main Bar	2"	0.8"
Material Concrete Probable f'_{co} Reinforcement f_y	 5000 psi Grade 40	 5000 psi Grade 40
Longitudinal Steel Total Steel Area Long. Steel Area Ratio	32 #14 72 in^2 2.55%	26 #6 11.44 in^2 2.53%
Transverse Steel Hoop Spacing Transverse Steel Ratio	#4 12" 0.118%	#2 5" 0.174%
Axial Load $P/(f'_{co}A_g)$	2544 kips 0.18	400 kips 0.177
Flexural Capacity M_u (Based on ACI)	 105056 kip.in	 6671 kip.in
Nominal Shear Stress $V_u/0.8A_g$	 129 psi	 128 psi

that the flexural capacities shown in Table 2.2 were obtained using the computer program developed by King [36] for ACI section analysis assessed at an extreme compressive strain of 0.003.

2.3.2 Column Reinforcement

Grade 40 reinforcement were used in the test columns except in the loadstub and strong footing where grade 60 steel were used. Figure 2.1(a) and (b) show the reinforcement details for the test column and footings. The longitudinal steel consists of 26 #6 bars uniformly distributed around the column, constituting a steel area ratio of 2.53%. The design is equivalent to 32 #14 bars in a 5 ft diameter prototype column. The use of #4 transverse steel at 12 inches centers in prototype columns is simulated by #2 hoops at 5 inches. It should be noted that the transverse steel in prototype column corresponds to a confining steel ratio of $\rho_s = 0.118\%$, whereas in the test columns, the design represents a slightly higher ratio of 0.174%. The confining steel ratio is defined as:

$$\rho_s = \frac{4A_{sh}}{sd_s} \tag{2.1}$$

where A_{sh} is the cross-sectional area of hoop; d_s is the core diameter measured along centerline of hoop; and s is the hoop spacing. If the same confining steel ratio is to be maintained while providing a proper scale of the prototype hoop spacing i.e. 0.4×12 inches $= 4.8$ inches, a hoop size smaller than #2 must be used. Without resorting to special fabrication, a compromise was reached by using #2 hoops with a slight increase of spacing to 5 inches. It should be noted that with the low transverse reinforcement ratio, simulation of antibuckling properties, which are largely related to transverse steel spacing, was felt to be

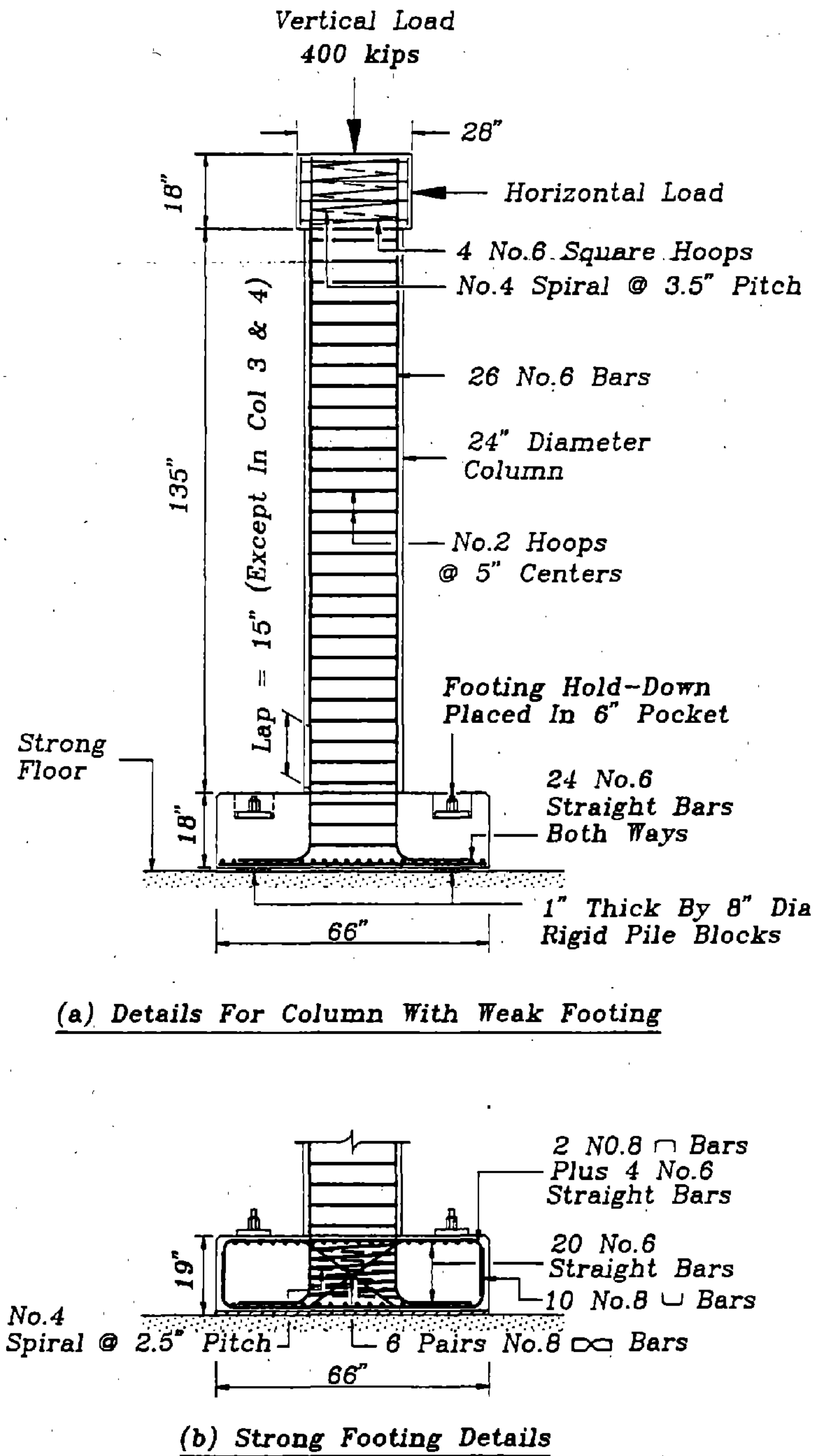

Figure 2.1: **Reinforcement Details for Test Columns**

more important than simulation of concrete confinement, which is more closely related to ρ_s. The cross-sections of the test columns are shown in Figure 2.2.

2.3.3 Footing Details

The reinforcement for the first pair of weak footings consisted of only straight bars (two orthogonal layers of 24 #6 bars each) in the bottom region of the footing as seen in Figure 2.1(a). The footing was supported off the test floor on six simulated pile-blocks (1 inch by 8 inch diameter). Horizontal translation was prevented by prestressing the footing to the test floor with a total force of 330 kips. The hold-down bolts for the footing were placed in 6 inch deep pockets to minimize any artificial influence on the column/footing joint by the compressive struts which may develop from the hold-down bolts.

Footing reinforcement was increased, after failure was observed with the above details in column 2, to include top and bottom layers of #8 bars bent at both ends, 6 pairs of #8 diagonal bars placed adjacent to the column/footing joint and #4 spiral at 2.5 inch pitch within the joint. Instead of using pile-blocks as support, the strong footing was uniformly placed on a thin layer of hydrostone and clamped against the test floor to alleviate the severe conditions associated with supporting on piles. In addition, the placing of hold-down bolts in sunken pockets was eliminated.

2.3.4 Axial Load

All test columns were subjected to the same axial load of 400 kips. The load level represents a nominal stress of $0.18f'_{co}$ which is considered to be a practical upper bound of the axial load that can be expected in single column bridge piers.

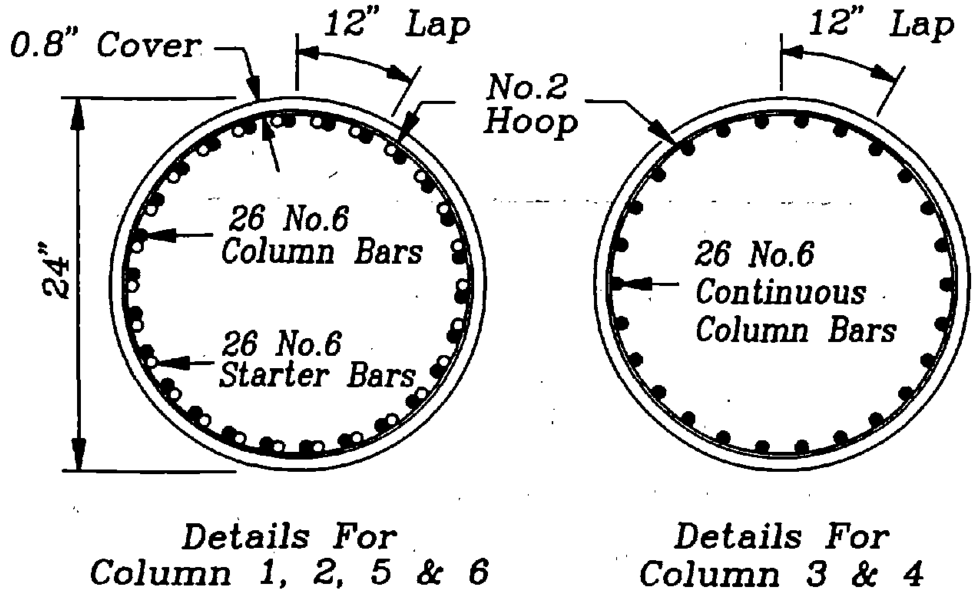

(a) 'As-Built' Columns - Lapped and Continuous

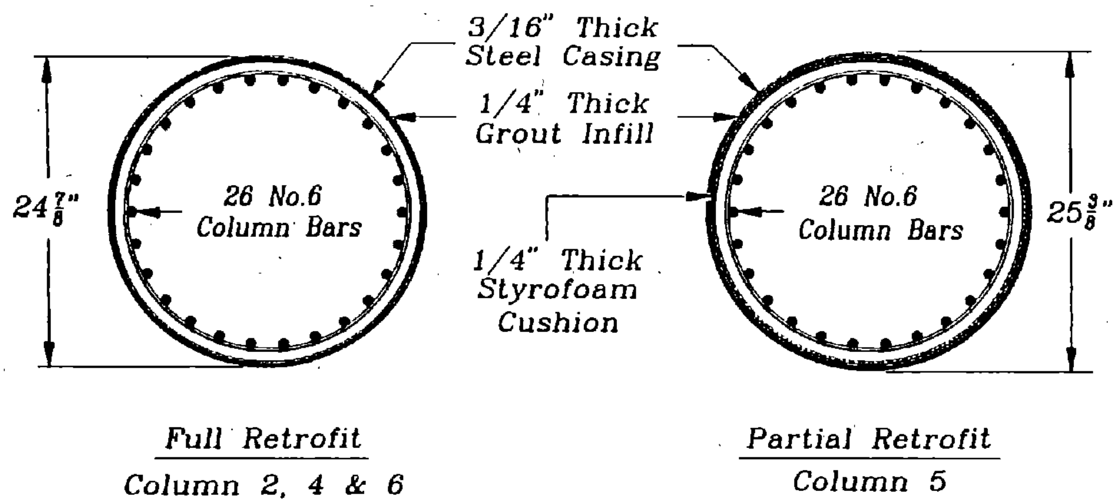

(b) Retrofitted Columns - Full and Partial Retrofit

Figure 2.2: Cross Section of Test Columns

Since column ductility capacity decreases with increasing axial load [37], the high design axial load would present a more severe test of the actual condition for bridge columns.

2.3.5 Concrete

Normal weight concrete with a target compressive strength of $f'_{co} = 5000$ psi at 28 days was used in the test columns. The concrete was designed to represent a 67% overstrength when compared to the typical 1960's design strength of 3000 psi. The overstrength is to reflect both the conservative concrete mix design and batching practices of the 1960's and the strength gain expected in more than twenty years of natural aging. Summaries of the mix design and compressive strengths are given in Appendix A.

2.3.6 Steel Jacket Length

Extension of the steel jacket to full height of the column is often not necessary for flexural retrofit. In determining the length of the steel jacket, the increase in moment demand on the column as a result of confinement by the steel jacket must be evaluated. Figure 2.3 shows the criterion used for the determination of steel jacket length. The bending moment at the base of the column corresponds to the plastic moment, M_p, which is assessed using a compressive strain of 0.005 in the extreme fiber of the concrete core. The Mander model for confined concrete [21], modified for confinement by steel jacket (Section 1.1), was used for the evaluation of M_p. The length of the jacket is terminated where the moment demand immediately above the jacket is less than 75% of the original flexural capacity M_u. Even though strain-hardening of the longitudinal steel is likely at

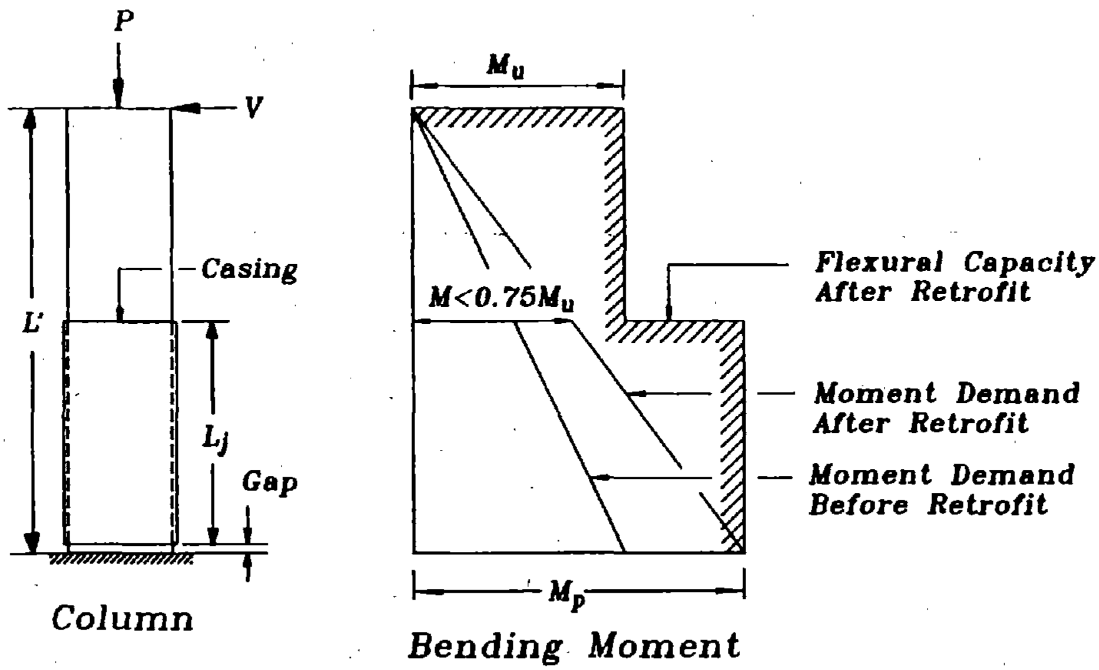

Figure 2.3: **Design Length of Steel Jacket**

ultimate displacement which will increase the moment demand above the jacket, the criterion is considered adequate in avoiding the formation of a plastic hinge above the jacket. The length of steel jacket L_j may be written to satisfy the inequality:

$$L_j > (1 - 0.75\frac{M_u}{M_p})L' - v_g \tag{2.2}$$

where L' is the height of the column; v_g is the vertical gap provided between the toe of the jacket and the top of the footing.

Using a 3/16 inch thick jacket for the test column, the value of M_p is 7366 kip.in. The original flexural capacity of the test column is $M_u = 6671$ kip.in (Table 2.2). If a vertical gap of 1 inch is used, the minimum jacket length is 45.2 inches. A practical jacket length of 48 inches was used.

Note that for proper confinement of the column concrete, the grout infill between the jacket and column must have sufficient strength to transfer the lateral pressure. The lateral pressure for retrofit application is however small compared to the compressive strength available from typical mix of cement-based grout. The uniform lateral confining pressure developed by the jacket, assuming f_{yj} = 36 ksi, is 551 psi for the test column (Eqn. 1.3 and 1.4). The grout compressive strength achieved for this study is about 2200 psi.

2.4 Test Setup

Two independent systems of loading were applied to the test columns using the test configuration shown in Figure 2.4. The axial force was applied using two 2 inch diameter high-strength steel bars before imposing lateral force to the column. Each bar was stressed with a center-hole jack which reacted against the test floor. The bar forces were transferred to the column by a cross-beam mounted on top of a heavily reinforced loadstub. Horizontal force was delivered by a double-acting actuator with a compression capacity of 150 kips and a tension capacity of 130 kips. The available stroke of the actuator was 18 inches. All the applied forces were measured by calibrated load-cells.

The design of the loading system assumed that the lateral force resisted by bending of the high-strength bars is small and that the bar forces will be introduced normal to the loadstub. This is justified in view of the flexibility of the bar. For example, the lateral force resisted by the bar is given by:

$$V_{bar} = \frac{3(EI)_{bar}\Delta'}{L_{bar}^3} \tag{2.3}$$

where $(EI)_{bar}$ and L_{bar} are the flexural rigidity and length of the bar, respectively, and Δ' denotes the top displacement of the bar. By substituting $(EI)_{bar}$ =

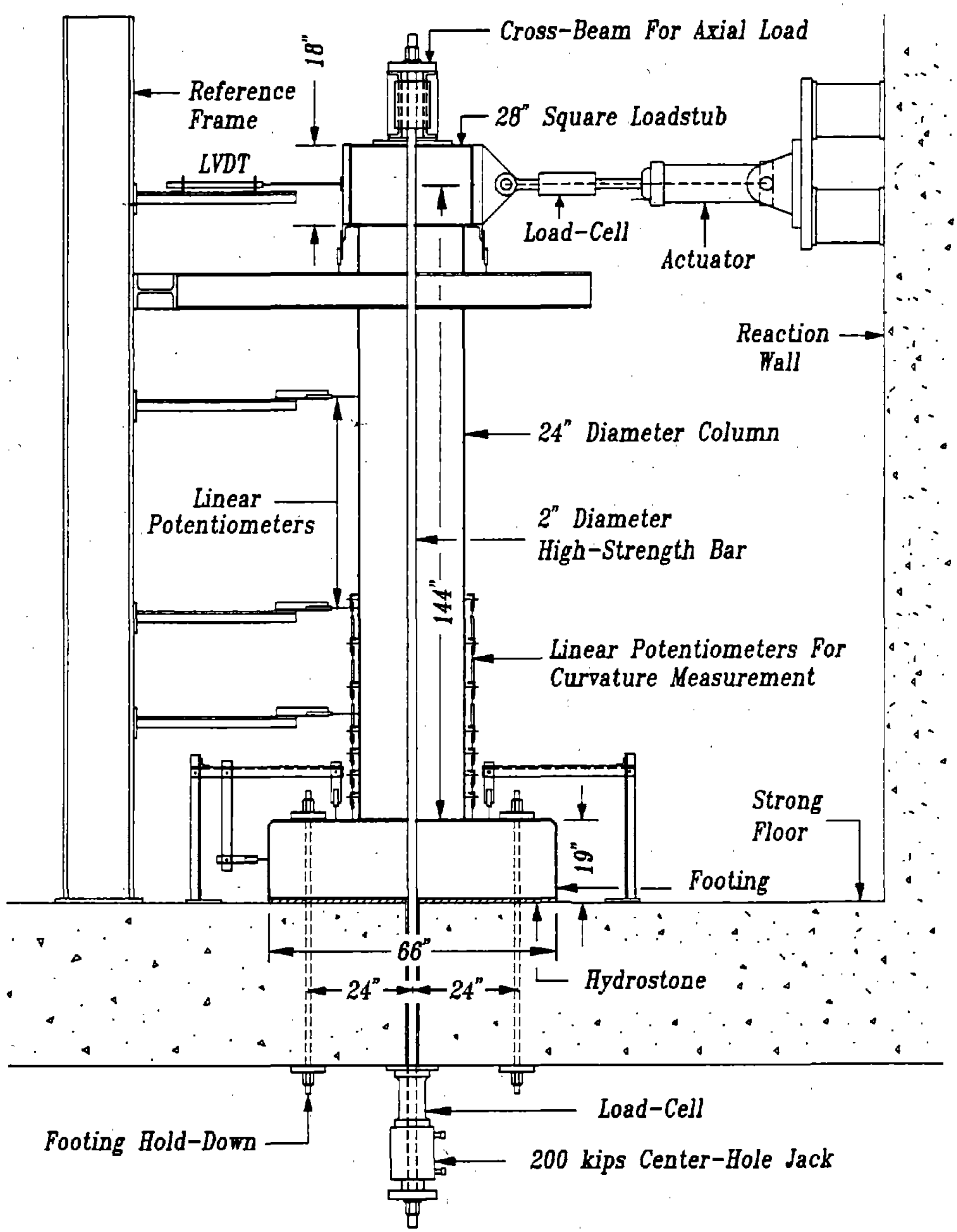

Figure 2.4: **Column Test Setup**

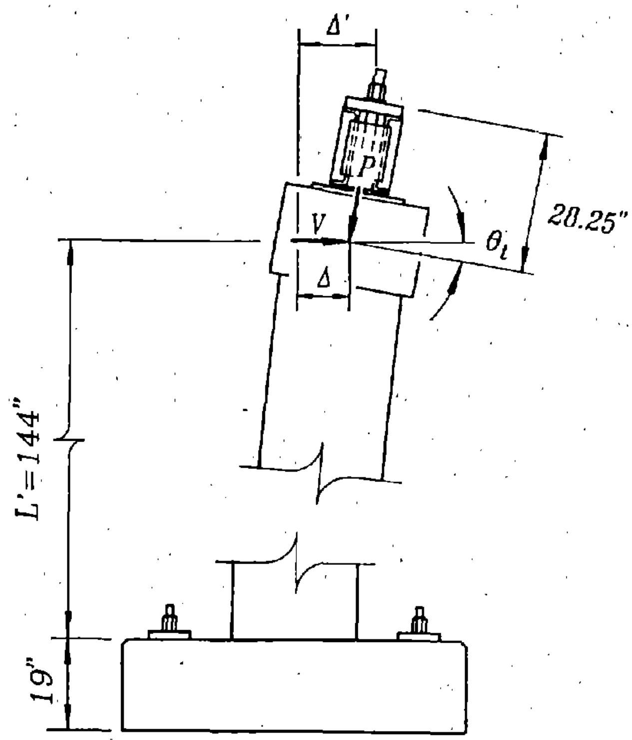

Figure 2.5: **Application of Column Forces**

22777 kip.in^2, L_{bar} = 191.25 inches (taking into account of the height of the cross-beam and footing); and $\Delta' = 10$ inches, gives $V_{bar} = 0.1$ kips which is very small compared with the level of lateral force applied.

The bending moment at the base of the column must however be corrected for the horizontal component of P which will vary with the rotation of the loadstub (see Figure 2.5). The correct bending moment M_b at the base of the column is given by:

$$M_b = (V - P\sin\theta_t)L' + P\cos\theta_t\Delta \tag{2.4}$$

where V = the lateral load as measured by the horizontal loadcell; L' = height of column; θ_t = rotation of loadstub; and Δ = horizontal displacement measured at the center of the loadstub. Eqn. 2.4 may be rewritten as:

$$M_b = R_f V L' \tag{2.5}$$

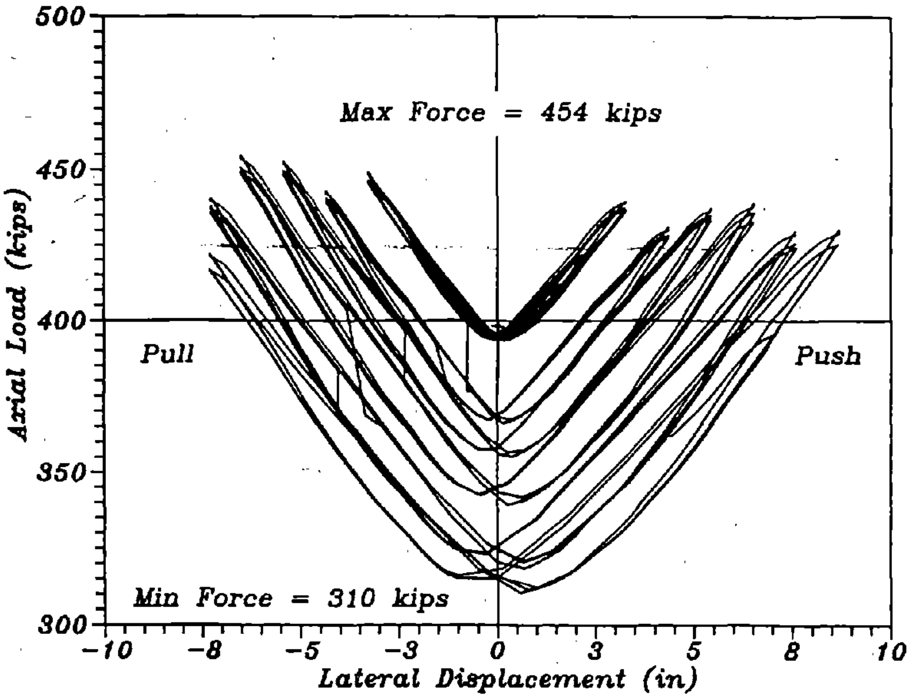

Figure 2.6: **Axial Force Variation during Column 4 Test**

where

$$R_f = 1 - \frac{P}{V}(\sin\theta_t - \frac{\Delta}{L'}\cos\theta_t) \qquad (2.6)$$

represents a correcting factor for the lateral load measured by the horizontal loadcell. The amount of correction is however relatively small. For instance, at the maximum stroke of the horizontal actuator, i.e. $\Delta = 9$ inches, the rotation of the loadstub θ_t was about 4^0. Thus, by substituting these values, and $P = 400$ kips, $V = 55$ kips into Eqn. 2.6, the correcting factor $R_f = 0.946$.

It should be noted that the axial force P will vary with the lateral displacement of the column. Since the neutral axis does not coincide with the centerline axis of the column, the formation of cracks in the column will impose an extension of the column, and hence of the bar which increases the axial force P. During testing of the columns, it was necessary to reduce the axial force after

$\mu = 3$ so that the forces remained within the design limit of the bars. Figure 2.6 shows the characteristic variation of axial force with displacement for column 4. It can be seen that an almost linear increase of axial force occurs at large column displacement.

The deflection at the level of lateral force application was recorded by a 20 inch DC operated linear variable differential transformer (LVDT), as shown in Figure 2.4. In addition, intermediate column displacements were measured by 4 inch linear potentiometers. The rotation of the loadstub was monitored by linear potentiometers mounted at the four corners of the loadstub. Linear potentiometers were also used to monitor the horizontal translation of the footing. No significant translation (less than 0.01 inch) of the footing was noted during testing of the columns.

The reinforcing steel as well as the steel jackets were instrumented with electrical resistance strain gages. The gages used were 120 Ω Showa gages Type N11-FA-5-120-11 which have a nominal length of 5 mm. The prepared surface was cleansed with methyl ethyl-ketone and wiped dry before gage installation. The bonding agent used was a super-adhesive (alpha cyanoacrylate monomer). All gages were coated with an acrylic based water-proofing agent and protected with a vinyl mastic membrane.

The curvatures within the potential plastic hinge region were measured using linear potentiometers mounted as shown in Figure 2.7. Pairs of 3/8 inch all-thread bars were cast in the columns to support aluminum angles to which the linear potentiometers were attached. The placement of linear potentiometers on the extreme tension and compression faces of the column allowed an average

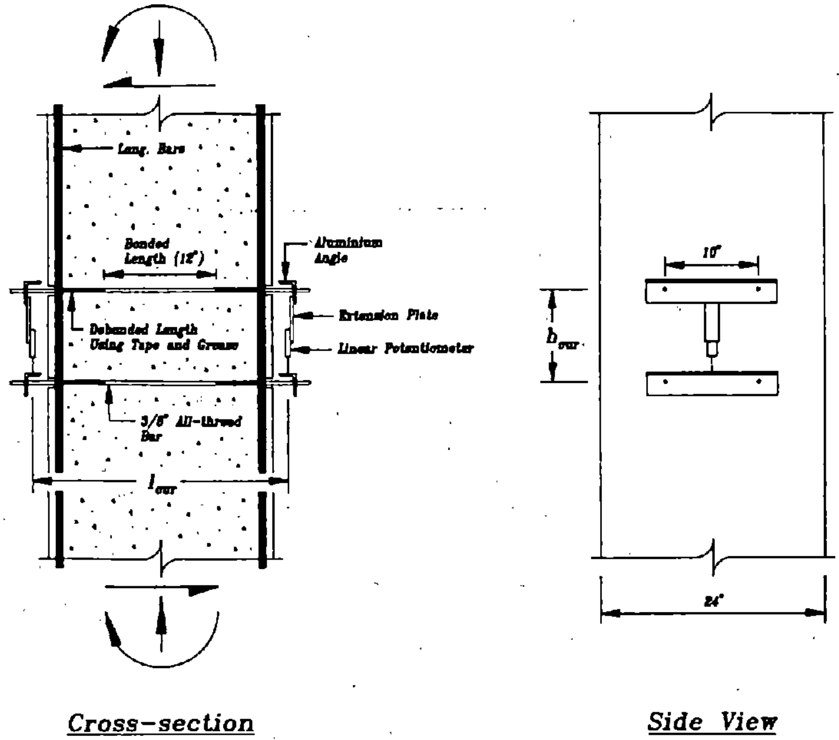

Figure 2.7: **Curvature Measurement**

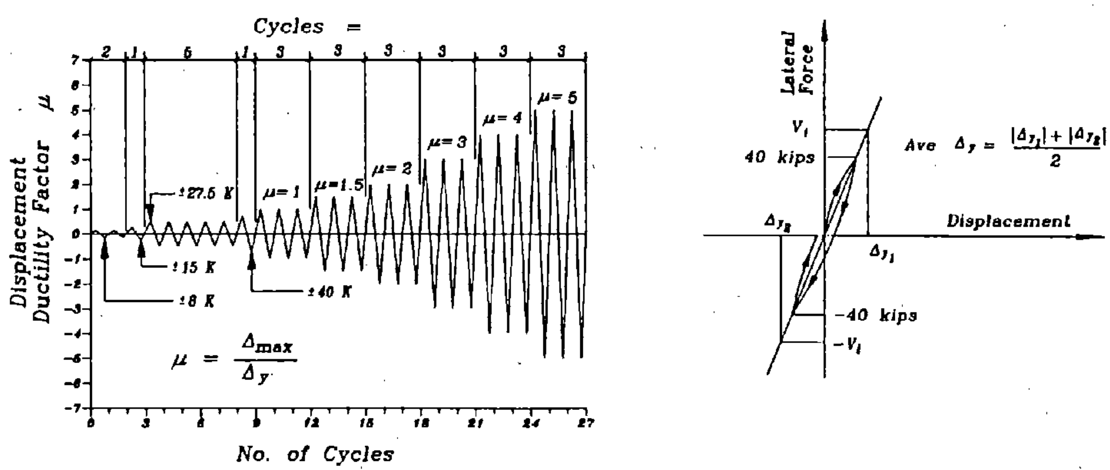

(a) Standard Loading History for All Test Columns *(b) Definition of Yield Displacement*

Figure 2.8: **Standard Force and Displacement Pattern**

curvature to be estimated:

$$\phi = \frac{\Delta_N - \Delta_S}{h_{cur} l_{cur}} \tag{2.7}$$

where Δ_N, Δ_S are the relative vertical displacements between the adjacent rods in the extreme faces; h_{cur} is the vertical distance between the adjacent curvature rods and l_{cur} is the horizontal distance between the pair of linear potentiometers.

All instrumentations were logged by a high-speed data acquisition system involving a VAX Station 2 minicomputer and a NEFF 470 (12-bit) analog-to-digital converter. The effective sampling rate of the converter is 19.5 Hz for a total of 512 data channels. The data acquisition system is driven by in-house developed software. In addition, a continuous real-time plot of the lateral load versus displacement was displayed on a X-Y plotter during testing.

2.5 Test Procedure

All test columns were subjected to the same lateral force and displacement pattern of increasing magnitude, as shown in Figure 2.8(a). Initial cycles were carried out under load control. Two cycles to ±8 kips, followed by one cycle to ±15 kips, were imposed to verify that both the load and data acquisition system were operating correctly, and to determine any cracks that may develop before 15 kips. Five cycles to ±27.5 kips corresponding to approximately 50% of nominal flexural strength were then applied to check for any premature bond failure at the lap-splice of the longitudinal reinforcement. One cycle to ±40 kips was carried out to define the experimental yield displacement. It should be noted that the force of 40 kips approximately corresponds to the theoretical first yield of the extreme tension steel. The experimental yield displacement Δ_y was determined by a linear extrapolation of the displacement at 40 kips to the ideal capacity V_i, as shown in Figure 2.8(b). The average of the displacements in the two directions was adopted as the experimental yield displacement i.e.

$$\Delta_y = \frac{|\Delta_{y1}| + |\Delta_{y2}|}{2} \tag{2.8}$$

where Δ_{y1}, Δ_{y2} = extrapolated yield displacements in the push and pull direction, respectively. For the 'as-built' column, the ideal capacity was assessed using an ultimate concrete compressive strain of 0.005, while for the retrofitted column, the ideal capacity corresponds to the lateral force at the development of the plastic moment, M_p, discussed earlier in Section 2.3.6. It is appropriate at this stage to define a parameter that will characterize the elastic lateral stiffness of the column i.e.

$$K^e_{col} = \frac{V_i}{\Delta_y} \tag{2.9}$$

The definition of K^e_{col} will allow a comparison of the column stiffness increase as a result of retrofit by the steel jacket.

Subsequent cycles beyond ± 40 kips were carried out under displacement control with three cycles being imposed at each ductility factor $\mu = \pm 1$, ± 1.5, ± 2, ± 3 etc., until the failure of the column or the stroke limit of the actuator. The displacement ductility factor is defined in the customary manner as:

$$\mu = \frac{\Delta}{\Delta_y} \tag{2.10}$$

Chapter 3

Observed Behavior of Columns

This Chapter describes the general observations made during testing of the columns. Even though the tests were carried out in the numerical order listed in the test matrix (Table 2.1), descriptions of the column behavior will be presented in two separate sections i.e. columns with lapped starter bars and columns with continuous reinforcement.

3.1 Columns with Lapped Starter Bars

3.1.1 'As-Built' - Column 1

Flexural cracking was first observed at the base of column 1 during the first cycle to 15 kips. The cracking subsequently spread to almost half the column height when the lateral force was increased to 27.5 kips. These cracks formed at near regular intervals of 5 inches and appeared to be influenced by the transverse hoop spacing. There was no observed cracking in the weak footing at this stage. Cracks outside the lap-splice region were wider than those within the splice length and were seen to extend more rapidly at higher forces. At this stage, the double amount of reinforcement in the lap-splice region clearly reduced the crack widths within the splice region.

Vertical splitting cracks first appeared on the tension face near the base of column at 40 kips, providing first visual evidence of incipient bond failure. More extensive vertical splitting cracks appeared in the lap-splice region after displacing the column to $\mu = 1.5$ (see Figure 3.1(a)). Spalling of cover concrete occurred on the tension face during the first pull cycle to $\mu = 1$ and became extensive at $\mu = 1.5$. A peak lateral force of 49 kips was recorded at $\mu = 1.5$ corresponding to a drift ratio ($\Delta/L' \times 100\%$) of 1.4% in the push direction. First evidence of footing distress was noted at $\mu = 1.5$ with a major crack on top of the footing propagating in the direction of lateral force. The crack was however stabilized by the rapidly degrading lateral strength associated with bond failure. Final failure of the column was caused by complete loss of cover concrete over the lap-splices, due to large displacement reversals, as seen in Figure 3.1(b). The second hoop above the base fractured during the second pull cycle at $\mu = 4$, indicating substantial strain beyond yield despite being anchored by a lap-splice in the cover concrete.

3.1.2 Retrofitted Column 2 - Weak Footing

The use of epoxy resin to seal the top and bottom of the steel jacket against grouting pressure presented minor difficulties in observing the formation of first cracking during the early stages of the loading. First cracking was noted in the epoxy seal at the base at 25 kips. Cracking above the jacket was first observed at 27.5 kips. A crack pattern similar to that of column 1 developed above the jacket at 40 kips. There was a slight inclination of the cracks above the jacket indicating the influence of shear on crack formation. Separation between the epoxy seal and column, and relative sliding between the jacket and column were noticeable at this stage. First cracking in the footing was also observed at 40 kips. The vertical crack appeared on top of the footing on the tension side of the loaded diameter propagating in the direction of lateral force. Without a top layer

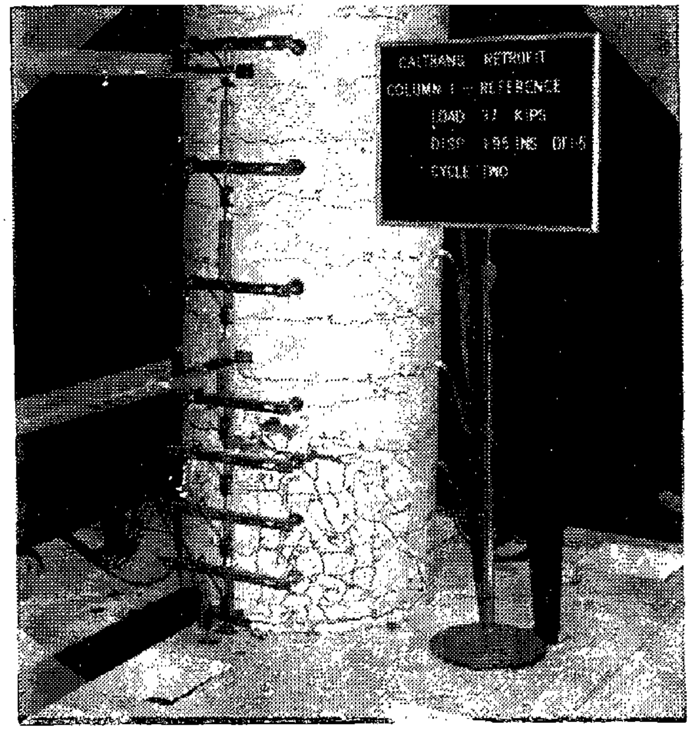

(a) **Crack Pattern at Lap-Splice of Column 1 at** $\mu = 1.5$

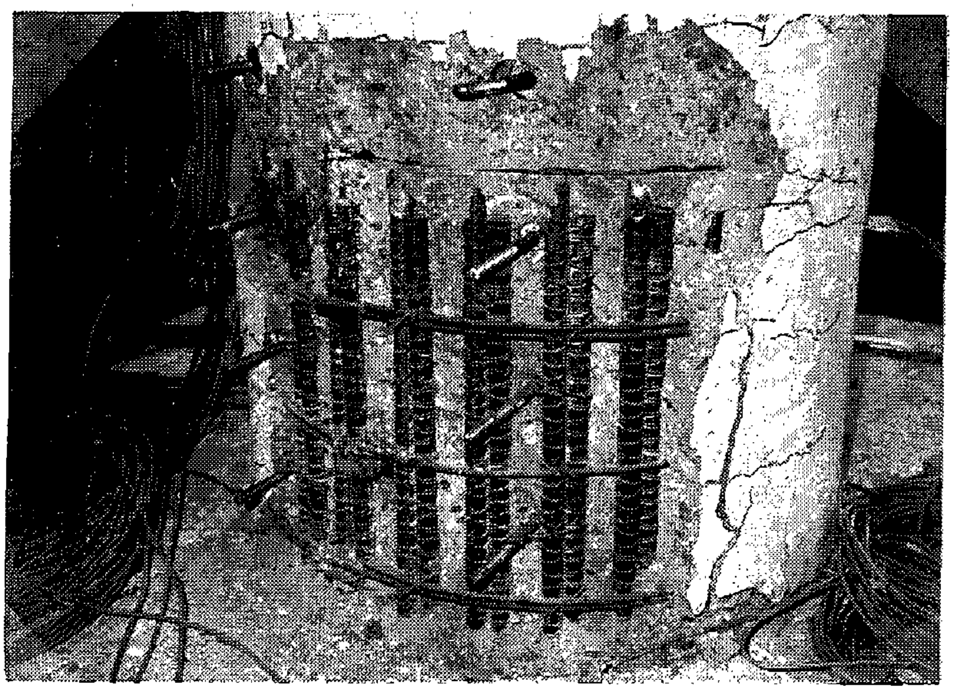

(b) Complete Loss of Cover Concrete in Column 1

Figure 3.1: **Failure of 'As-Built' Column 1 with Lapped Starter Bars**

of reinforcement in the footing, the crack continued to widen as displacements to $\mu = 1$, 1.5 and 2 were imposed. A maximum lateral force of 58.5 kips was recorded during the first push cycle to $\mu = 3$ corresponding to a drift ratio of 2.5%. Stable response of the column was maintained in the first two cycles to $\mu = 3$, but a brittle failure of the footing occurred in the third cycle, resulting in a rapid drop of vertical and lateral force resistances. The failure occurred in the joint region under the column and developed into the full crossed crack pattern under cyclic load reversals, as shown in Figure 3.2(a) and (b). Analysis of footing failure will be further discussed in Chapter 5.

3.1.3 Full Retrofit - Column 6

Column 6 was constructed to duplicate column 2, but with a redesigned footing so that response at large lateral displacement could be studied. Initial behavior of column 2 and 6 were similar, except that the support of column 2 footing on pile-blocks resulted in increased footing flexibility, and hence in slightly larger lateral displacements than for column 6.

No visible cracking was observed in column 6 at the lateral force of 15 kips. There was however minor separation of the epoxy seal from the column surface at the top of the jacket at 20 kips. Four flexural cracks developed above the jacket at 25 kips, with the first crack appearing at approximately 8 inches from the top of the jacket. The cracks were again well spaced at about 5 inches apart. It is clear that the transverse hoops were acting as crack initiators. Minor extension of the cracks occurred upon force increase from 25 to 27.5 kips. A symmetrical crack pattern developed in the column under the two directions of loading. Five cycles to 27.5 kips however did not produce any significant

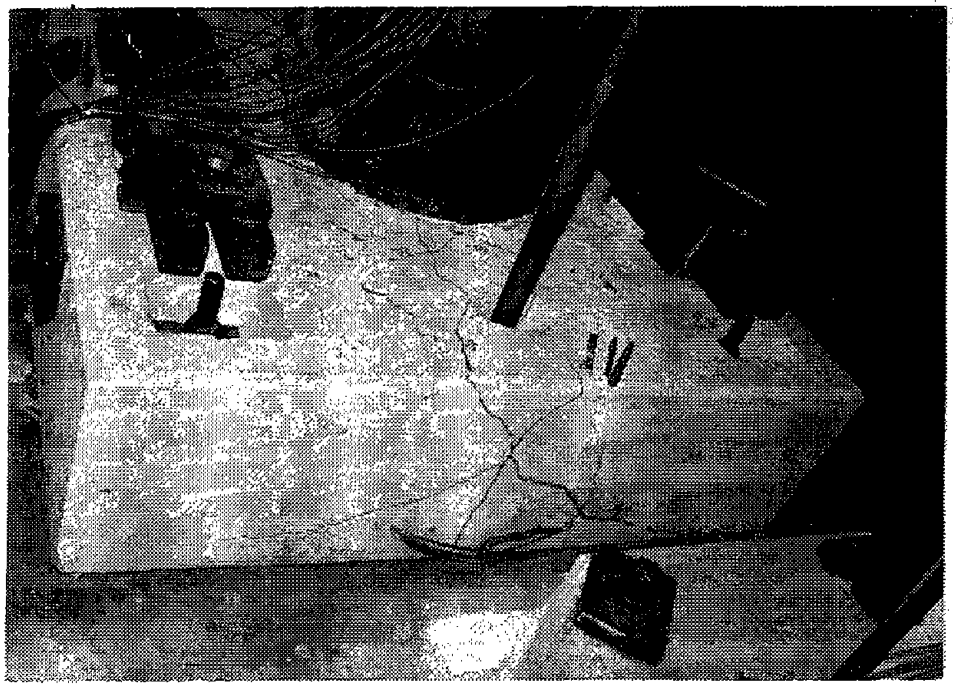

(a) East Face of Footing

(b) West Face of Footing

Figure 3.2: Weak Footing Joint Shear Failure in Retrofitted Column 2

extension of these cracks nor the formation of new cracks. At 40 kips, the spread of cracking up the column was about 2/3 of the column height.

Cracking in the epoxy seal at the base of the column was first noted at a force of 30 kips, and upon loading to 40 kips, the epoxy crack widened sufficiently to allow the crack in the column to become visible. The crack continued to widen as the displacement to $\mu = 1$ was imposed. This is expected since the inelastic rotation of the column was concentrated over a small plastic region. The epoxy seal at the base of column finally spalled off after $\mu = 1.5$ and minor crushing of concrete cover was evident at $\mu = 2$. Cracks appeared on top of the footing at $\mu = 3$ and were seen to radiate from the column in a fan-like manner. Large inelastic strains were developed in the starter bars and the penetration of these strains into the footing led to splitting and eventual spalling of the cover concrete from the footing surface at $\mu = 5$. The spalling exposed part of the starter bars and created an unsupported length of reinforcement of approximately 2.5 inches. Concurrent spalling of concrete inside the jacket was also noted on the compression side. Subsequent displacement to higher ductilities resulted in buckling of the starter bars when in compression and straightening when the direction of applied lateral force was reversed. The cyclic buckling and re-straightening of the starter bars resulted in low-cycle fatigue fractures, as shown in Figure 3.3(a). The first fracture of the starter bar occurred during the first push cycle to $\mu = 8$.

The steel jacket was successful in preventing a bond failure at the lap-splice, and in allowing the strength of the starter bars to be developed. Column behavior was stable prior to the bar fracture and a maximum lateral force of 77 kips was noted at first push cycle to $\mu = 7$, corresponding to a drift ratio of 5.3%. Figure 3.3(b) shows the symmetrical crack pattern of the column near the end

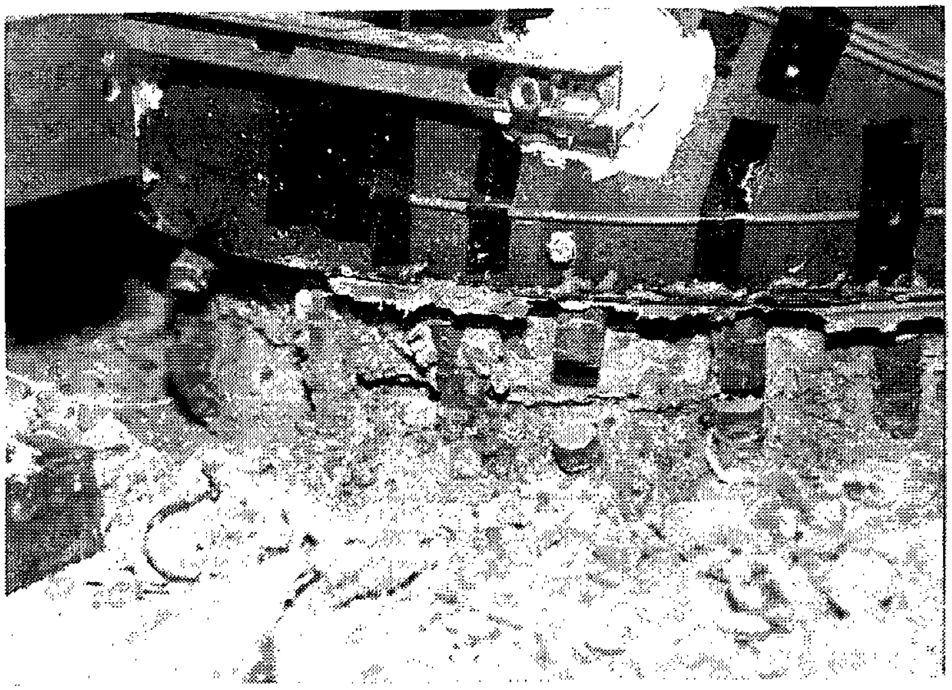

(a) Low-Cycle Fatigue Fracture of Longitudinal Reinforcement

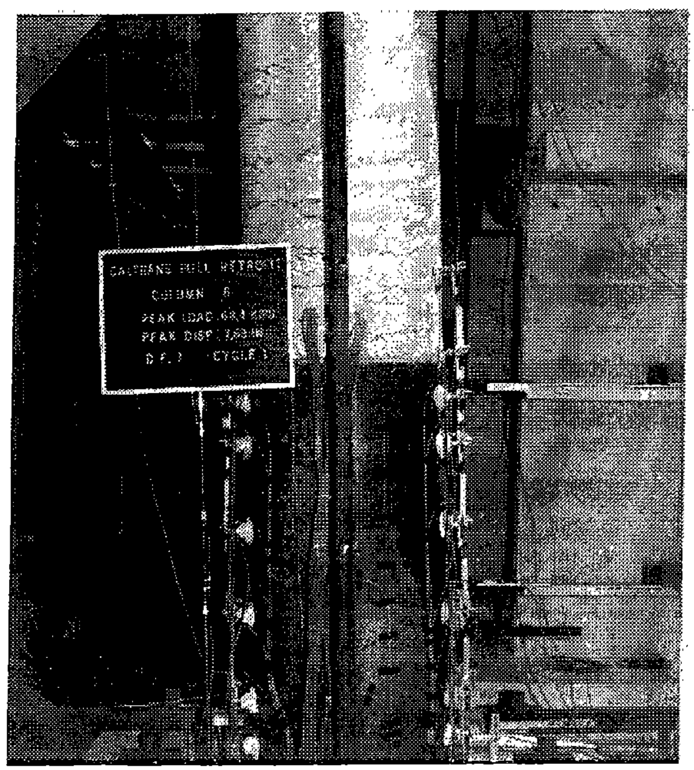

(b) Crack Pattern at $\mu = 7$

Figure 3.3: Failure Mode of Column 6 (Retrofit, With Laps)

of the test.

3.1.4 Partial Retrofit - Column 5

Figure 3.4(a) shows the styrofoam wrap prior to the installation of the steel jacket. The soft styrofoam wrap in column 5 caused an early separation of the epoxy seal from the column surface at a lateral force of 15 kips. Despite the separation, there was no observed cracking in either the epoxy or column.

Three flexural cracks first appeared above the jacket at 20 kips. The cracks were 10, 15 and 20 inches from the top of the jacket. Upon loading to 27.5 kips, cracking spread to almost 36 inches above the jacket, and a symmetrical crack pattern was again observed on the column. A maximum force of 47 kips was recorded during the first push cycle to $\mu = 1.5$ after which the lateral strength decreased as bond failure of the lap-splice became progressively more pronounced. The peak force was slightly lower than its 'as-built' counterpart - column 1, due to the lower concrete strength in column 5 (see Table A.1 in Appendix A for concrete strengths). Unlike column 2 or 6, there was no observed damage to the footing of column 5. The bond failure which occurred at the lap-splice prevented the development of yield of the main reinforcement and the penetration of large inelastic strains into the footing. Despite imposing a final lateral displacement of 8.7 inches in the push direction, the toe of the steel jacket did not bear against the footing, and the vertical load carrying capacity of the column was successfully maintained. The final displacement corresponds to a displacement ductility factor of $\mu = 7.5$ or a drift ratio of 6%. The lateral displacement in the pull direction was however slightly smaller, as limited by the stroke of the actuator to 7 inches. The general view of column 5 at $\mu = 5$ is shown in Figure 3.4(b). Note the excellent condition of the footing.

3.1.5 Repaired Column 1-R

A provision for increasing the strength of the footing was made during the construction of the first pair of weak footings in anticipation of footing failure, by casting conduits in the footing parallel to the loading axis to allow post-tensioning of the footing. Figure 3.5(a) shows the strengthening of the footing using four $1\frac{3}{8}$ inch diameter Dywidag bars. A total of 300 kips was applied to the footing in the direction of lateral force application. Further relief to the footing was provided by placing the footing in a uniform bearing instead of pile-block supports. There was no further development of cracks in the footing during the repair test of the column.

The loss of cover concrete during the initial test of the column presented a problem for containing the grout at the base. It was decided to extend the jacket to the top of the footing to ensure a complete seal against the grouting pressure. Without a vertical gap, the jacket was seen to bear against the footing even at early stages of loading. High hoop strains at the base of the jacket caused noticeable jacket deformations at $\mu \geq 4$. Figure 3.5(b) shows the condition of the jacket at the end of test. Note the belling out of the jacket over the bottom 6 inches.

The general behavior of column 1-R was surprisingly good. For lateral forces below 40 kips, there was no extension of previously existing cracks nor the formation of new cracks. At displacement ductility factor of $\mu = 3$ or drift ratio of 2.7%, the column registered a peak lateral force of 57 kips, which exceeded the 'as-built' maximum force of 49 kips, and also the theoretical 'as-built' flexural

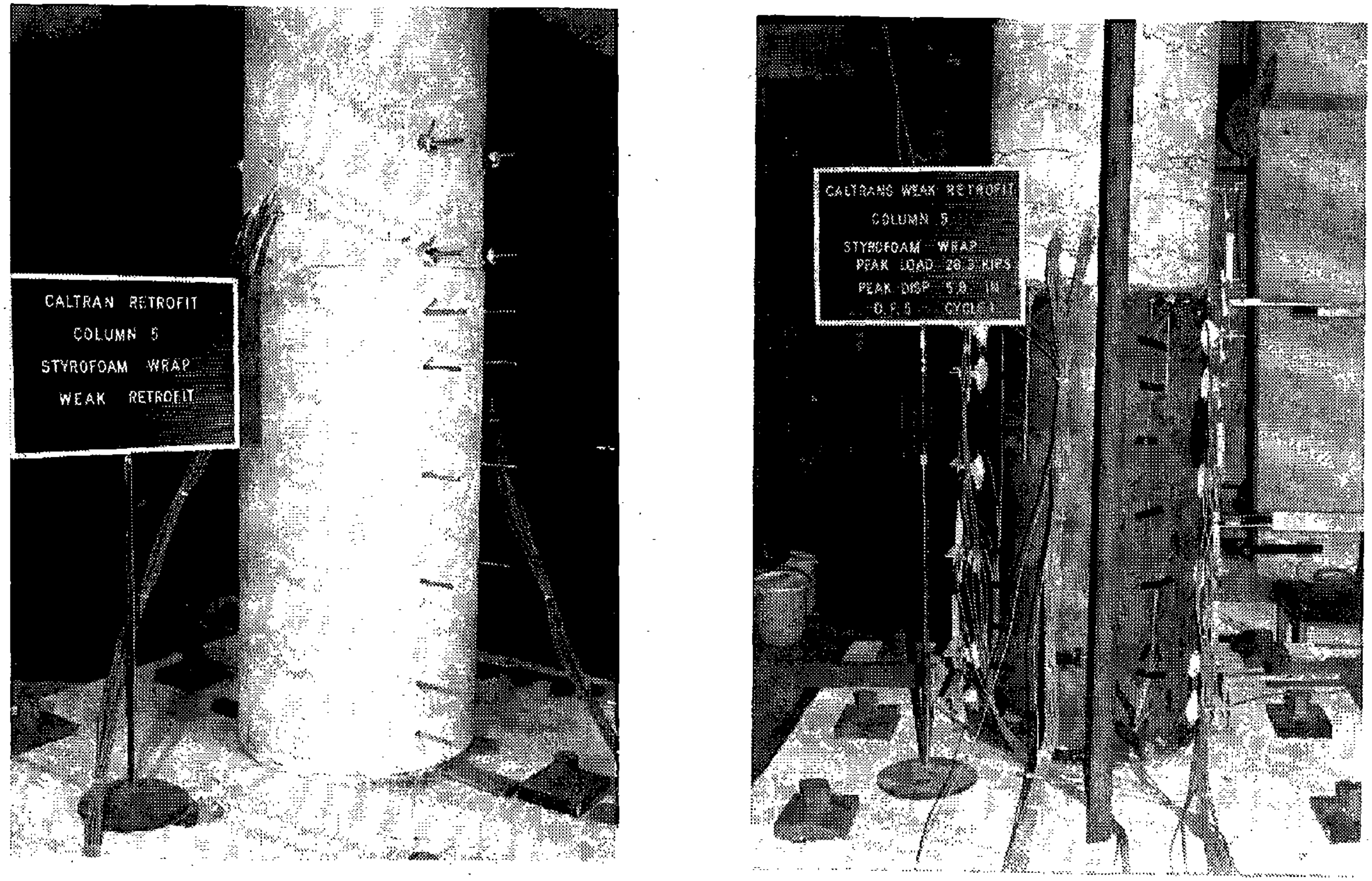

(a) Styrofoam Wrap on Column 5 prior to Steel Jacketing

(b) Condition of Column 5 at $\mu = 5$

Figure 3.4: Styrofoam Wrap and Crack Pattern in Column 5 (Partial Retrofit)

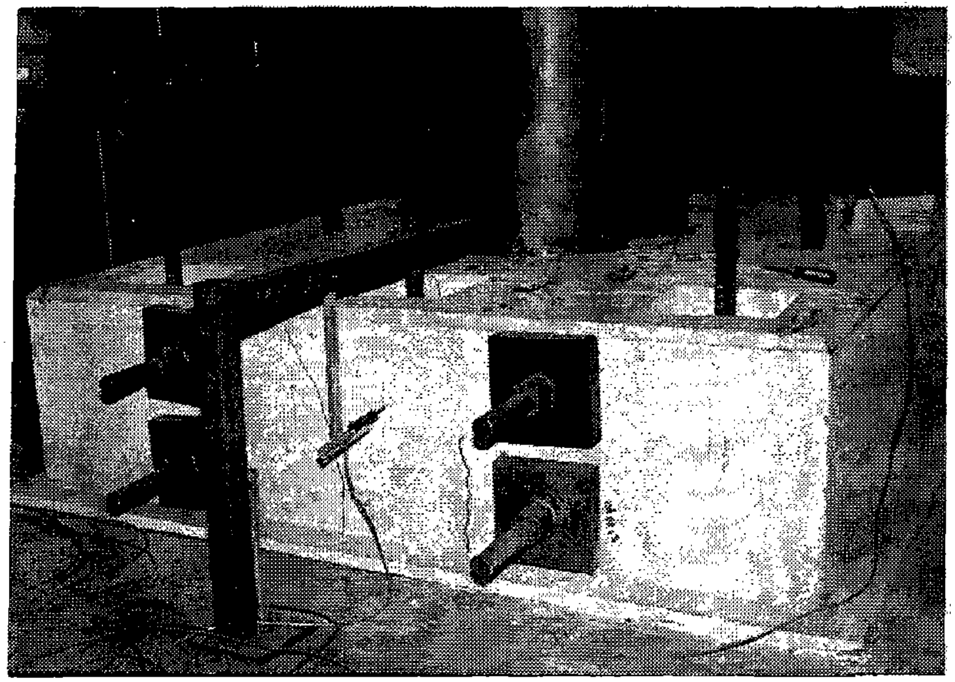

(a) Strengthening of Weak Footing

(b) Local Buckling of Steel Jacket at $\mu = 6$

Figure 3.5: Repaired Column 1-R During Testing

strength. The peak force in the repaired column however was smaller than that of column 6 indicating a reduced strain-hardening as the result of eventual bond failure at the lap-splice region. The column was subjected to further cycles of displacement to $\mu = 6$ or a drift angle of 5.4%, with only gradual degradation of lateral strength. Removal of the steel jacket after test confirmed that bond failure had occurred.

3.2 Columns With Continuous Reinforcement

3.2.1 'As-Built' - Column 3

Unlike column 1, first cracking in column 3 was not apparent at 15 kips. Two cracks appeared at 12 and 15 inches above the base at 18 kips. First cracking of the base was observed at 21 kips. Cracking spread to half the column height at 27.5 kips. Increased loading to 40 kips and $\mu = 1$ produced only minor extension of the crack lengths. First evidence of concrete crushing was noted at the base at $\mu = 1.5$ in the push direction. Crushing was delayed in the pull direction until $\mu = 2$. Spalling of the cover concrete on both faces of the column occurred at $\mu = 3$. Incipient buckling of the longitudinal bars was obvious at $\mu = 4$, corresponding to a drift ratio of 3%. The second hoop above the base fractured during the second pull cycle to $\mu = 5$. The first hoop, as well as third and fourth, did not fracture but showed some slip in their lap-splices. The loss of lateral restraint by these transverse hoops allowed further outward bowing of the longitudinal reinforcement in compression. Repeated cycles to a displacement ductility factor $\mu = 5$ resulted in the destruction of the concrete compression zone and eventual loss of the lateral strength of the column. The confinement failure associated with inadequate transverse reinforcement is shown in Figure

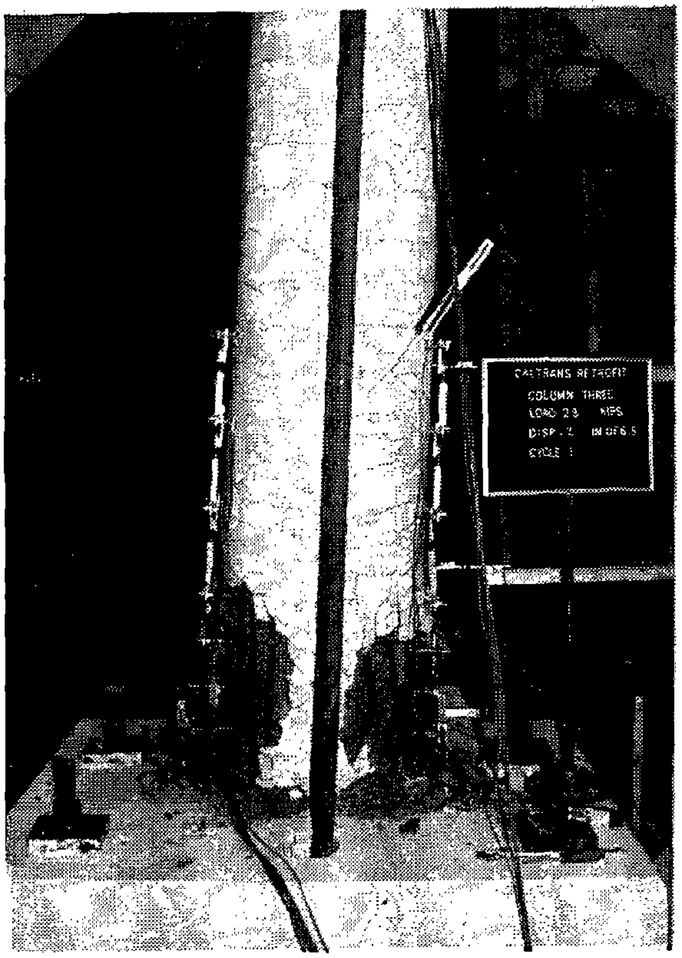

Figure 3.6: **Confinement Failure of Column 3 ('As-built', No Laps)**

3.6.

3.2.2 Full Retrofit - Column 4

The basic behavior of column 4 was very similar to that of column 6. Cracking in the epoxy seal at the base was first observed at 19 kips. Cracking above the jacket was noted at 24 kips, and epoxy separation from the column surface was first noticeable at 27.5 kips. First crushing of the concrete cover occurred at the toe of the jacket at $\mu = 3$. Relative slip between the base of the jacket and the column increased with ductility factor, and was about 5/16 inch at $\mu = 5$. A fan-like crack pattern similar to that observed on the footing of column 6 was well developed at $\mu = 3$ and significant spalling of cover concrete on the footing occurred at $\mu = 6$, as seen in Figure 3.7(a). A maximum lateral force of 73 kips was recorded during the first push cycle to $\mu = 8$ or a drift ratio of 6%. The cyclic displacements imposed on the column led to the eventual loss of the cover concrete on the footing, fully exposing the internal reinforcement. Longitudinal bars were seen to buckle under compression and straightened when lateral force was reversed. As discussed earlier, the cyclic process of compression buckling and tension straightening led to low-cycle fatigue fracture of the main reinforcement. First fracture occurred during the third push cycle to $\mu = 8$, slightly later than column 6 which occurred during the first push cycle. The low-cycle fatigue fracture of the extreme longitudinal reinforcement, is seen in Figure 3.7(b).

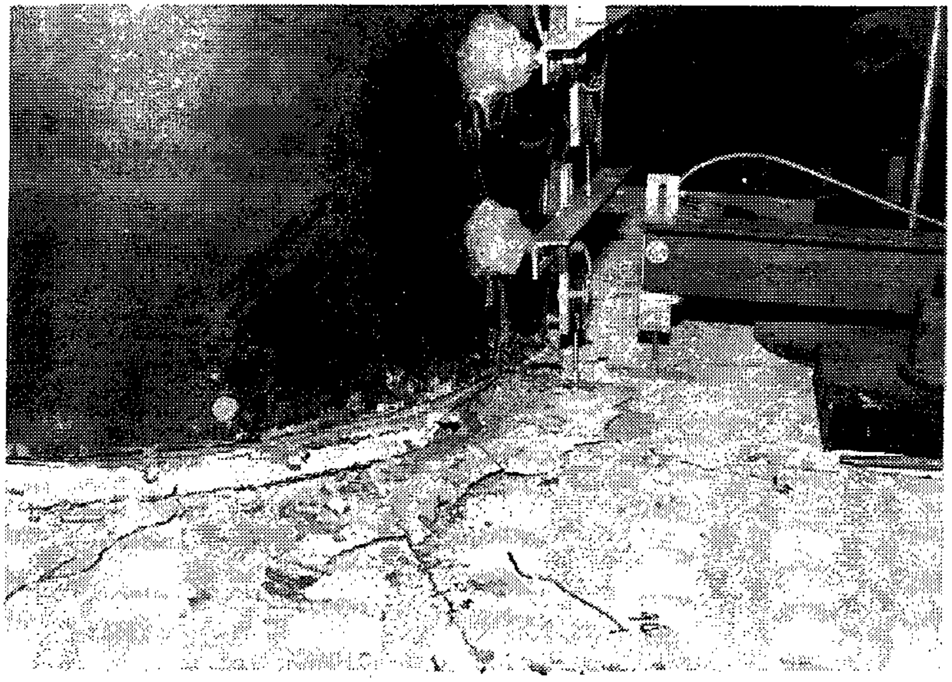

(a) Shallow Spalling of Cover Concrete in Footing

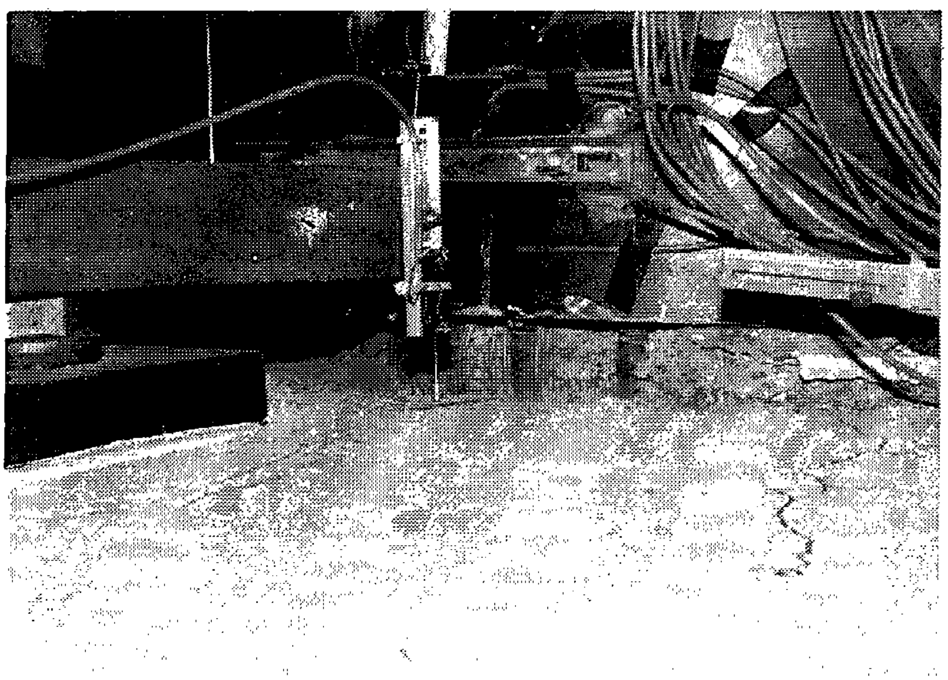

(b) Low-Cycle Fatigue of Longitudinal Reinforcement

Figure 3.7: **Failure Mode of Column 4 (Retrofit, No Laps)**

Chapter 4

Experimental Results

4.1 Lateral Load Versus Displacement Response

As noted previously in Chapter 2, the bending moment at the base of the column is not given by the product of the measured lateral force and column height but must include a correction for the horizontal component of the applied axial force. The correction factor for the measured lateral force at first peaks of each ductility factor, R_f defined in accordance with Eqn. 2.6, is shown in Table 4.1. It can be seen that the correction for the lateral force is small, typically less than 5%. It should be noted that the loadstub rotation for repaired column 1-R was not recorded for $\mu \leq 3$ and thus the factor R_f could not be determined. In the ensuing discussions, the lateral force referred to is that **measured** by the horizontal loadcell. A comparison of the corrected and uncorrected response is included for column 4 in section 4.1.2.2.

In the plots of lateral force versus displacement, V_y is the theoretical lateral force corresponding to first yield of the extreme tension reinforcement, V_i is the lateral force corresponding to the theoretical ideal flexural capacity of the unconfined column section, and V_p is the theoretical lateral force at the development of the plastic moment M_p (defined in Section 2.3.6). The dashed lines representing V_y, V_i or V_p in the plots have been divided by the R_f factors to denote a 'positive' $P-\Delta$ effect. Note that positive displacement indicates the push direction in these plots.

Table 4.1: **Correction Factors R_f for Measured Lateral Force**

(a) <u>**Push Direction**</u>

Column	1	2	3	4	5	6	1-R
$\mu = 1$	0.978	0.984	0.973	0.973	0.970	0.976	-
$\mu = 1.5$	0.973	0.981	0.971	0.973	0.968	0.969	-
$\mu = 2$	0.971	0.983	0.968	0.971	0.962	0.968	-
$\mu = 3$	0.967	0.983	0.968	0.975	0.964	0.964	-
$\mu = 4$	-	-	0.964	0.977	0.958	0.964	0.963
$\mu = 5$	-	-	0.955	0.975	0.944	0.962	0.958
$\mu = 6$	-	-	-	0.973	0.934	0.956	0.956
$\mu = 7$	-	-	-	0.974	-	0.951	-
$\mu = 7.5$	-	-	-	-	0.928	-	-
$\mu = 8$	-	-	-	0.976	-	0.950	-

(a) <u>**Pull Direction**</u>

Column	1	2	3	4	5	6	1-R
$\mu = -1$	0.984	0.978	0.981	0.982	0.978	0.977	-
$\mu = -1.5$	0.985	0.978	0.976	0.981	0.975	0.978	-
$\mu = -2$	0.982	0.979	0.976	0.979	0.971	0.977	-
$\mu = -3$	0.974	0.978	0.978	0.983	0.973	0.976	-
$\mu = -4$	-	-	0.976	0.985	0.972	0.972	0.981
$\mu = -5$	-	-	0.969	0.984	0.960	0.973	0.980
$\mu = -5.67$	-	-	-	-	-	-	0.985
$\mu = -6$	-	-	-	0.986	0.960	0.976	-
$\mu = -6.7$	-	-	-	0.988	-	-	-
$\mu = -7$	-	-	-	-	-	0.980	-

4.1.1 Columns With Lapped Starter Bars

4.1.1.1 Column 1 - Reference 'As-built'

Figure 4.1 shows the measured lateral force versus displacement response of the 'as-built' column with lapped starter bars. The initial response of the column up to five cycles at 27.5 kips showed very little degradation in strength. Minor hysteretic response is noticeable in the one cycle to $\pm$40 kips. The displacements at 40 kips were 1.02 and -0.98 inches in the push and pull direction respectively. Extrapolation of displacements to the ideal capacity (V_i = 52 kips) gives the experimental yield displacement of Δ_y = 1.297 inches, and the lateral stiffness for the column, as defined by Eqn. 2.8, is 40.1 kip/in.

The lateral force recorded at $\mu = 1$ exceeded the theoretical first yield lateral force of V_y = 42 kips, indicating some of the starter bars were yielding. There was very minor degradation of lateral strength between successive cycles to $\mu = 1$. A maximum lateral force of 49 kips was noted during the push cycle to $\mu = 1.5$ and was 94% of the theoretical ideal capacity V_i. The peak force reduced to 42 kips in the pull direction. It is probable that large compression strains developed during $\mu = 1.5$ causing vertical micro-cracking on the compression side. Upon force reversal, the capacity of the cover concrete to resist the splitting force was reduced and hence the lower measured lateral force. The second cycle to $\mu = 1.5$ produced a 18% reduction in the peak force. The reduction was however smaller in the third cycle (about 12%). Subsequent response beyond $\mu = 1.5$ was characterized by very rapid strength degradation with severely pinched hysteresis loops. The second and third cycle showed smaller reduction in peak force than at $\mu = 1.5$. The lateral strength envelope is seen to degrade asymptotically from

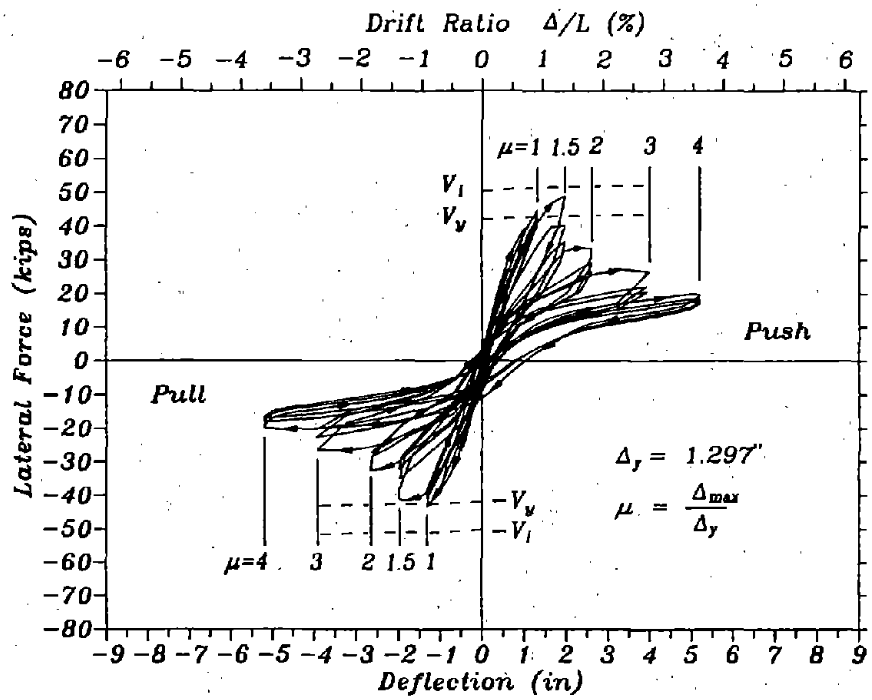

Figure 4.1: **Measured Lateral Force-Deflection Hysteresis Loops for Column 1**

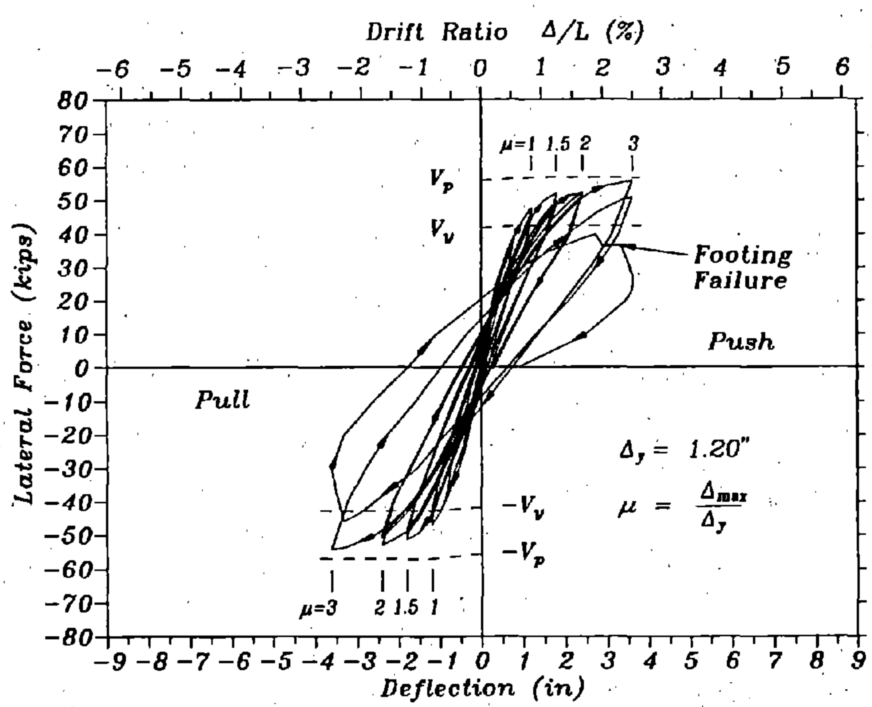

Figure 4.2: **Measured Lateral Force-Deflection Hysteresis Loops for Column 2**

μ = 1.5 to a lateral force of about 20 kips. The degraded lateral strength of the column corresponded to the lateral force resisted by the axial force and is discussed further in Section 5.2.

4.1.1.2 Column 2 - Retrofit, Weak Footing

The lateral force versus displacement curve for column 2 is shown in Figure 4.2. Note that the predicted first yield lateral force is the same as that of column 1 i.e. V_y = 42 kips. This can be expected since the confining effect of the steel jacket is not mobilized until larger column displacements. The plastic lateral force predicted was V_p = 58.4 kips; ≈ 12% larger than the ideal capacity V_i of column 1.

The initial response of column 2 was similar to that of the 'as-built' column, except for an increase in the lateral stiffness. The displacements measured at 40 kips were 0.789 and -0.857 inches in the push and pull direction respectively; both were smaller than that measured in column 1. The extrapolation of the displacements to the plastic lateral force gives the experimental yield displacement of Δ_y = 1.20 inches and a lateral stiffness of K^e_{col} = 48.7 kip/in for the column, indicating a 21 % increase over the 'as-built' column. Although part of the stiffness increase is attributed to the steel jacket, incipient bond failure at the lap-splice of the 'as-built' column is felt to have resulted in a larger yield displacement and a degraded stiffness.

Stable response was noted for displacement to $\mu = \pm 1$, ± 1.5 and ± 2. Unlike the rapid degradation of lateral strength noted in column 1 after $\mu = 1.5$, the lateral force for column 2 continued to increase up to $\mu = 3$ with very little degradation between successive cycles. The plastic lateral force V_p was reached in the first cycle to $\mu = 3$ after which a significant drop in lateral force was recorded, especially during the second cycle in the pull direction, as a result of the footing shear cracking. The footing collapsed during the third cycle to $\mu = 3$, destroying the ability of the test unit to carry the vertical force.

4.1.1.3 Column 6 - Retrofit, Strong Footing

The response of column 6 built with a strengthened footing and retrofitted with a steel jacket exhibited remarkably stable hysteresis loops up to $\mu = 7$, as shown in Figure 4.3. The loops were characterized by a relatively high energy absorption and low reduction of peak lateral force upon recycling to a given ductility level.

The displacements measured at 40 kips were 0.809 and -0.765 inches in the push and pull direction respectively. The extrapolation of the displacements to the plastic lateral force ($V_p = 55.4$ kips) gave an experimental yield displacement of $\Delta_y = 1.09$ inches and a lateral stiffness of $K^e_{col} = 50.8$ kip/in. The lateral stiffness was 4% higher than that of column 2, due in part to a reduction in footing rotation as a consequence of the continuous support along the footing instead of pile-block supports.

The peak lateral forces exceeded the plastic lateral force V_p after $\mu = 2$ as a result of strain-hardening in the longitudinal reinforcement. The maximum lateral force of 77 kips occurring at $\mu = 7$ was 39% above V_p. Low-cycle fatigue fracture of the longitudinal reinforcement which occurred during the first cycle to $\mu = 8$, was accompanied by comparatively rapid strength degradation, although good energy absorption capacity was maintained. Note that the displacement at $\mu = 7$ corresponded to a drift ratio (displacement divided by height) of 5.3%.

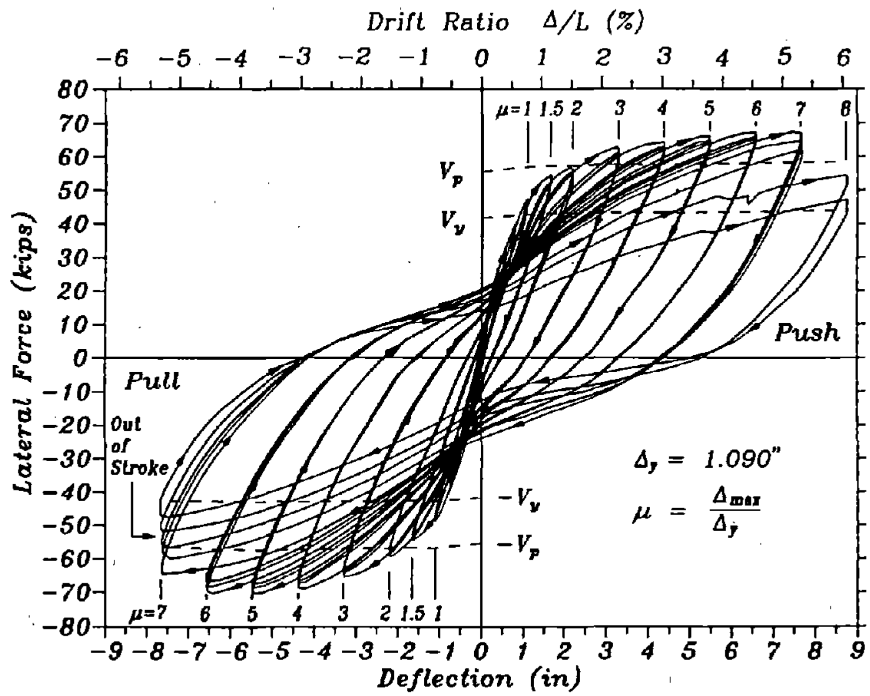

Figure 4.3: Measured Lateral Force-Deflection Hysteresis Loops for Column 6

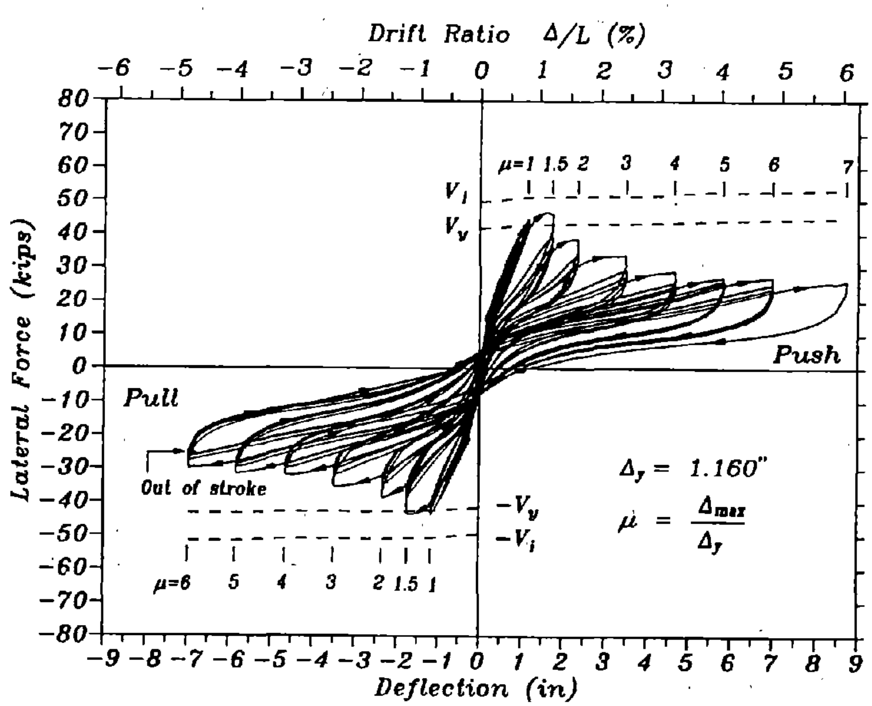

Figure 4.4: Measured Lateral Force-Deflection Hysteresis Loops for Column 5

4.1.1.4 Column 5 - Partial Retrofit

The hysteretic response of column 5, shown in Figure 4.4, exhibited similarity to that observed for column 1. The displacements measured at 40 kips were 0.915 and -0.930 inches in the push and pull direction respectively. The extrapolation of the displacements to the ideal lateral force ($V_i = 50.3$ kips) gave an experimental yield displacement of $\Delta_y = 1.16$ inches and a lateral stiffness of $K^e_{col} = 43.4$ kip/in. The lateral stiffness was 8% larger than that of column 1. The increase is consistent with that observed between column 2 and 6 due to the placing of the footing in uniform bearing instead of on pile-block supports.

A maximum lateral force of 46 kips was recorded in the push direction prior to reaching $\mu = 1.5$, and was 6% less than that measured for column 1 possibly due to weaker lap-splices resulted from the slightly lower concrete strength. The degradation of peak forces between the second and third cycles were comparable with that of column 1 at $\mu = 1.5$. The presence of steel jacket however prevented complete loss of cover concrete and therefore a less rapid degradation of strength for $\mu \geq 3$. Note that even at large displacements, the lateral strength does not degrade to as low a level as for column 1, indicating some residual bond strength.

4.1.1.5 Column 1 - Repaired

The hysteresis loops for column 1 after repair with a steel jacket are shown in Figure 4.5. The experimental yield displacement determined during initial test i.e. $\Delta_y = 1.297$ inches was used as the inelastic displacement increment. Even though the behavior was not as good as that of column 6, there was a significant improvement over its initial performance. The repaired response was almost identical to its 'as-built' response up to $\mu = 1$. The column first reached its ideal lateral force at $\mu = 1.5$ with very minor degradation in strength between the successive cycles to the same displacement. The lateral force continued to increase until a maximum of 54 kips was observed at $\mu = 3$. The subsequent strength envelope showed comparatively slow degradation. Note that at $\mu = 6$, corresponding to a drift ratio in excess of 5%, the lateral strength was still more than 85% of ideal strength. Although bond failure at the lap-splice still occurred, the clamping pressure across the lap provided by the hoop action of the jacket resulted in frictional restraint of the slip. Compared to column 6, the energy dissipation was, however, reduced as signified by the area within the loops.

4.1.2 Columns With Continuous Reinforcement

4.1.2.1 Column 3 - Reference 'As-built'

With continuous longitudinal reinforcement, column 3 showed a favorable increase in flexural strength and ductility over column 1, as can be seen by comparing Figure 4.1 and 4.6. The displacements at 40 kips were 0.900 and -0.852 inches in the push and pull direction respectively. The extrapolation of the displacement to the ideal capacity ($V_i = 49.3$ kips) gave a yield displacement of $\Delta_y = 1.082$ inch. The corresponding lateral stiffness was $K^e_{col} = 45.6$ kip/in; about 14% larger than that of column 1. Note, however, that some of this increase can be attributed to the different footing support conditions.

The ideal lateral strength of the column was first exceeded at $\mu = 2$. Note that a slightly larger lateral force was recorded in the pull direction. The maximum lateral force recorded was 55 kips at $\mu = 3$; about 11% higher than the

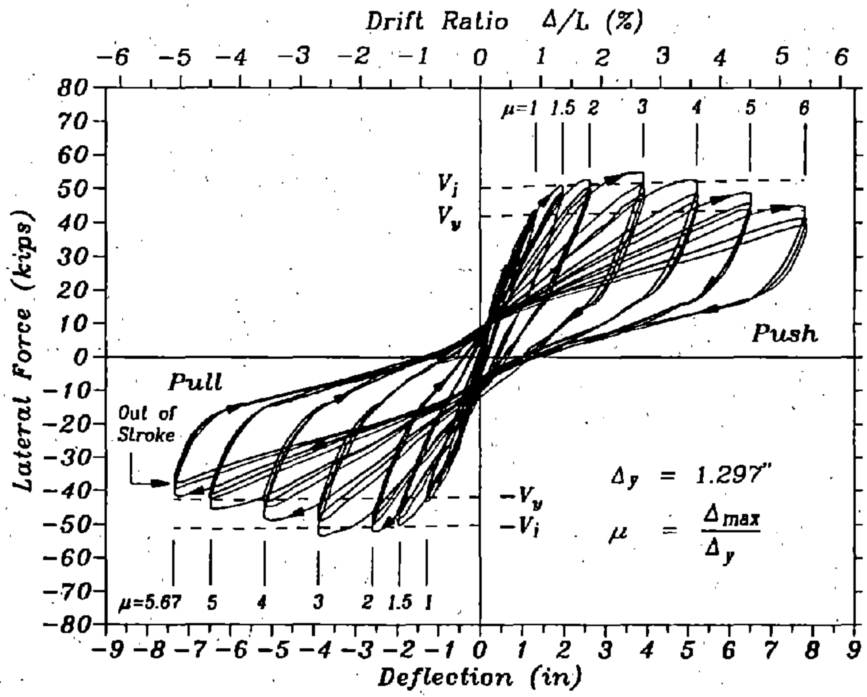

Figure 4.5: Measured Lateral Force-Deflection Hysteresis Loops for Repaired Column 1 - R

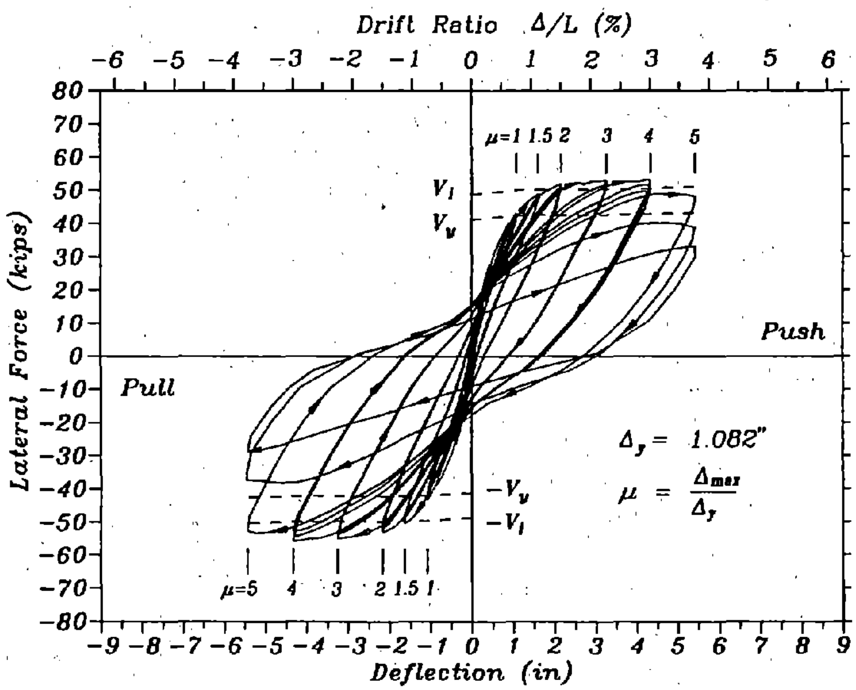

Figure 4.6: Measured Lateral Force-Deflection Hysteresis Loops for Column 3

ideal capacity. The hysteresis loops were stable up to $\mu = 4$ and showed good energy dissipation. There was practically no degradation of lateral strength between the three successive cycles to each ductility factor. The confinement failure at $\mu = 5$, however, was accompanied by relatively rapid strength degradation. Despite the good performance at $\mu = 4$, it would be unwise to rely on a value greater than $\mu = 3$ which corresponded to the onset of cover spalling, for assessing the dependable performance of similar existing bridge columns.

4.1.2.2 Column 4 - Retrofit, Strong Footing

Figure 4.7 shows the measured lateral force versus displacement hysteresis loops for column 4. The hysteretic response of column 4 was very similar to that of column 6. Displacements at 40 kips were 0.814 and -0.742 inches in the push and pull direction respectively, and extrapolation to the plastic lateral force (V_p = 55.9 kips) gave an experimental yield displacement of $\Delta_y = 1.084$ inches. The corresponding lateral stiffness was 51.6 kip/in, about 2% higher than that of column 6. The plastic lateral force was first exceeded at $\mu = 3$ indicating strain-hardening in the longitudinal steel. There was a minor drop in peak lateral force after three cycles to each ductility factor. A maximum lateral force of 73 kips occurred during the first push cycle to $\mu = 8$. Failure by low-cycle fatigue fracture occurred after two cycles to $\mu = 8$ corresponding to a drift ratio of 6%.

As an illustration, the hysteretic response of column 4 was corrected for the horizontal component of the axial force, as outlined in Section 2.4. The corrected hysteresis loops are shown in Figure 4.8. There is very little difference between the measured and corrected plots. A slight reduction in the lateral force was noted in the corrected hysteresis loops at large column displacements.

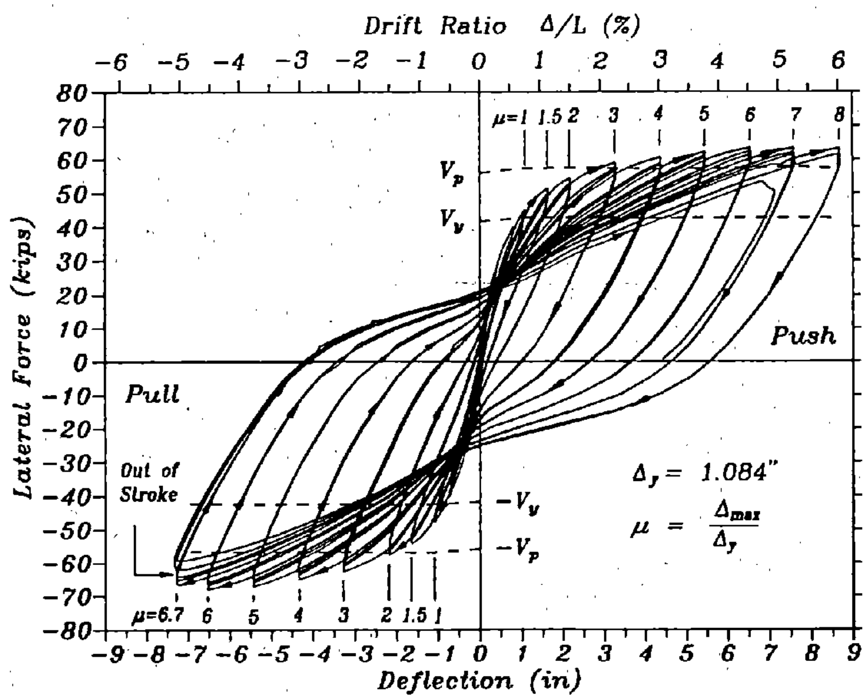

Figure 4.7: **Measured Lateral Force-Deflection Hysteresis Loops for Column 4**

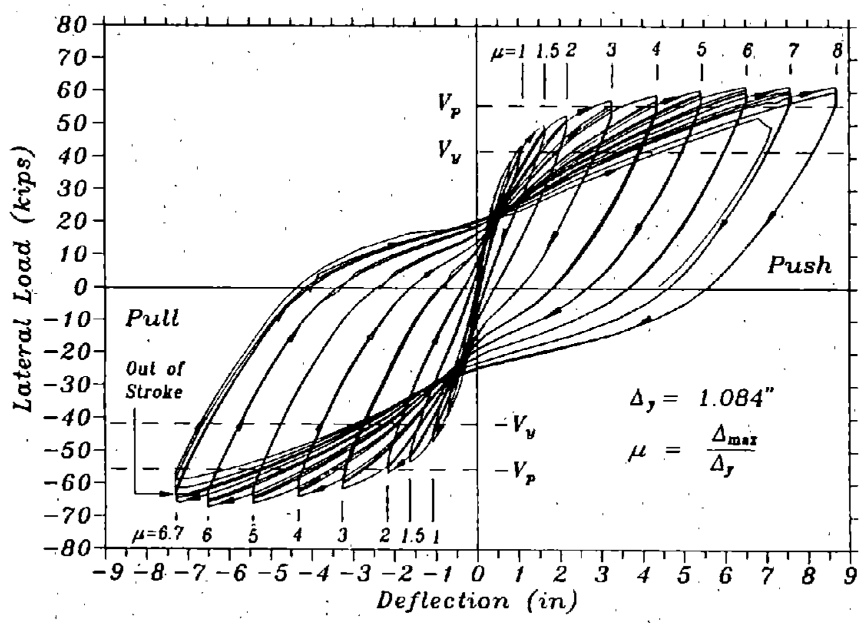

Figure 4.8: **Corrected Lateral Force-Deflection Hysteresis Loops for Column 4**

The cumulative energy dissipated by the column as obtained by the area under the hysteresis loops were 7823 and 7678 kip.in for the measured and corrected hysteresis loops, respectively. The difference between the two energies was only 2%.

4.2 Column Curvatures

Distributions of column curvatures are presented in this section. The curvatures are defined in accordance with Eqn. 2.7. Different scales have been used for the 'as-built' and retrofitted columns. The plotted curvatures are the first cycle peak values for each ductility factor.

The presence of lap-splices in column 1 strongly influences the development of curvatures in the lap region. Figure 4.9 shows a noticeable reduction of curvature at mid-height of the lap-splice due to the stiffening effect of the doubled reinforcement. In contrast, column 3 showed a more gradual distribution of curvature up the column in Figure 4.10. For a given ductility level, the base curvature in the column 3 was less than that of column 1. For instance, at $\mu = 3$, the base curvature (averaged in the two directions) was 23×10^{-4} rad/in for column 1, whereas the base curvature for column 3 was only 15×10^{-4} rad/in. The stiffening effect of the lap-splice requires a larger inelastic rotation to be developed at the base for a given displacement. At a height of 25 inches, column 3 showed a substantial increase of curvature after $\mu = 3$ as a result of increasing moment, and strain penetration up the column. This is not apparent in the profiles for column 1 as a result of the reduced lateral forces sustained by this column.

Curvature distributions for column 5 are shown in Figure 4.11. Note that

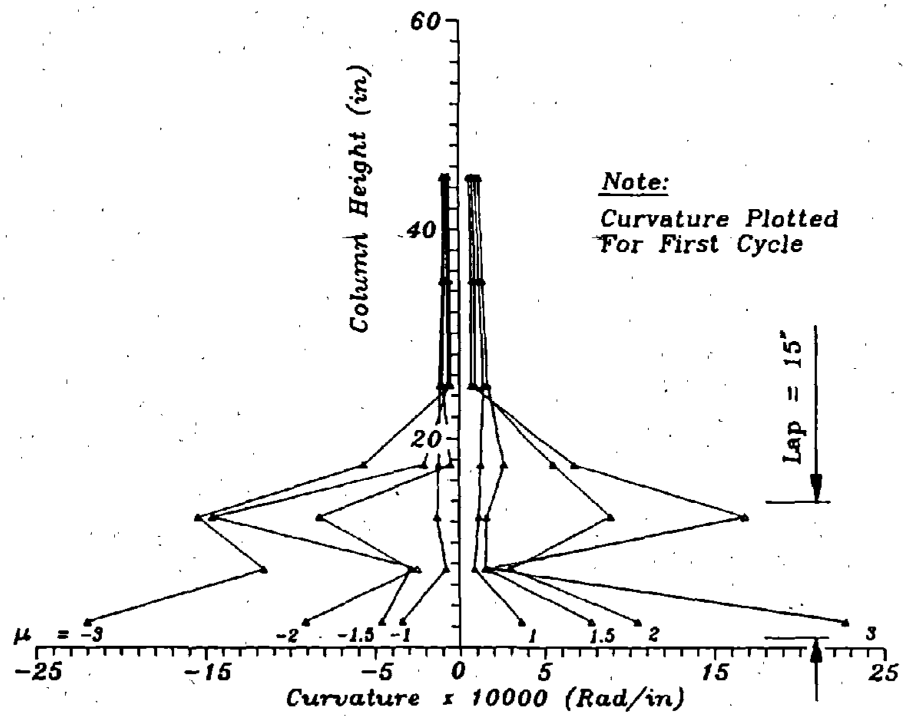

Figure 4.9: **Curvature Distribution in Column 1 ('As-built', With Laps)**

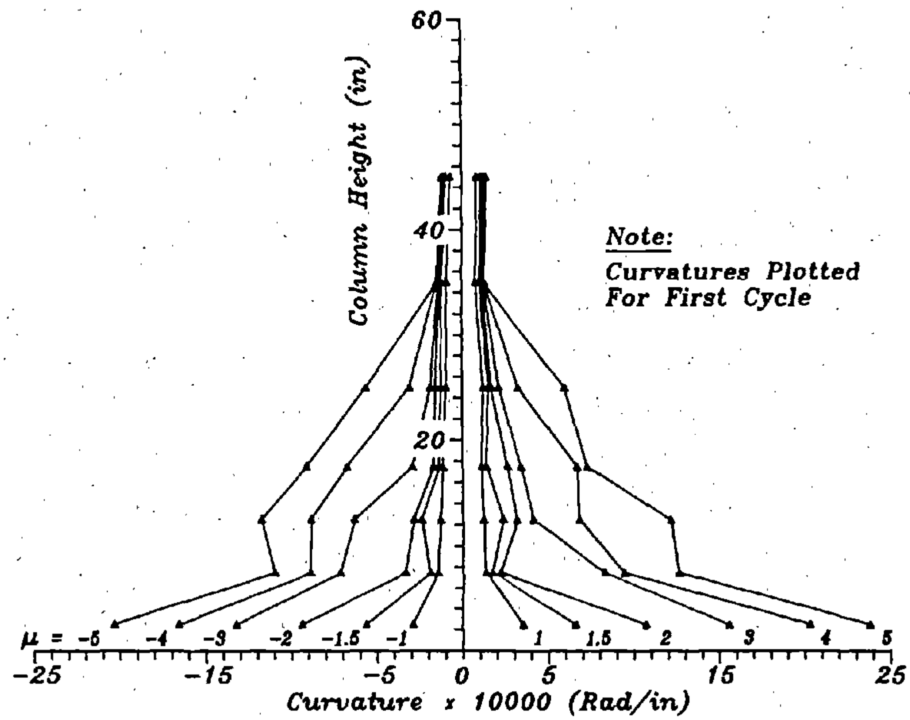

Figure 4.10: **Curvature Distribution in Column 3 ('As-built', No Laps)**

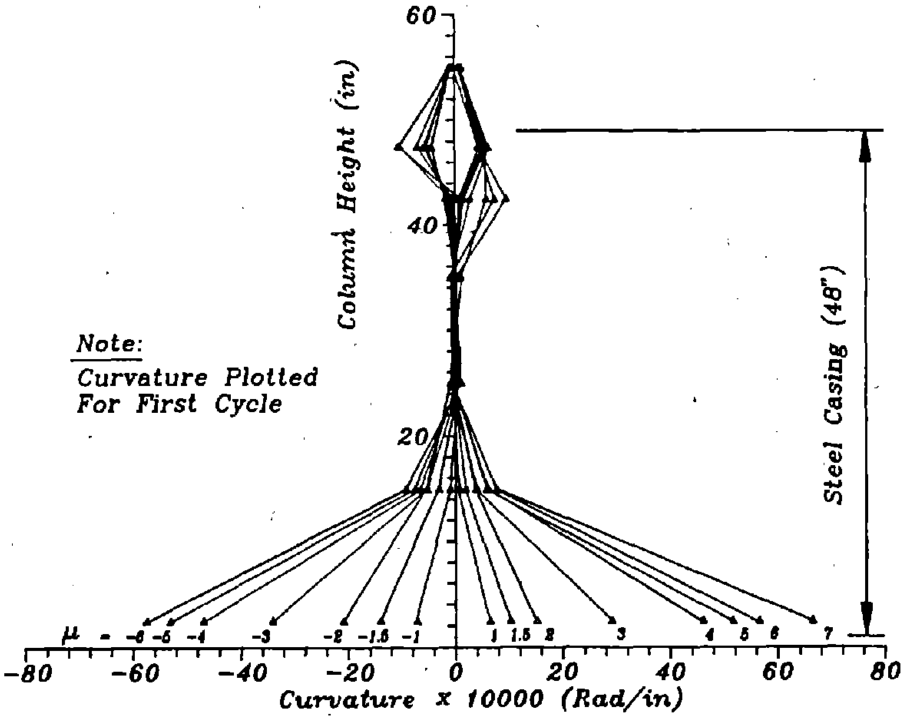

Figure 4.11: Curvature Distribution in Column 5 - Partial Retrofit

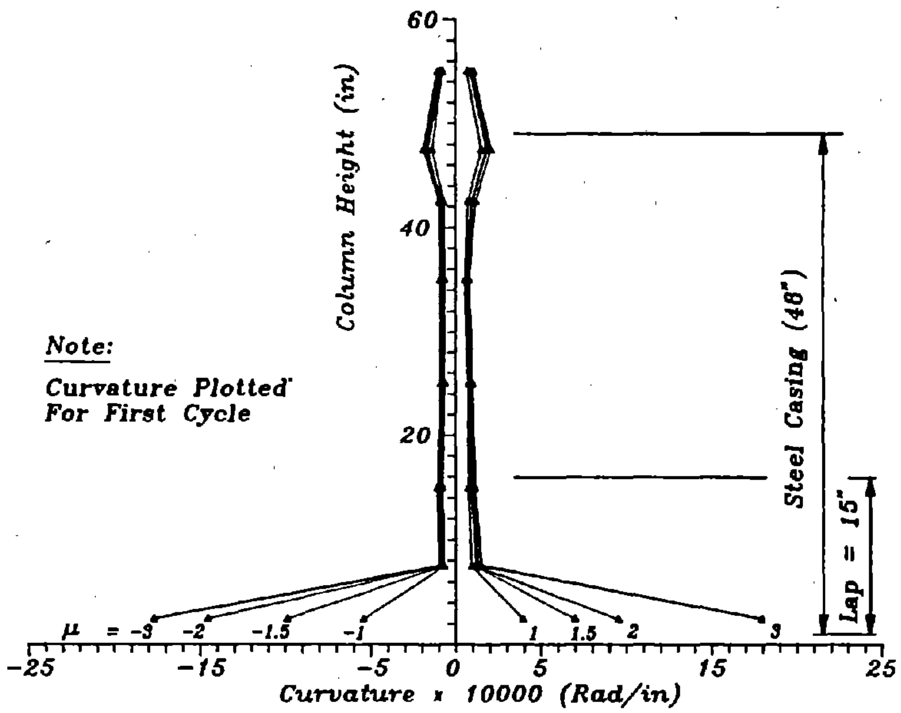

Figure 4.12: Curvature Distribution in Column 2 - (Retrofit, With Laps)

the curvature reduction due to stiffening effect of doubled reinforcement in the lap-splice region could not be measured due to malfunctioning in one of the linear potentiometers at that location. For displacement ductility factors $\mu \geq 2$, column 5 showed a larger base curvature than did column 1. The additional restraint by the steel jacket forced further concentration of the inelastic rotation at the base. Unusually large curvatures were measured near the top of the jacket, even at initial stages of loading. A possible explanation was the bending of the curvature rods due to relative slip between the jacket and column. The rods were bearing on the steel jacket even before the start of the test, despite oversized holes being provided during fabrication of the jacket.

Curvature distributions for column 2 are plotted in Figure 4.12. Note that column 2 showed a smaller base curvature at $\mu = 3$ than column 1 i.e. 18×10^{-4} rad/in compared with 23×10^{-4} rad/in. The deformation of column 1 after incipient bond failure was mainly effected by a continuous opening of a single crack at the base of the column. Despite the influence of the steel jacket in column 2, the inelastic rotation did not occur over a single crack but was distributed over a slightly greater height. The curvature distribution in column 2 also showed a small increase above the jacket, as expected from the reduction of flexural rigidity at that section.

Figure 4.13 and 4.14 show the curvature distributions for retrofitted columns 4 and 6. The concentration of large inelastic rotations at the base of the column is very distinct in these plots. Note the added stiffening effect of the lap-splice which reduces the curvatures inside the jacket of column 6 compared with column 4.

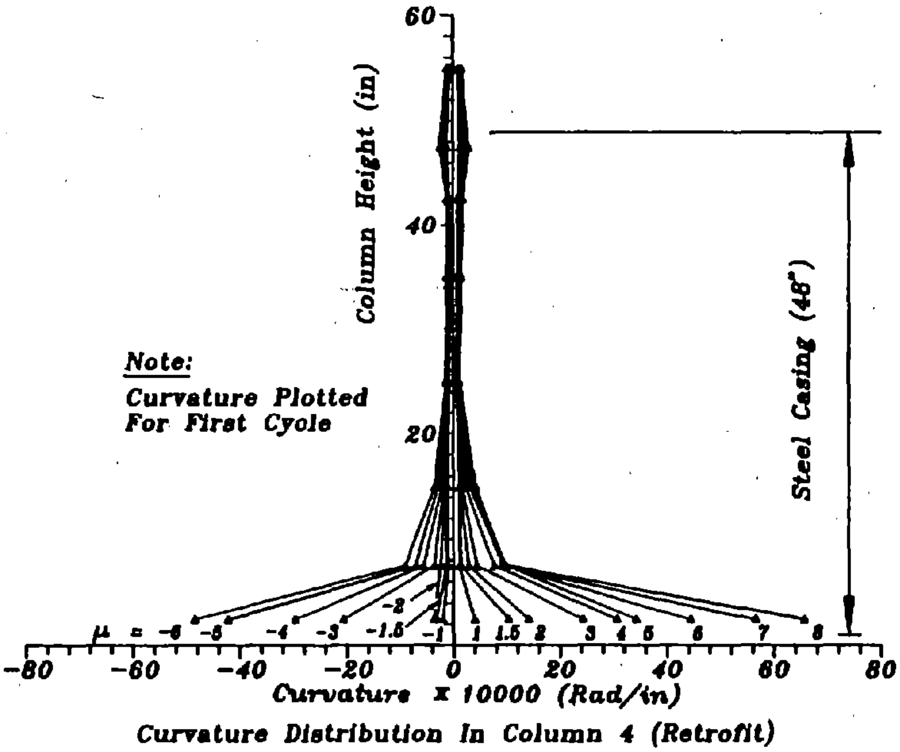

Figure 4.13: Curvature Distribution in Column 4 - (Retrofit, No Laps)

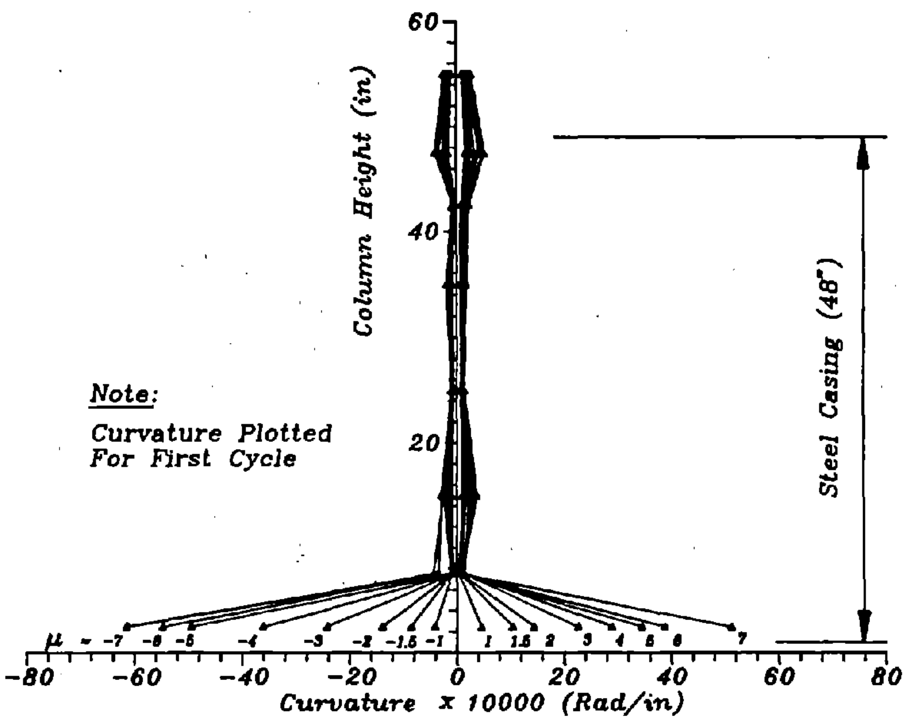

Figure 4.14: Curvature Distribution in Column 6 - (Retrofit, With Laps)

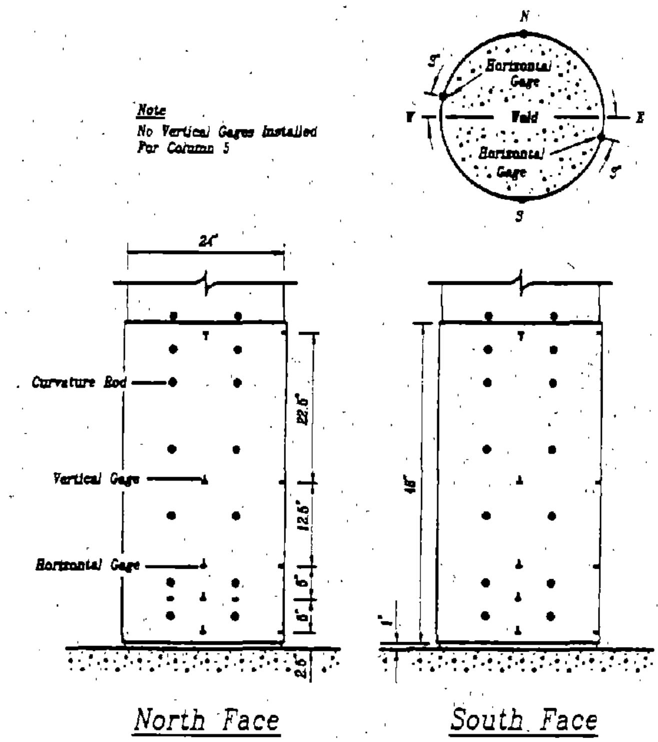

Figure 4.15: **Strain Gage Layout on Steel Jacket**

4.3 Steel Jacket Stresses and Strains

Orthogonal pairs of strain gages were affixed in the vertical and horizontal directions on the longitudinal tension and compression generators of the jacket. In addition, horizontal strain gages were placed 3 inches away from the east and west generators. The deviation of these gages from the east and west generators was necessary in order to avoid the welded longitudinal seams of the jacket. It should be noted that no vertical gages were placed on the jacket of column 5 since the use of styrofoam wrap was expected to prevent any significant development of vertical stresses. Figure 4.15 shows a typical strain gage layout used for column 2, 4 and 6.

4.3.1 North - South Generators

As observed earlier in discussion of the lateral force versus displacement response, the use of a fully grouted jacket increases the lateral stiffness of the column. The increase depends on the effectiveness of the bond transfer between the jacket and column. A plot of the vertical stress instead of strain distribution would enable the level of bond stress at the jacket/grout interface to be determined. To this end, the measured orthogonal strains on the jacket were converted into stresses, using the procedure outlined in Appendix B. Since strains exceeded yield at higher ductility levels, the conversion required considerations of plasticity theory.

4.3.1.1 Vertical Stress Distribution

Figure 4.16(a) and (b) show the development of vertical stresses on the north and south generators of the jacket for column 2 during the push cycle. Slightly higher vertical stresses were noted on the compression generator due to the better frictional characteristics associated with dilation of the compressed concrete. For example, at $\mu = 2$, the peak vertical stress on the compression side was -15 ksi, whereas on the tension side the peak vertical stress was 12 ksi. The average slope of the vertical stress distribution implied a bond stress of 117 psi and 94 psi on compression and tension sides of the column respectively.

Figure 4.17(a) and (b) show the same distributions for column 4, but up to the larger displacement ductility factor of $\mu = 6$. Vertical stresses larger than that of column 2 were noted. For example, compressive stress as high as -22 ksi was measured at displacement ductility factor of $\mu = 6$. On the tension side, a slightly smaller vertical stress of 20 ksi was measured. Note again the better

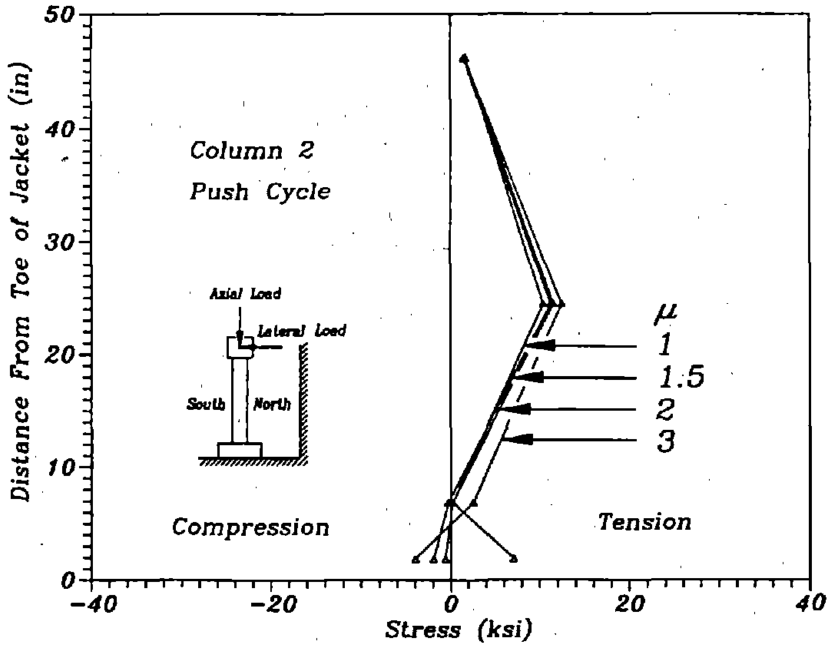

(a) Tension Generator (North)

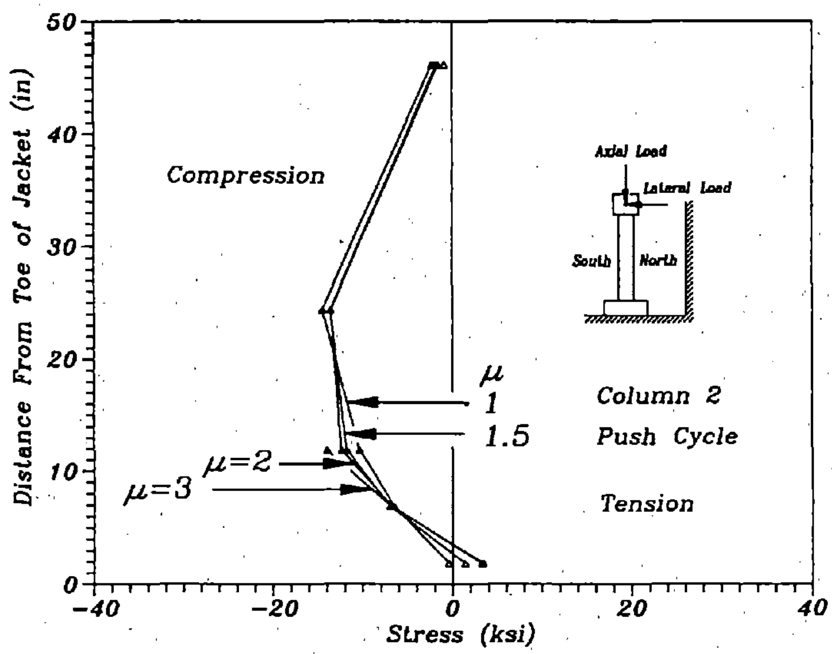

(b) Compression Generator (South)

Figure 4.16: N-S Vertical Stresses on Jacket of Column 2 (Retrofit, With Laps)

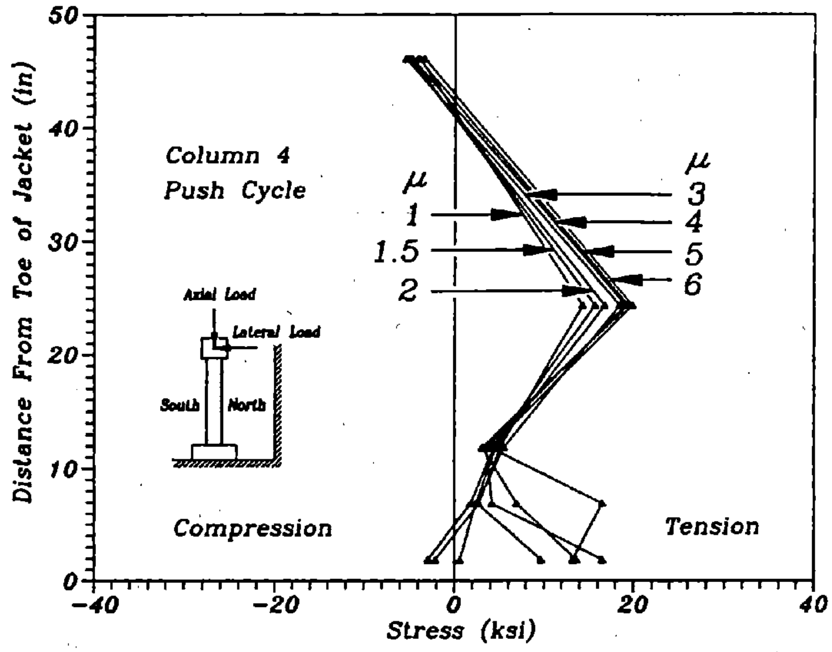

(a) Tension Generator (North)

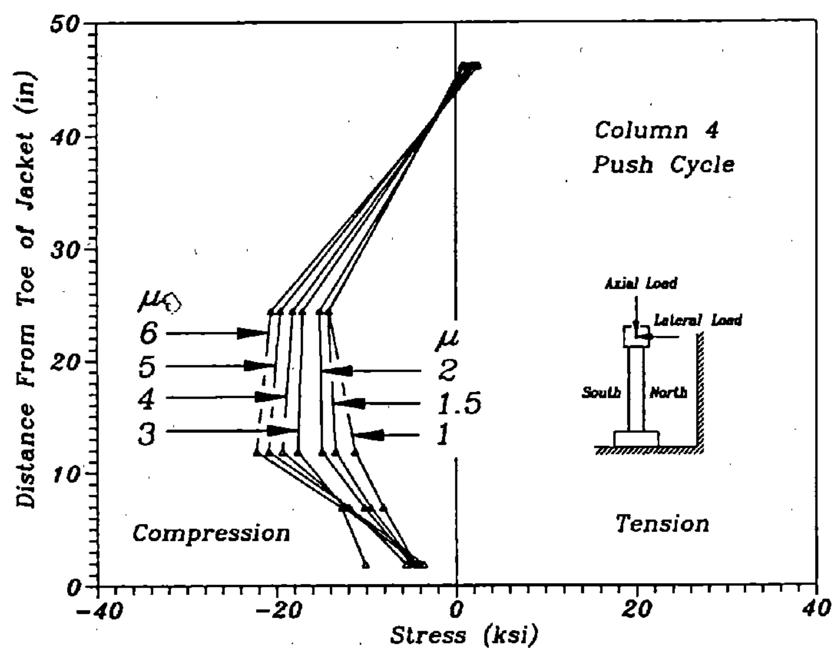

(b) Compression Generator (South)

Figure 4.17: **N-S Vertical Stresses on Jacket of Column 4 (Retrofit, No Laps)**

bond transfer on the compression side, as evidenced by the maximum vertical stress occurring at quarter height from the toe of the jacket. Near the top of the jacket, the vertical stresses reversed, apparently due to local bending at that location. The use of epoxy resin as sealant against grouting pressure resulted in a relatively strong bond of the jacket to the column. The lateral displacement of the column resulted in local bending of the jacket since the bond transfer from the column to the jacket must act at an eccentricity equal to half the jacket wall thickness.

The distributions of vertical stresses on the jacket of column 6 are shown in Figure 4.18(a) and (b). The vertical stresses were approximately 20% higher than those recorded for column 4. At a displacement ductility factor of $\mu = 6$, the stresses were -27.5 and 26 ksi on the compression and tension generators respectively. Section analysis carried out at $\mu = 6$, assuming full composite action, gave the respective vertical stresses of -36.8 and 36.2 ksi at the same height. The smaller measured vertical stresses implied that relative slip had occurred between the jacket and grout infill. High tension stresses at the base of the jacket on the compression side (Figure 4.18(b)) indicate the presence of localized plate bending.

4.3.1.2 Circumferential Stress Distribution

Figure 4.19(a) and (b) show the circumferential stress distributions on the tension and compression generators of the jacket for column 2 during the push cycle. A near uniform distribution of circumferential stress was noted on the tension generator with magnitude less than 12 ksi. In contrast, large tension circumferential stresses were recorded on the compression generator at the two

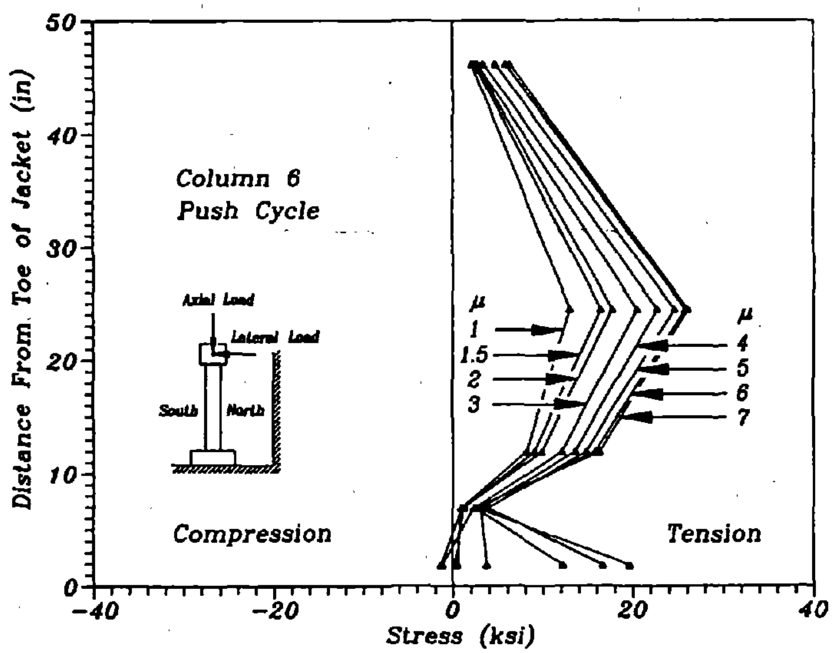

(a) Tension Generator (North)

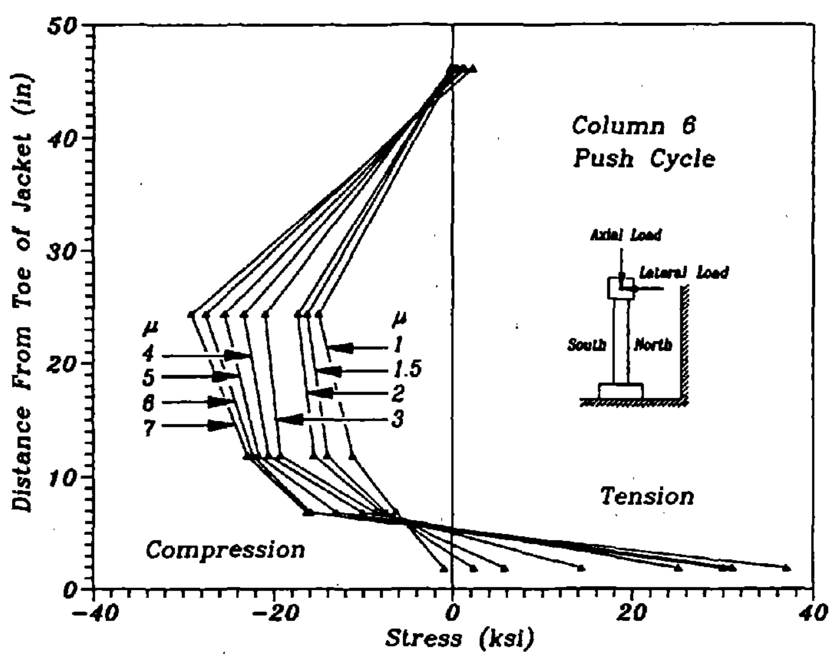

(b) Compression Generator (South)

Figure 4.18: N-S Vertical Stresses on Jacket of Column 6 (Retrofit, With Laps)

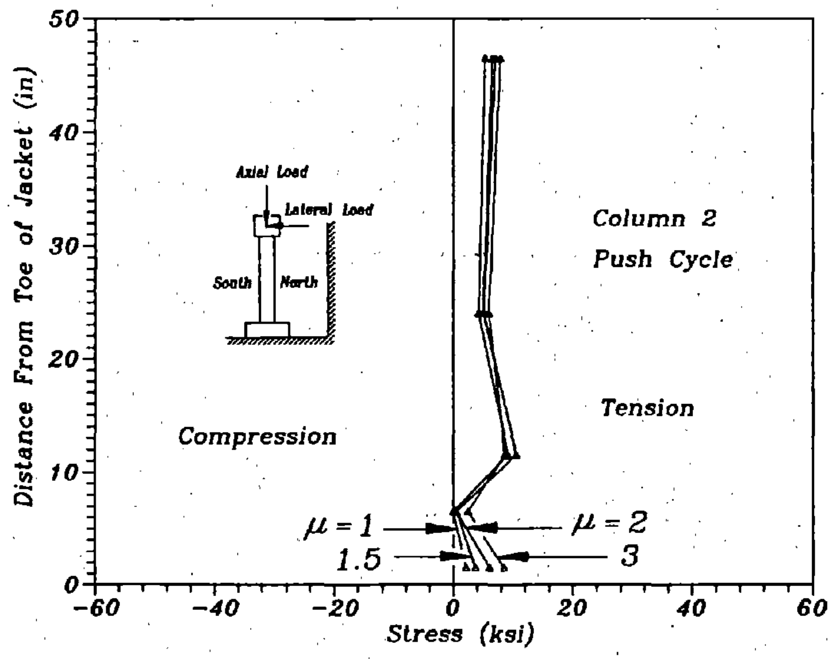

(a) Tension Generator (North)

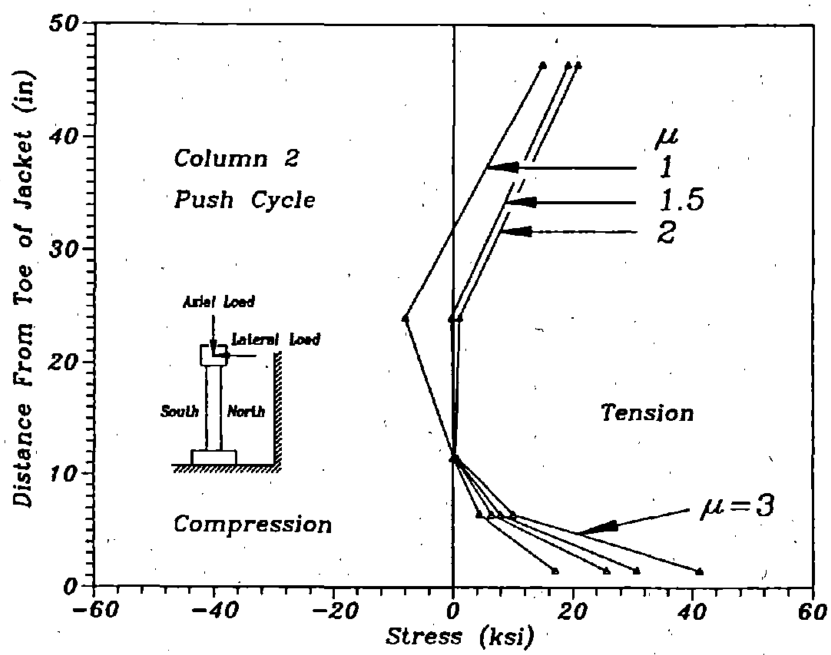

(b) Compression Generator (South)

Figure 4.19: N-S Circumferential Stresses on Jacket of Column 2 (Retrofit, With Laps)

ends of the jacket. The stresses decreased rapidly until almost zero at mid-height of the jacket. Tensile stress as high as 41 ksi was measured at the toe of the jacket at $\mu = 3$, as a result of confinement of the compressed concrete. The relatively large compressive stress noted at mid-height of the compression generator at $\mu = 1$ was probably due to an unstable strain gage at that location.

Figure 4.20(a) and (b) show the circumferential stresses on the tension and compression generators of the jacket for column 4 during the first peak of the push cycle. On the tension generator, some erratic variation of circumferential stresses was noted, especially close to the two ends of the jacket, possibly due to instability of the strain gages. Circumferential tension was noted on the compression side and was considerably larger than that on the tension side, as a result of Poisson's ratio effects, and the confining action of the jacket at the base of the jacket. It is interesting to note, however, that the circumferential tensions were of approximately equal magnitude near the two ends of the jacket. The peak circumferential tension at the toe of the jacket was 45 ksi, whereas the circumferential tension was 42 ksi near the top. The relatively large circumferential stresses near the top of the jacket may be due to a continuity of column curvature inside the stiffer jacket causing local bearing of the column on the jacket, thus inducing the large circumferential stresses in the jacket. The yield strength of the jacket based on tension test of two inch wide strip was 47 ksi, as given in Table A.1 of Appendix A.

Figure 4.21(a) and (b) show similar circumferential stress distributions on the jacket of column 6 during the push cycle. The north generator showed a relatively uniform distribution of circumferential tension. In contrast, large circumferential stresses were measured on the south generator especially near

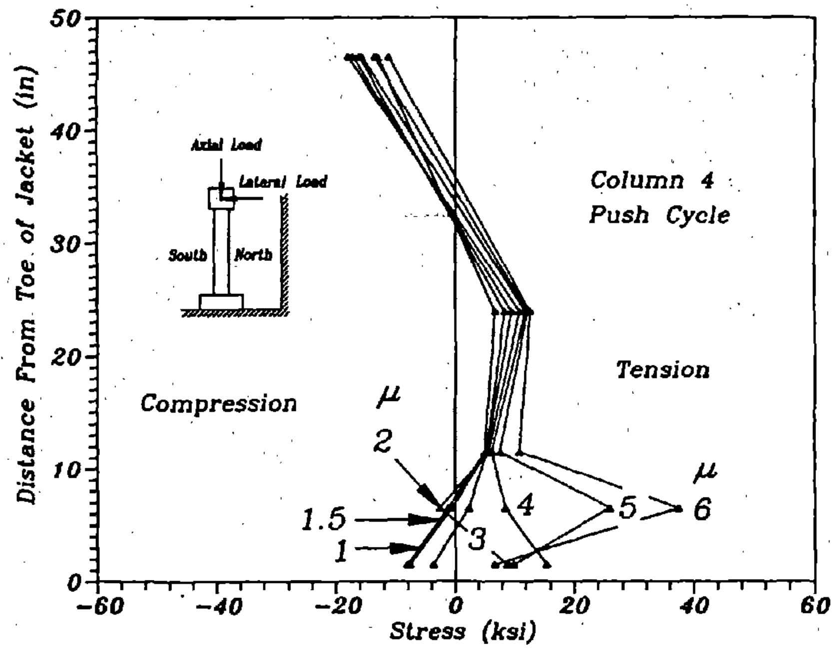

(a) Tension Generator (North)

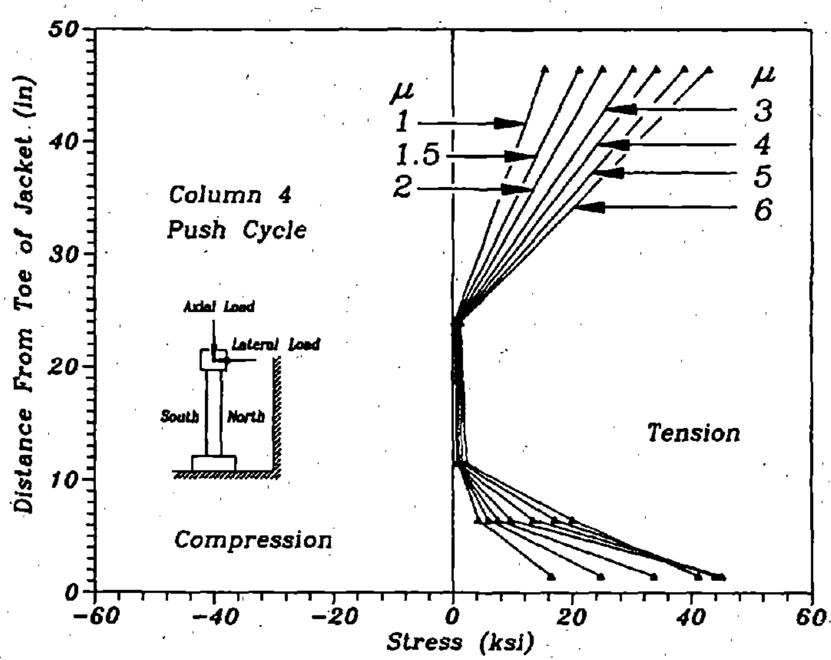

(b) Compression Generator (South)

Figure 4.20: N-S Circumferential Stresses on Jacket of Column 4 (Retrofit, No Laps)

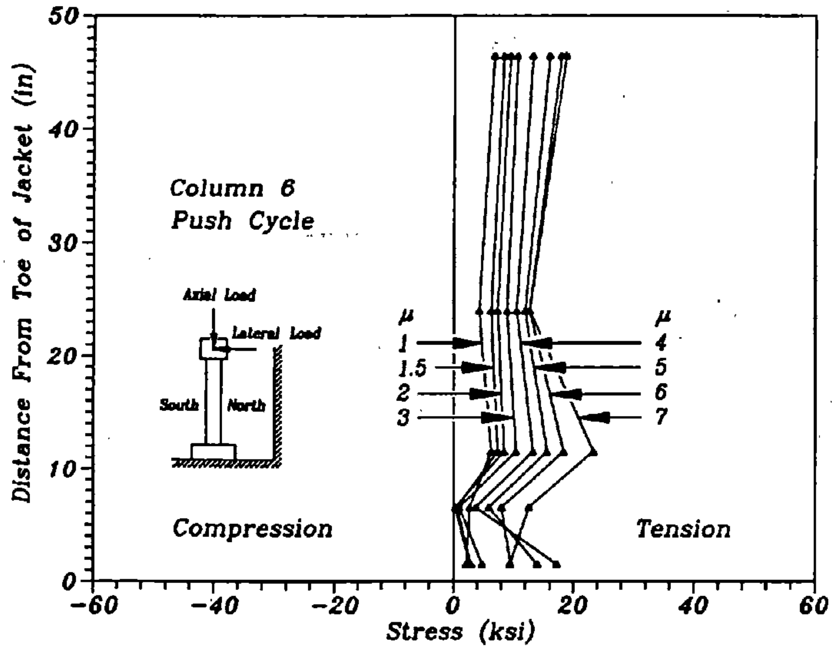

(a) Tension Generator (North)

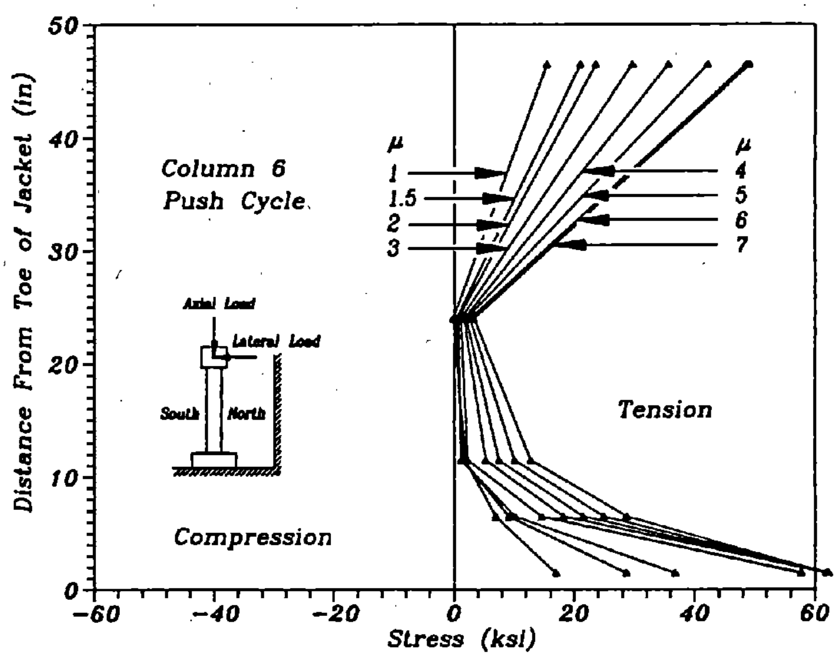

(b) Compression Generator (South)

Figure 4.21: **N-S Circumferential Stresses on Jacket of Column 6 (Retrofit, With Laps)**

the top and bottom of the jacket. Figure 4.21(b) shows a circumferential tension at the toe of the jacket larger than the yield strength of the jacket which was 54 ksi. This was not a result of strain-hardening, but was due to the large vertical tensile strain measured near the toe and the elliptical nature of Von Mises yield criterion used for stress-strain conversion (see Figure B.2 in Appendix B). Note that, compared to column 4, the circumferential stress distribution on the tension generator of the jacket of column 6 was more stable near the toe of the jacket.

4.3.1.3 Circumferential Strains - Column 5

Since only horizontal strain gages were installed on the jacket of column 5, the data will be presented in terms of measured strains. Figure 4.22(a) and (b) show the distributions of circumferential strains on the north and south generators of the jacket for column 5 during the push cycle. Note that the top strain gage was not installed on the south generator of the jacket and the vertical scale on Figure 4.22(b) has been enlarged to cover only half of the jacket. At $\mu = 1$, circumferential strains are less than 100×10^{-6} at all locations, but there is a substantial increase in strains between $\mu = 1$ and $\mu = 2$, particularly on the compression generator. A relative large increase of circumferential strain was also noted on both generators of the jacket from displacement ductility factor of $\mu = 4$ to 6. The magnitude of circumferential strains was about twice as large on the compression generator as on the tension generator. This is of course associated with the larger lateral dilation of concrete in compression. On the north generator, only the lower half of the jacket showed any significant residual circumferential strains. The south generator showed circumferential strains as high as 1900×10^{-6} occurring near the toe of the jacket at $\mu = 6$, indicating that

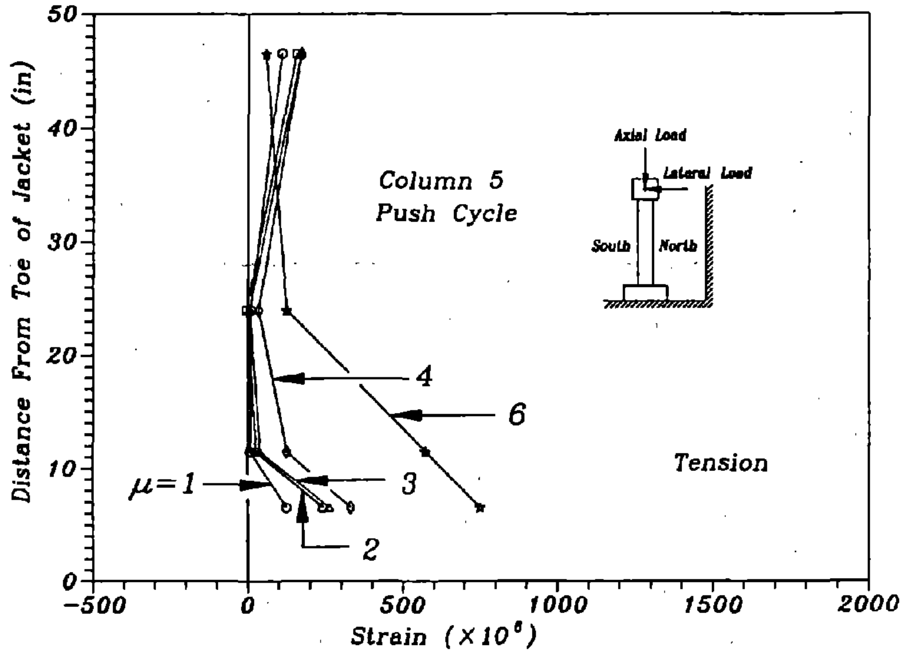

(a) Tension Generator (North)

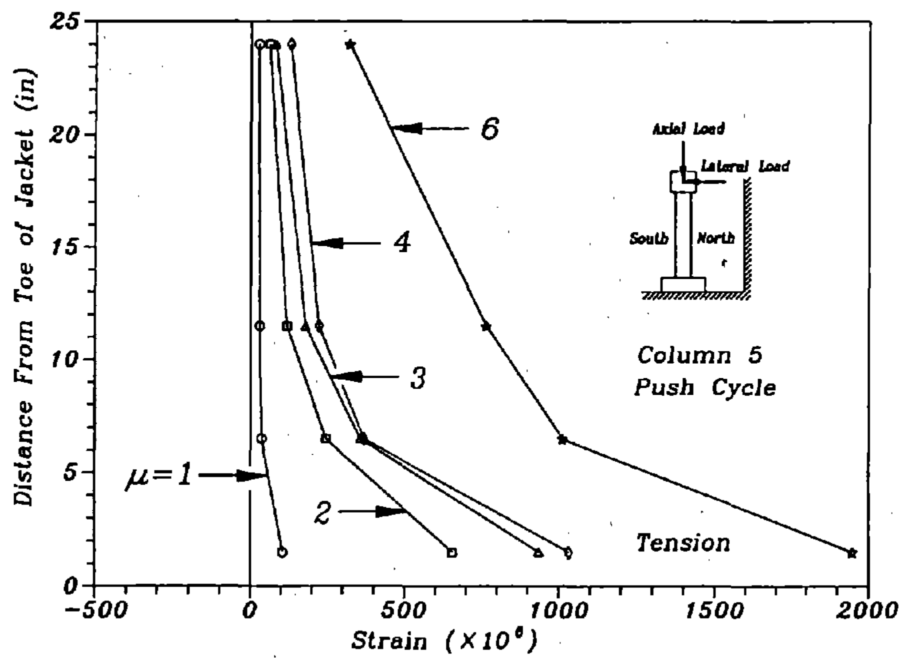

(b) Compression Generator (South)

Figure 4.22: **N-S Circumferential Strains on Jacket of Column 5 (Partial Retrofit)**

the jacket was functioning as intended to contain the failing lap-splices.

4.3.2 East-West Generators (Shear Strains)

The circumferential strains on the east and west generators of the jacket for column 2 are shown in Figure 4.23(a) and (b). These locations are subjected to the circumferential stresses due to shear forces as well as the restraint due to confinement of the compression zone by the jacket. Both directions of lateral loading were included in the plot. Similar distribution of circumferential strains were noted for the east and west generators. The largest circumferential strains occurred at the toe of the jacket, with a magnitude of 500×10^{-6} being recorded at $\mu = 3$. The strain at the top of the jacket was about 75% of the strain recorded at the toe.

The circumferential strain distributions on the east and west generators of the jacket for column 4 are shown in Figure 4.24(a) and (b). Tensile strains occurred over the entire length of jacket except at mid-height of the west generator where a very small initial compressive strain was measured at $\mu = 1$, possibly due to thermal effects. In the toe region, the circumferential strain was about twice than that near the top of the jacket. The largest tensile strain was about 1000×10^{-6} i.e. ≈ 62 % of yield strain.

The jacket for column 6 exhibited similar distributions of circumferential strains to the other two retrofitted columns, as seen in Figure 4.25(a) and (b). There were, however, slightly larger circumferential strains near both ends of the jacket when compared to column 4. The magnitude of tensile strain near the toe was 1100×10^{-6}.

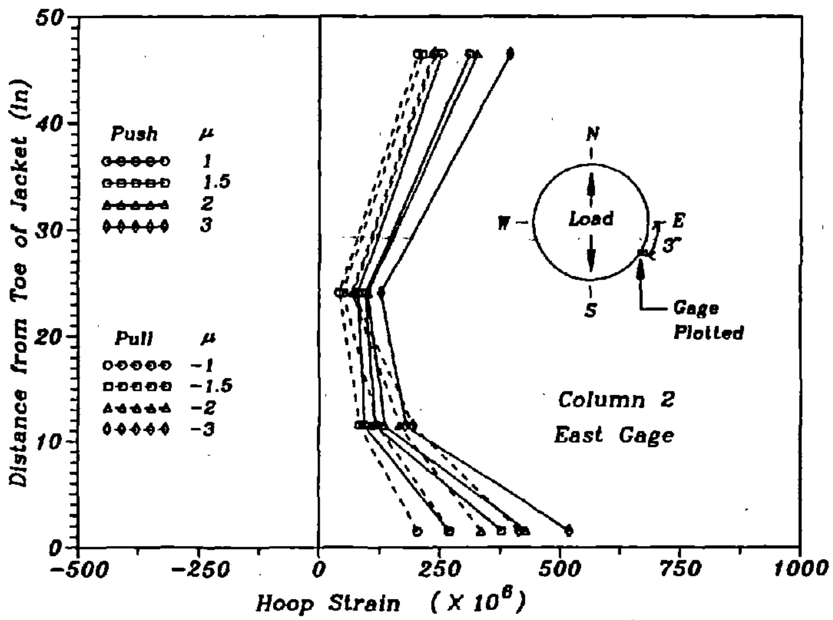

(a) East Generator

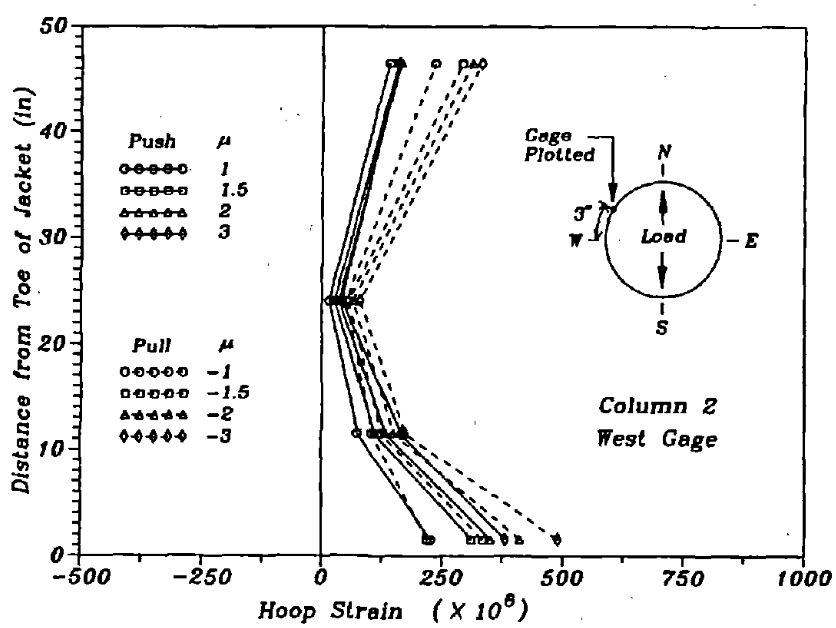

(b) West Generator

Figure 4.23: E-W Circumferential Strains on Jacket of Column 2 (Retrofit, With Laps)

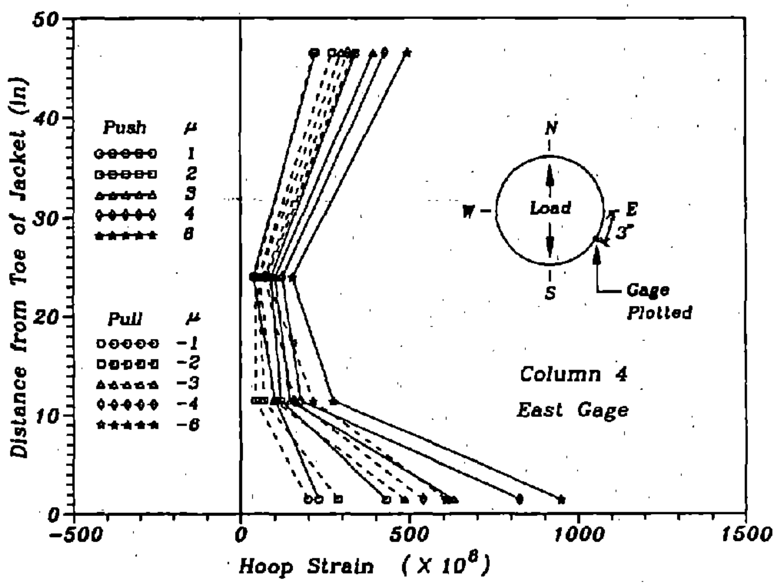

(a) East Generator

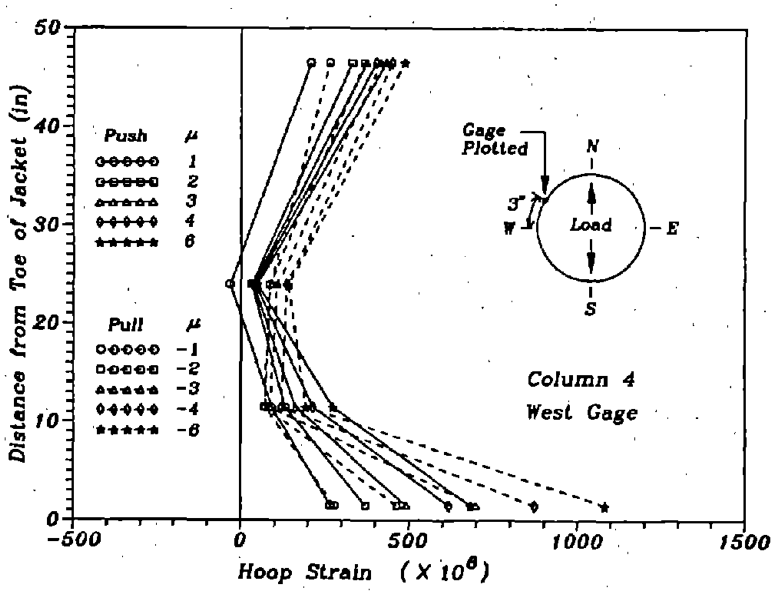

(b) West Generator

Figure 4.24: **E-W Circumferential Strains on Jacket of Column 4 (Retrofit, No Laps)**

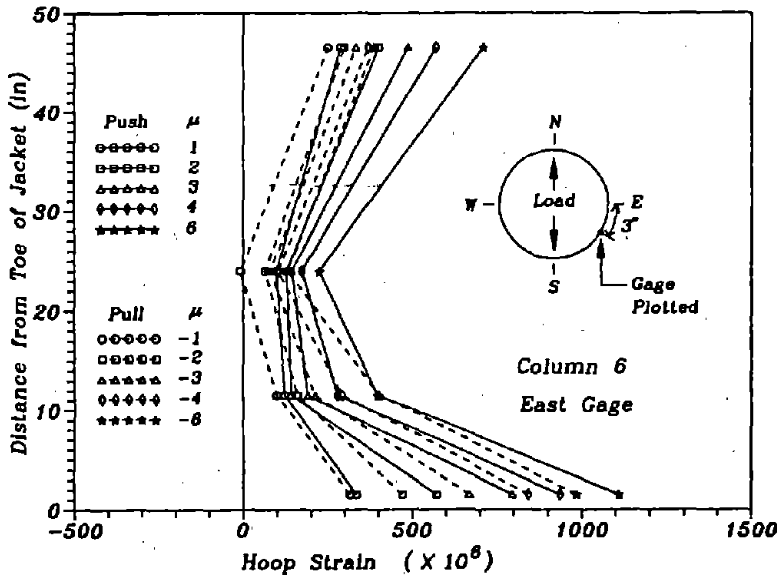

(a) East Generator

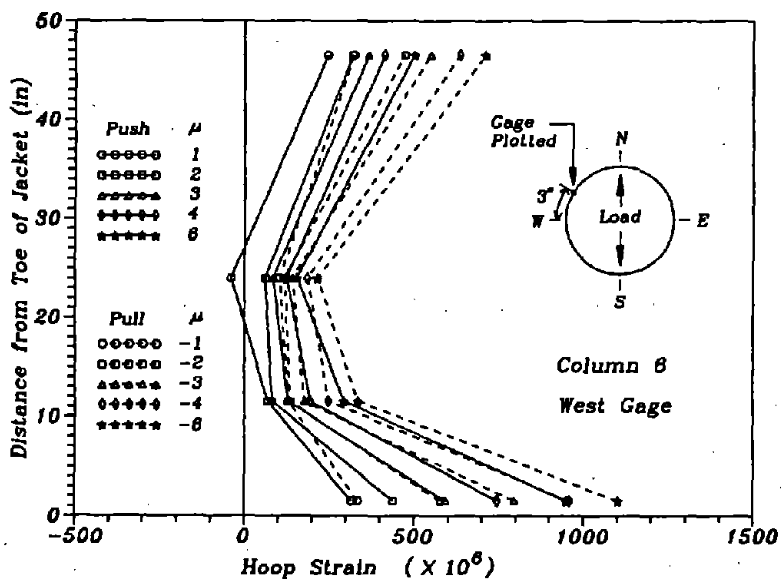

(b) West Generator

Figure 4.25: E-W Circumferential Strains on Jacket of Column 6 (Retrofit, With Laps)

4.4 Longitudinal Bar Strains

4.4.1 Starter Bar Strains Versus Displacements

Figure 4.26 and 4.27 show the variation of extreme starter bar strains with column lateral displacements and the yield strain indicated as ϵ_y for reference. A proportional increase of strain was observed for displacement less than 0.8 inch. Early bond failure at the lap-splice region resulted in smaller strains being developed in the starter bars of the 'as-built' and partially retrofitted columns than in the full retrofit columns, even for displacement less than $\mu = 1$. Column 1 showed the starter bar strain reaching yield at a displacement of 1.3 inches, while the peak strain in column 5 was only 80% of the yield strain. In contrast, the fully jacketed columns (column 2 and 6) exhibited a very rapid increase in strain at $\mu = 1$. Significant residual tensile strain was noted in column 6 after the initial excursion beyond yield in the push direction.

Note that in Figure 4.26(a) and (b), column 5 shows a change in the strain of the north starter bars from compressive to tensile as displacements were increased in the pull direction, even though no yield excursion was evident during the entire load history. The anomaly may be attributed to local bending of the starter bar in the compression zone as a result of large local curvature at the column base. Strain gages were installed on the starter bars facing inward, and in spite of overall compression in the bar, tension was developed by local bending on the strain gage face. In the tension zone, however, the starter bars were subjected to less severe bending as a result of wide base crack and the neutral axis depth being closer to the compression zone. Similar, though less dramatic behavior is exhibited by the column 1 starter bar in Figure 4.27. Note that the

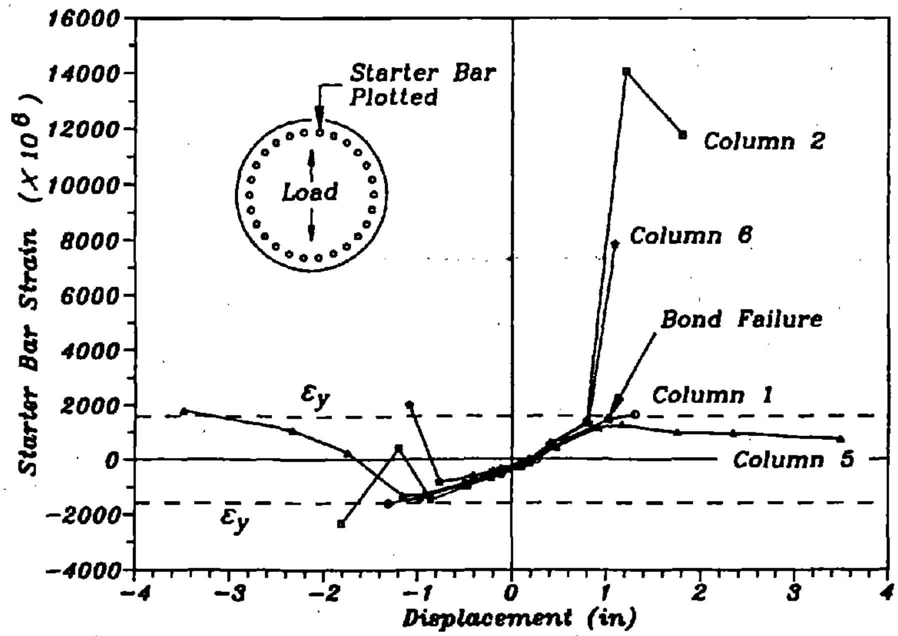

(a) Right Starter Bar

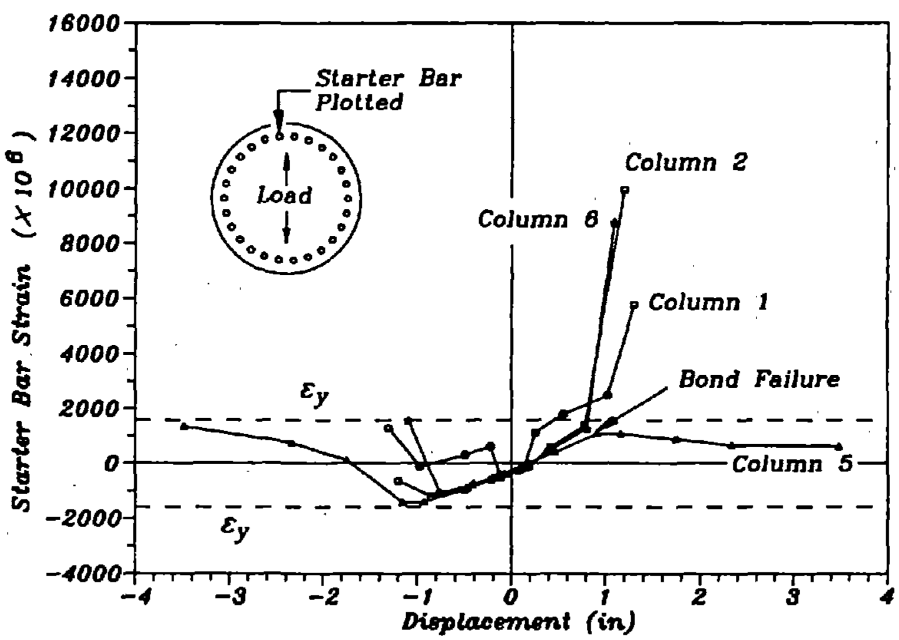

(b) Left Starter Bar

Figure 4.26: North Starter Bar Strain Versus Displacement

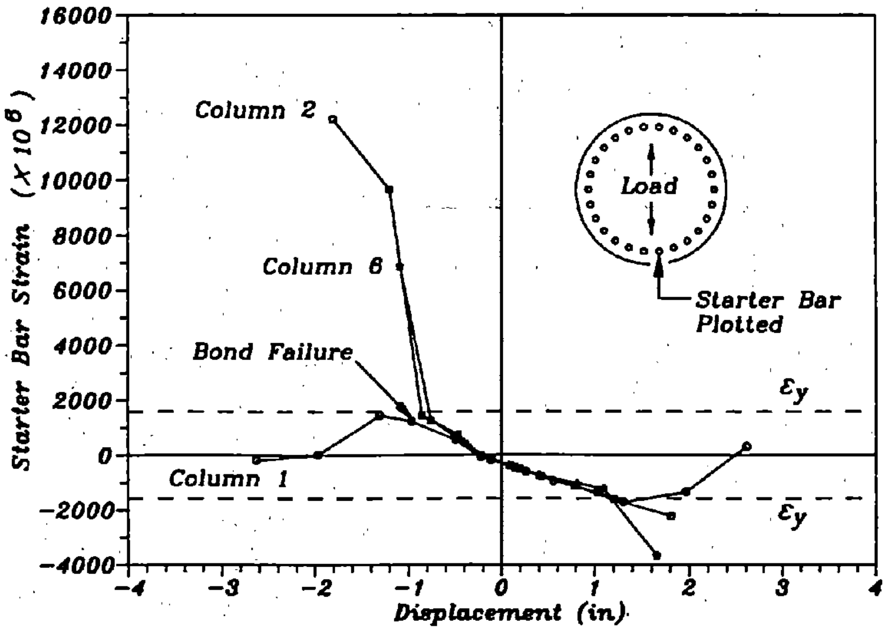

(a) Right Starter Bar

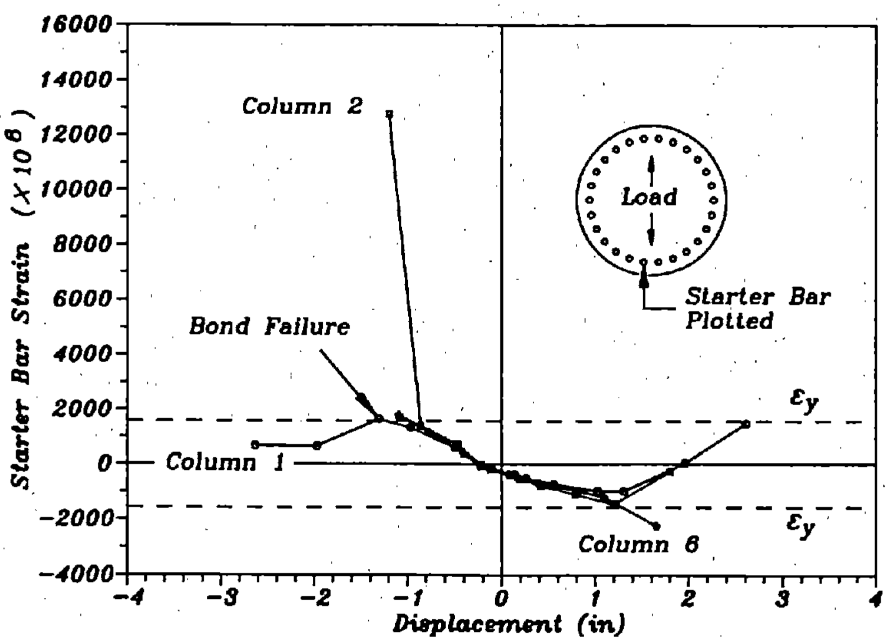

(b) Left Starter Bar

Figure 4.27: South Starter Bar Strain Versus Displacement

envelope for column 5 showed a more gradual degradation after $\mu = 1$ than column 1.

4.4.2 Strain Profiles

4.4.2.1 Column 1 - 'As-built', With Laps

Figure 4.28(a) and (b) show the strain profiles of the sections as measured by the strain gages at the base of the column and at top of the lap, respectively. Near-linear strain profiles were apparent in Figure 4.28(a) at low levels response, up to a displacement ductility factor of $\mu = 1$. Strains exceeding yield was noted in six of the outer most bars on the tension side at $\mu = 1$. The neutral axis depth was about 10 inches at $\mu = 1.5$. Tensile strains due to local bending of starter bars, discussed above, was evident in the compressive zone at $\mu = 2$,.

The strain profiles at the end of the laps showed smaller slopes, as expected, since the section was subjected to a smaller bending moment. The near linear strain profiles are also apparent at low ductilities. Note that substantial compressive strains of $\approx 3000 \times 10^{-6}$ were registered by the extreme compressive steel at $\mu = 1.5$, and may be a result of local bending in the bars.

4.4.2.2 Column 3 - 'As-built', No Laps

The strain profiles at the base section and at 12.5 inches from the base of column 3 are shown in Figure 4.29(a) and (b) which have been plotted with a larger vertical scale. The linearity of the strain profiles at low ductilities is more distinct than with column 1. A large increase in the curvature at the base section, as signified by the slope of the strain profile, occurred between displacement ductility factors of $\mu = 1$ and 1.5. Substantial tension yielding up

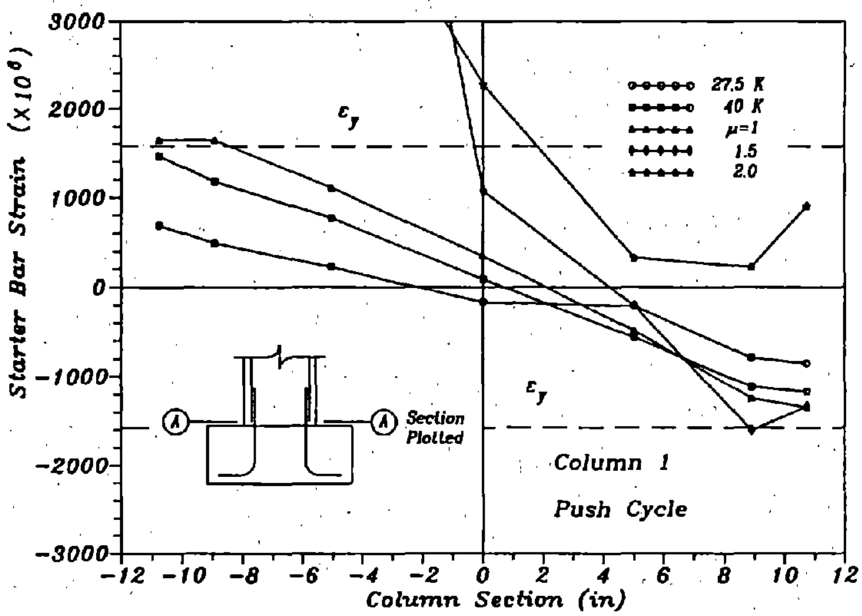

(a) At Base of Column

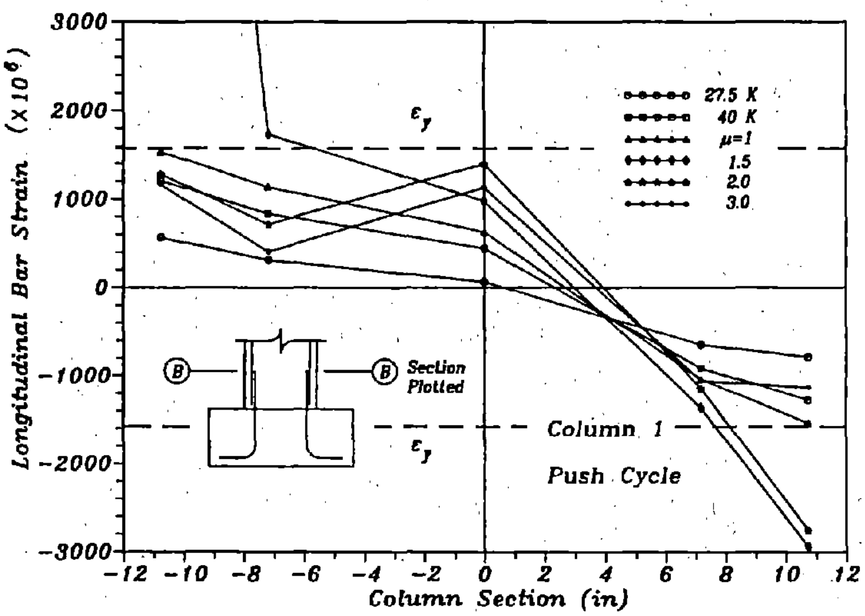

(b) At Top of Lap-Splice

Figure 4.28: **Strain Profiles in Column 1 ('As-built', With Laps)**

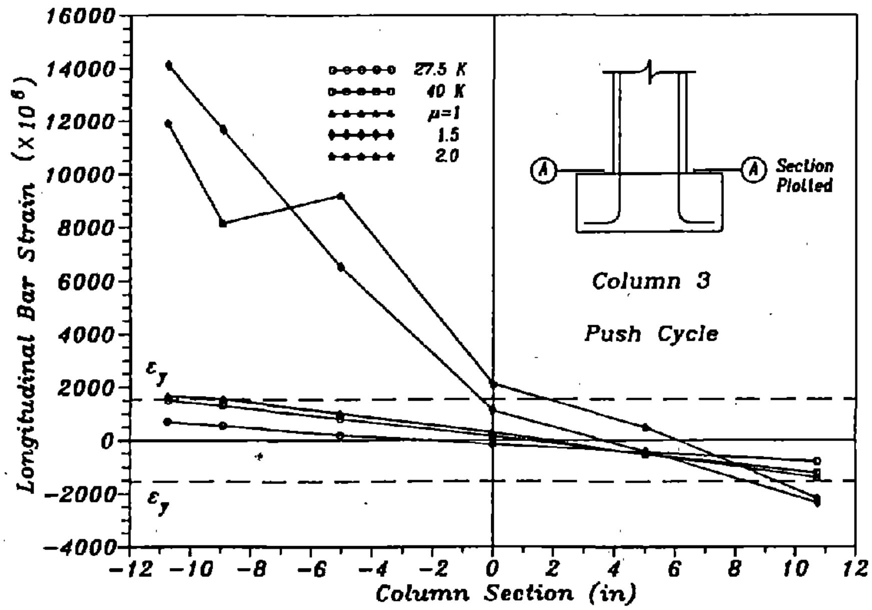

(a) At Base of Column

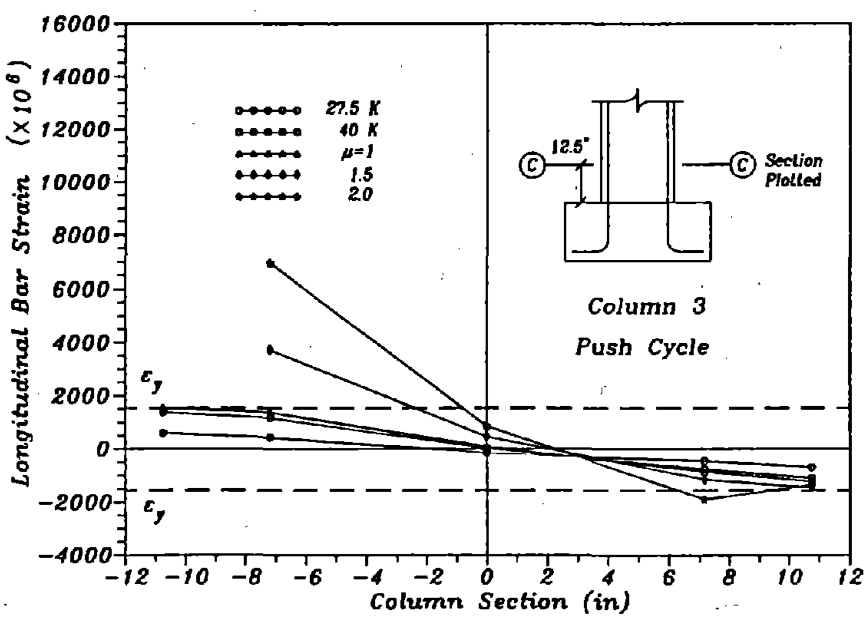

(b) At 12.5 inches above Column Base

Figure 4.29: **Strain Profiles in Column 3 ('As-built, No Laps)**

to a strain of 14000×10^{-6} was observed at $\mu = 1.5$. There was also noticeable yielding in the extreme compressive steel. At ductilities greater than $\mu = 2$, the extreme fiber strains exceeded the range of the data acquisition system.

4.4.2.3 Column 6 - Retrofit, No Laps

The strain profiles at the base of the column and above the steel jacket for column 6 are shown in Figure 4.30(a) and (b). At the base of the column, tensile strains as high as 8000×10^{-6} were measured in extreme tension steel at the early stage of $\mu = 1$. The increase in section curvature from $\mu = 1$ to 1.5 was also more rapid than the previous 'as-built' columns. The observation is consistent with the increased curvature measured by the linear potentiometers, discussed in Section 4.2. Extreme tension reinforcement strains were beyond the operating range of the data acquisition system for $\mu \geq 2$.

Figure 4.30(b) shows smaller strains above the steel jacket. The extreme tension steel however exceeded the yield strain at $\mu = 1.5$. First yielding of extreme compressive steel was evident at $\mu = 2$. Compared to the base section, the strain profile above the jacket showed a more gradual increase in slope. There was however substantial spread of yielding across the section at $\mu = 6$. The strain profiles indicate that compression strains at the extreme compression fiber of the concrete were always less than the crushing strain of the concrete, taken to be 5000×10^{-6}.

4.4.2.4 Column 4 - Retrofit, No Laps

The strain profiles at the base of column 4 are shown in Figure 4.31(a). Unlike column 6 which showed large tensile strain in the extreme tension steel at

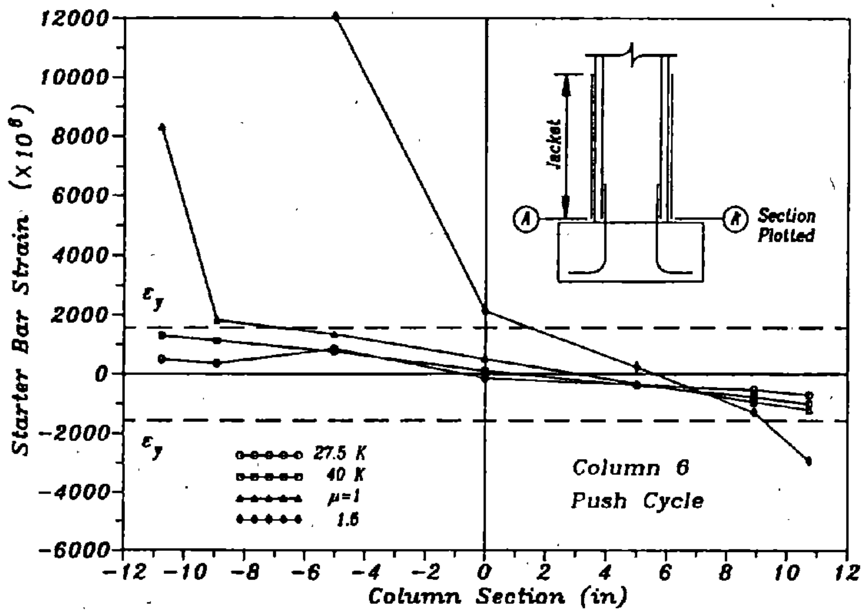

(a) At Base of Column

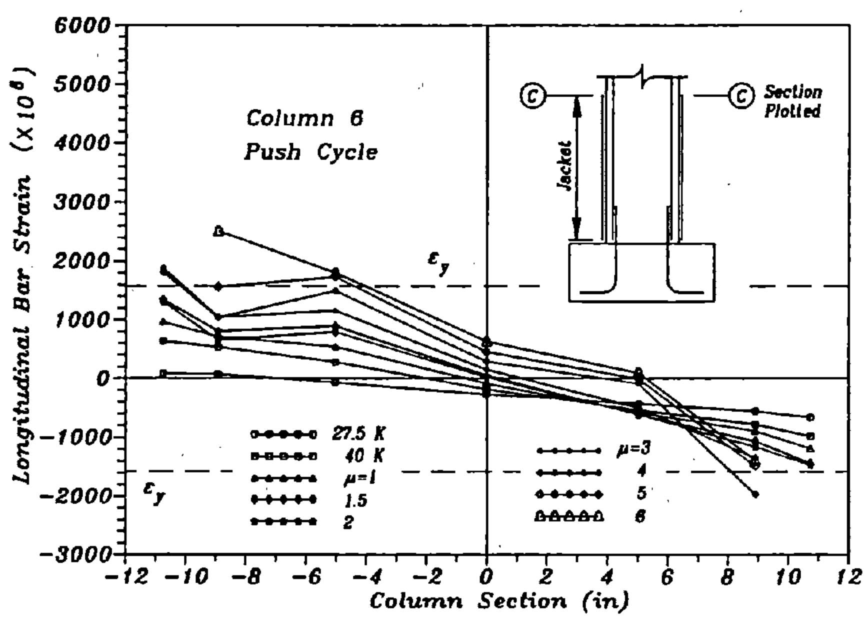

(b) Above the Steel Jacket

Figure 4.30: Strain Profiles in Column 6 (Retrofit, With Laps)

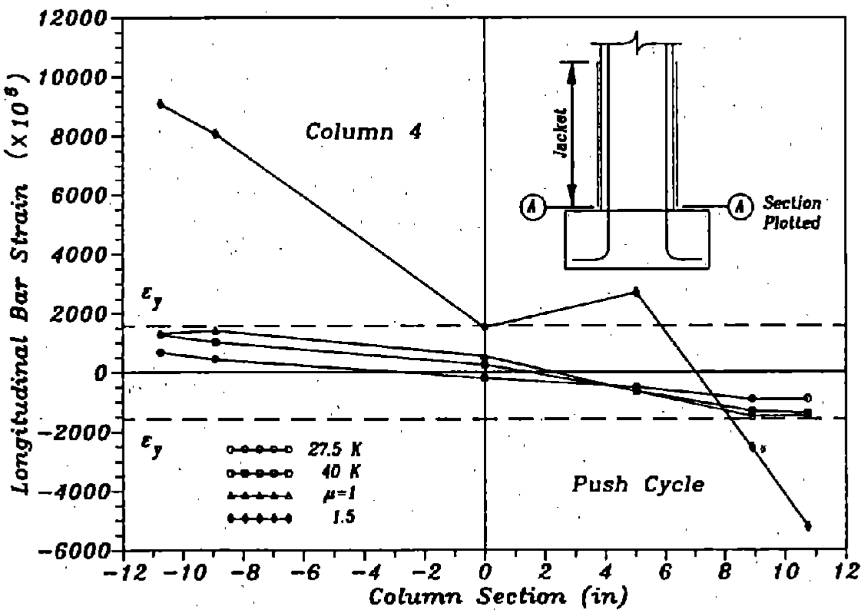

(a) At Base of Column

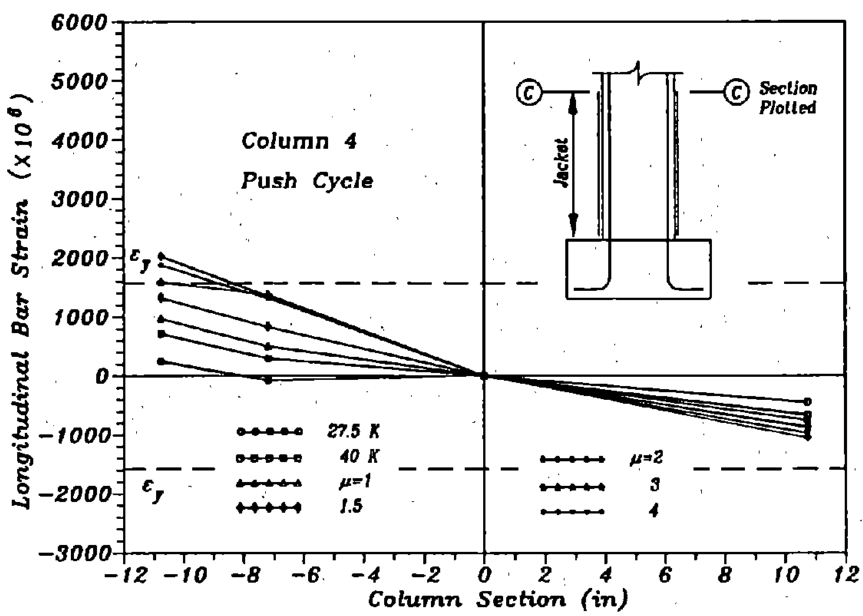

(b) Above the Steel Jacket

Figure 4.31: Strain Profiles in Column 4 (Retrofit, No Laps)

the early stage of $\mu = 1$, this behavior was delayed for column 4 until $\mu = 1.5$. This may be attributed to the increase in curvature at the base section due to stiffening effect of the lap-splices in the longitudinal steel in column 6. Even though strains exceeding 8000×10^{-6} were noted in the tension steel at $\mu = 1.5$, these values are smaller than strains recorded for column 6 at the same ductility factor.

Strain profiles above the jacket of column 4 are shown in Figure 4.31(b). The profiles were similar to those of column 6. Yielding in the extreme tension reinforcement is noted at $\mu \geq 2$. The strain gages in the compression zone for the push cycle failed during construction of the column, except in the extreme location. Also the reliability of the strain gage at mid-section of the column which showed values within $\pm 10 \times 10^{-6}$ throughout the entire test is doubtful. Moment-curvature analysis had indicated a neutral axis depth of about 8 inches or less (see Section 5.5), which does not agree with the measured strains.

4.4.3 Strain Penetration in Footing

The starter bars of column 6 were instrumented with strain gages to determine the extent of strain penetration into the footing. Figure 4.32(a) and (b) show the distributions of starter bar strains in the footing for the extreme north and south starter bars. For the north starter bar in Figure 4.32(a), strains decreases linearly with depth at lateral forces of 27.5 and 40 kips. The distribution at $\mu = 1$, however, showed deviation from a linear profile due to large yielding strain developing on top of the footing. For the south starter bar, linear distributions were noted up to $\mu = 1$, as shown in Figure 4.32(b). Both the north and south starter bars show strains near yielding in tension at depth of 5 inches at $\mu = 2$

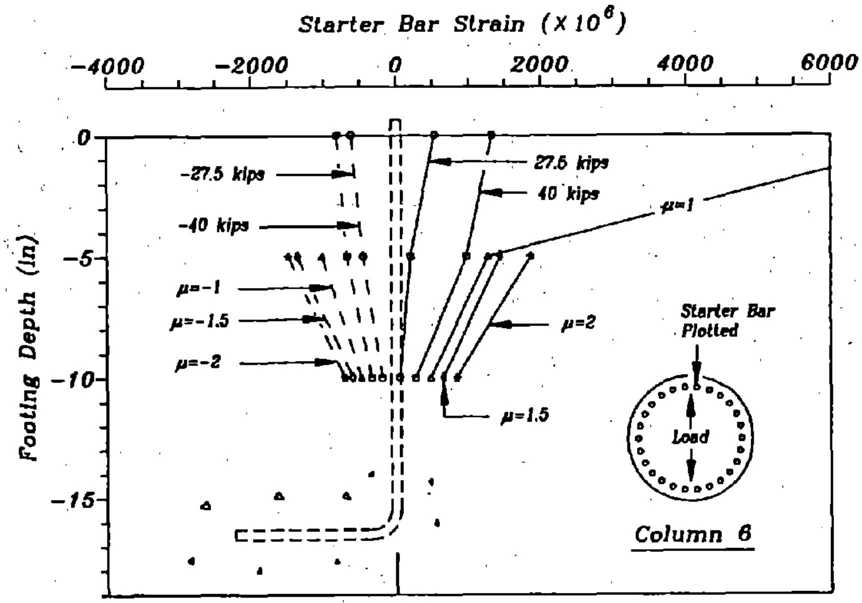

(a) North Starter Bar

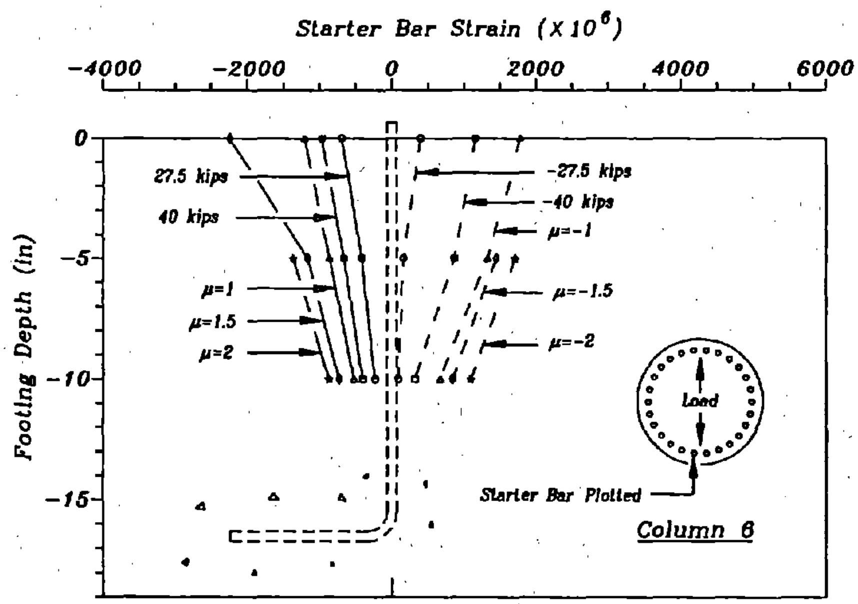

(b) South Starter Bar

Figure 4.32: **Strain Penetration into Footing of Column 6**

and these strains decreased to below 850×10^{-6} at depth of 10 inches. The strain gage at the depth of 5 inches was lost after $\mu = 2$, and subsequent starter bar strains at 10 inches depth were not plotted.

The slopes of the starter bar strains, when multiplied by $E_s A_b / \Sigma_{bar}$, where E_s = elastic modulus for the reinforcing bar, A_b and Σ_{bar} = cross-sectional area and perimeter of the reinforcing bar respectively, gives an estimation of the bond stresses in the bar. In this case, $A_b = 0.44$ in^2 and $\Sigma_{bar} = 2.36$ inches for #6 bar, and $E_s = 28.7 \times 10^6$ psi (Appendix A for steel properties); thus a multiplication factor of 5.35×10^6 psi.in is appropriate. For instance, the bond stress for the north starter bar, which shows a best-fit slope of 110×10^{-6}/in at a lateral force of 40 kips, is $110 \times 5.35 = 589$ psi or $\approx 8\sqrt{f'_{co}}$ where $f'_{co} = 5425$psi for column 6 (see Table A.1 in Appendix A). Table 4.2 summarizes the bond stresses for the north and south starter bars in tension and compression. It can be seen that the bond stresses, which reflect strain dissipation in the starter bars, increases with the lateral displacements of the column, and are larger for tension strains than for compression strains. The strain profiles indicated maximum bond stress of about $15\sqrt{f'_{co}}$ in tension. Note that the basic development length for reinforcing bar, as required by the ACI 318 Code [38], implies a bond strength of $10.7\sqrt{f'_{co}}$ for #6 bars.

4.5 Hoop Reinforcement Strains

Strain gages were installed on the hoop reinforcement in the four principal directions; the gages at the north and south generators were intended to monitor the confining effect of the hoops, while the gages on the east and west generators of the hoops were to monitor shear influences. Note that different scales have been

Table 4.2: **Bond Stresses for Starter Bars in Footing**

Load	North Starter	South Starter
27.5 kips	268 psi	-246 psi
-27.5 kips	-230 psi	182 psi
40 kips	589 psi	-305 psi
-40 kips	-273 psi	460 psi
$\mu = 1$	851 psi	-369 psi
$\mu = -1$	-589 psi	605 psi
$\mu = 1.5$	963 psi	-451 psi
$\mu = -1.5$	-856 psi	675 psi
$\mu = 2$	1116 psi	-506 psi
$\mu = -2$	-856 psi	675 psi

used for the retrofitted and 'as-built' columns; and positive μ denotes the push direction of loading, while negative μ denotes the pull direction of loading. It should also be noted that, for the push cycle, the north generator corresponded to the longitudinal tension face of the column, while the south generator corresponded to the longitudinal compression face of the column, and vice-versa.

4.5.1 North-South Generators

4.5.1.1 Columns with Lapped Starter Bars

(a) Column 1 'As-Built'

Figure 4.33(a) shows the hoop reinforcement strains measured at different height on the north generator of the hoop reinforcement in column 1. A dramatic increase of tensile strains occurred in the second hoop between displacement ductility factors of $\mu = 1.5$ and 2. The tensile strains were larger in the push than in the pull direction at $\mu = 2$, even though the north generator had corresponded to the tension side of the column in the push direction, indicating that the strains

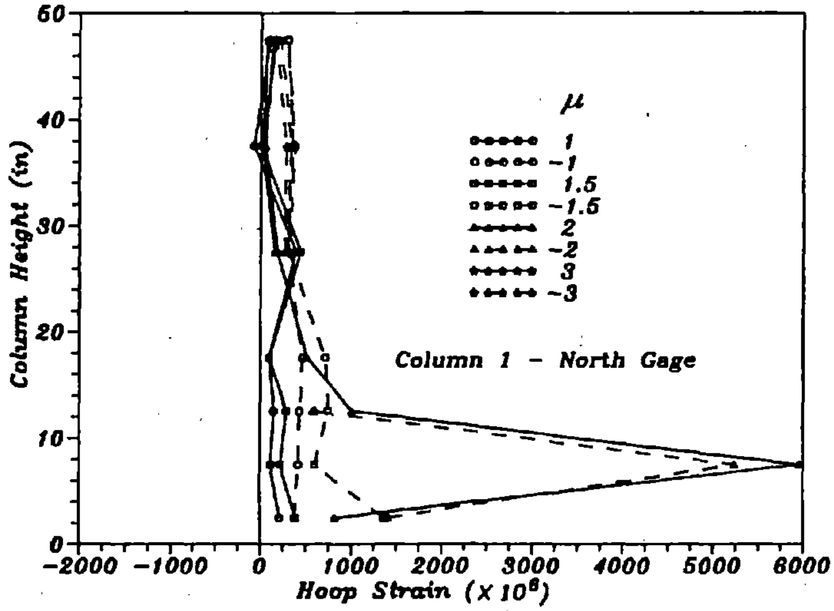

(a) North Generator

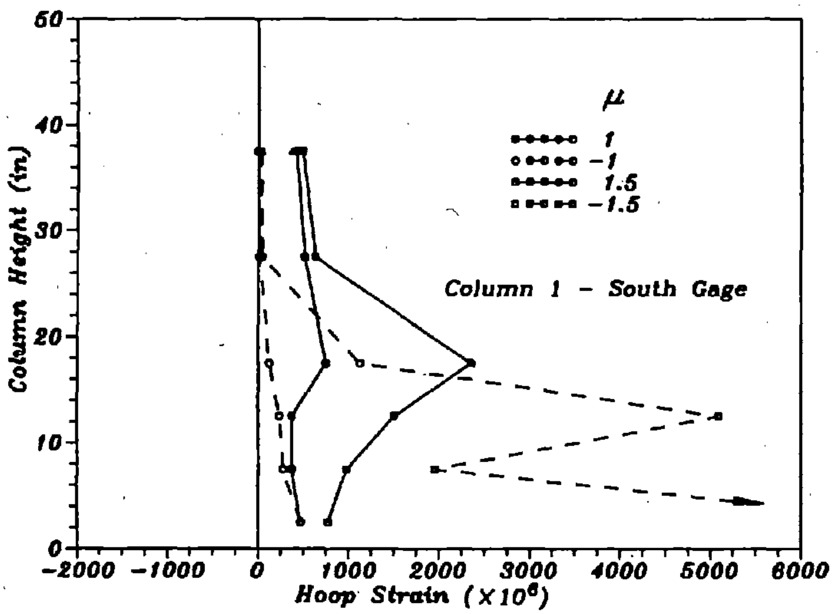

(b) South Generator

Figure 4.33: N-S Hoop Reinforcement Strains - Column 1 'As-Built'

were associated with the bond failure at the tension laps. A tensile strain as high as 6000×10^{-6} was recorded in the second hoop at $\mu = 2$ in the push direction. The first hoop showed a smaller strain of 1500×10^{-6}, due to restraint by the footing. The third hoop, being close to the end of the lap-splice, was less affected by the bond failure and hence exhibited smaller tensile strain. It is of interest to note that the hoop at level 2 was capable of sustaining strains considerably in excess of yield, despite the ends being lapped in the cover concrete. As noted earlier in Section 4.1.1, the second hoop fractured during the second pull cycle to $\mu = 4$.

The hoop reinforcement strains on the south generator of column 1 is shown in Figure 4.33(b). The strain gages on the 9^{th} and 10^{th} hoops were damaged during construction of the column and the strain gages on the bottom four hoops on the south generator were not operational after $\mu = 1.5$. Despite the loss of data, a near uniform distribution of hoop reinforcement strains was evident at $\mu = 1$. There was, however, a significant increase in hoop reinforcement strains between $\mu = 1$ and 1.5. Unlike the north generator, the third hoop registered a larger increase in strains than the second hoop. Up to the stage of $\mu = 1$, the recorded strains were larger in the push than in the pull direction for all the hoops as a result of lateral expansion of the concrete compression zone. At $\mu = 1.5$, however, the hoop reinforcement strains became reversed and were larger in the pull direction for the bottom three hoops, primarily due to the dilation associated with splitting cracks generated by bond failure at the lap-splices.

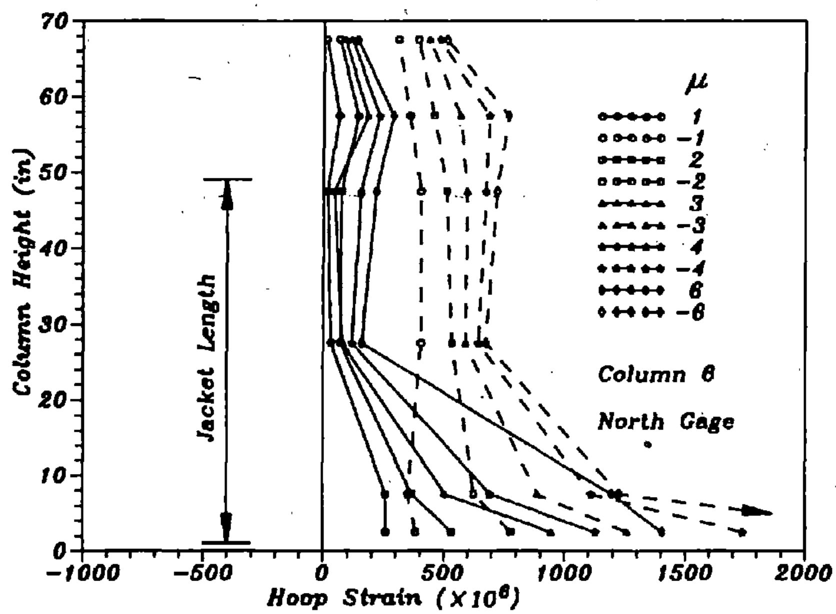

(a) North Generator

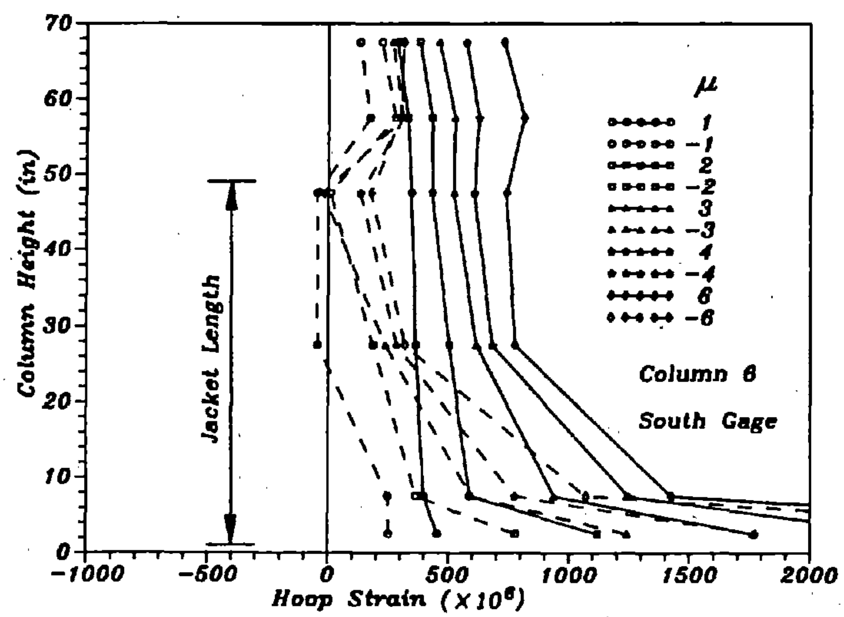

(b) South Generator

Figure 4.34: N-S Hoop Reinforcement Strains - Column 6 'Retrofitted'

(b). Column 6 'Retrofitted'

The hoop reinforcement strains on the north generator of column 6 is shown in Figures 4.34(a). Unlike column 1, the tensile strains were larger in the pull than in the push direction primarily due to confinement action of the jacket. Since there was no bond failure at the lap-splices, the tensile strains in the hoops were caused by the lateral dilation of concrete in compression. Even though not apparent in the enlarged scale for the retrofitted column, the presence of the steel jacket significantly reduced the magnitude of the hoop tension. For example, at $\mu = 2$, the second hoop showed a tensile strain of only 10% of that measured in column 1. All instrumented hoops indicated strains below yield for displacement ductility factor up to $\mu = 6$, except for the first hoop which was located at 2.5 inches above the footing. As observed in Chapter 4, the progressive spalling of cover concrete on top of the footing and inside the jacket after $\mu = 5$ led to the buckling of longitudinal bars which induced larger tensile strains in the first hoop.

The hoop reinforcement strains on the south generator of column 6 are shown in Figure 4.34(b). The strains were very similar to that observed for the north generator except the magnitudes were reversed for the two directions of loading. All recorded hoop strains were below yield up to $\mu = 6$, except for the first hoop which showed first yielding at $\mu = 3$. The hoop strains immediately above the jacket were slightly larger than the hoop strains inside the jacket for $\mu \geq 3$ due to the termination of confinement by the steel jacket.

4.5.1.2 Columns with Continuous Reinforcement

(a) Column 3 'As-Built'

Figure 4.35(a) shows a relatively uniform distribution of hoop reinforcement strains on the north generator of column 3. Larger hoop reinforcement strains were recorded on the tension generator of the column. The hoop strains were however below yield at $\mu = 4$, indicating bond failures at the lap-splices of the hoop reinforcement, since cover spalling and longitudinal bar buckling were apparent at this stage. It must however be noted that the second hoop which was not instrumented, was able to sustain yield of the hoop bar until fracture at $\mu = 5$, as noted in Section 4.2.

Figure 4.35(b) shows larger hoop reinforcement strains being recorded on the south generator than on the north generator of column 3. The first hoop showed a tensile strain of 2900×10^{-6} at $\mu = 3$, compared to a hoop strain of 1500×10^{-6} being recorded on the north generator at $\mu = 4$ in the pull direction. The larger recorded strains seemed to suggest an earlier compression buckling of the longitudinal reinforcement on the south generator, and might be due to an unintentional eccentricity of the axial force on the column.

(b) Column 4 'Retrofitted'

The distribution of hoop strains on the north generator of column 4 is shown in Figure 4.36(a). The first hoop registered the largest strain on the north generator with a magnitude of about 900×10^{-6} and very small strains (less than 200×10^{-6}) were recorded for the hoop at mid-height of the steel jacket. The north generator corresponded to the longitudinal tension face of the column during the push cycle. In the pull direction of loading, however, large increase in

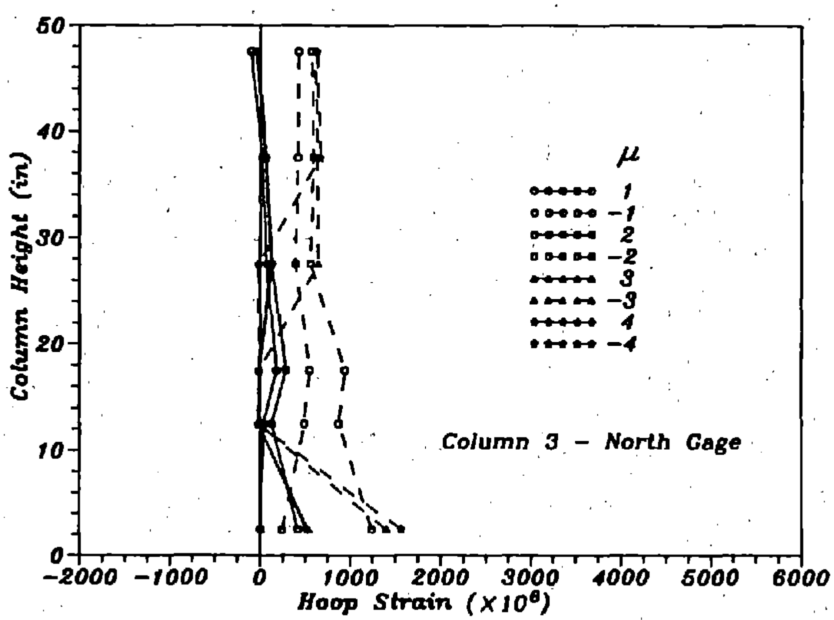

(a) North Generator

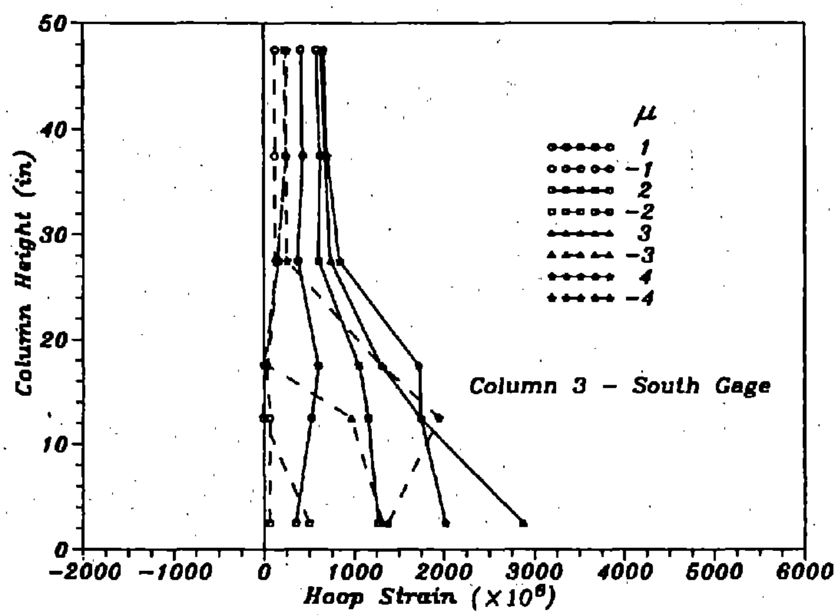

(b) South Generator

Figure 4.35: **N-S Hoop Reinforcement Strains - Column 3 'As-Built'**

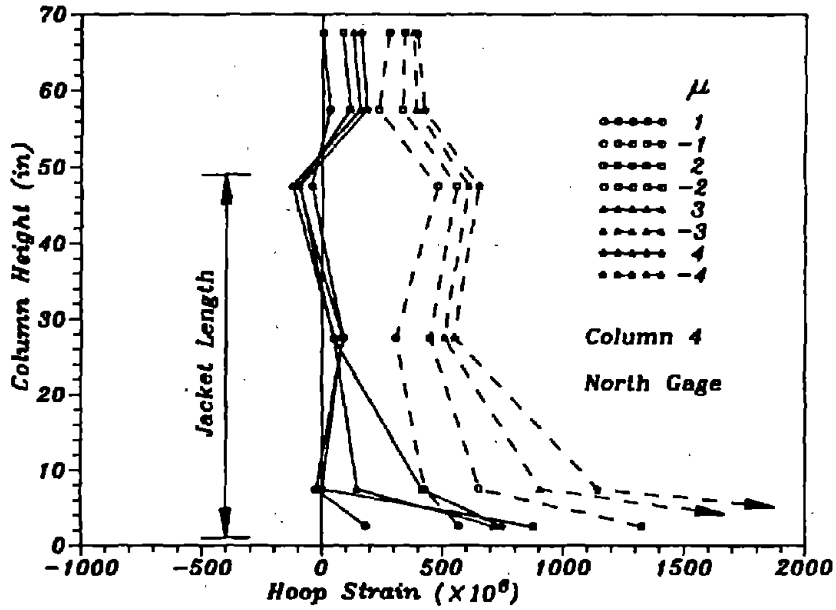

(a) North Generator

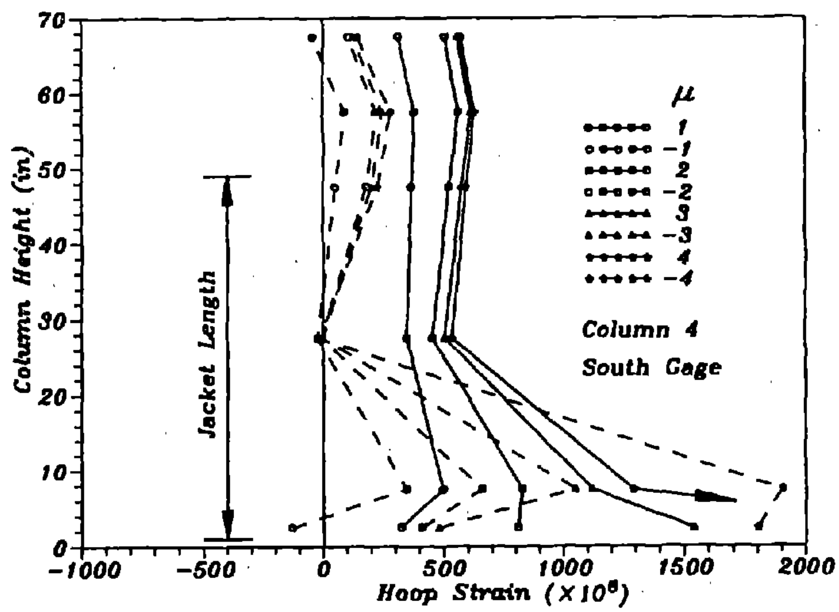

(b) South Generator

Figure 4.36: N-S Hoop Reinforcement Strains - Column 4 'Retrofitted'

the hoop reinforcement strains were recorded for the north generator. The first hoop, as a result of spalling of concrete inside the jacket near the toe, registered strains beyond yield of the hoop steel for $\mu \geq 3$. The hoop reinforcement strains at the mid-height of the jacket increased to about 550×10^{-6} at $\mu = 4$, primarily due to the lateral dilation of concrete in the compression zone. Note that the distribution of hoop reinforcement strains is similar to that of column 6 with about the same magnitude being noted at mid-height of the jacket (compare Figure 4.34(a) and Figure 4.36(a)).

The distribution of hoop reinforcement strains on the south generator of column 4 is shown Figure 4.36(b). The distribution of hoop reinforcement strains were similar to that on the north generator, except for a reverse in strain magnitude for the two directions of loading. Relatively large increase in the hoop reinforcement strains was observed for the south generator of the bottom two hoops. The largest tensile strain recorded was in the first hoop with first yielding occurred at $\mu = 3$ in the push direction of loading. Compared to column 6, the hoop reinforcement strains at mid-height of the jacket were slightly smaller for the same ductility factor. For instance, at $\mu = 4$, the hoop strain at mid-height of jacket for column 4 was about 550×10^{-6}, whereas the strain in column 6 was about 700×10^{-6}.

4.5.2 East-West Generators

4.5.2.1 Columns with Lapped Starter Bars

(a) Column 1 'As-Built'

Figure 4.37(a) shows the hoop reinforcement strains on the east generator of column 1. Significant tensile strains were recorded on the east generator in the bottom three hoops of column 1, as a result of bond failure at the lap-splice of the longitudinal reinforcement. The magnitude of tensile strains were however smaller than those measured on the north and south generators. For example, at $\mu = 2$, the largest tensile strain noted in the third hoop was 3800×10^{-6}, compared to 6000×10^{-6} on the north generator. The tensile strains in the third hoop on the east generator increased significantly to 5800×10^{-6} at $\mu = 3$. The first and second hoops, however, showed only half the magnitude measured by the third hoop. Negligible tensile strains were noted above the sixth hoop.

Figure 4.37(b) shows the hoop reinforcement strains on the west generator of column 1. A similar increase of the hoop reinforcement strains was noted between $\mu = 1$ and 1.5, indicating bond failure at the lap-splices of the longitudinal steel on the west generator as well. The largest strain recorded was in the third hoop, with magnitude 4500×10^{-6} at $\mu = 3$; slightly smaller than the magnitude recorded for the corresponding east generator. A compressive strain of about 500×10^{-6} was noted initially at $\mu = 1$ at the mid-height of jacket, possibly due to instability of the particular strain gage.

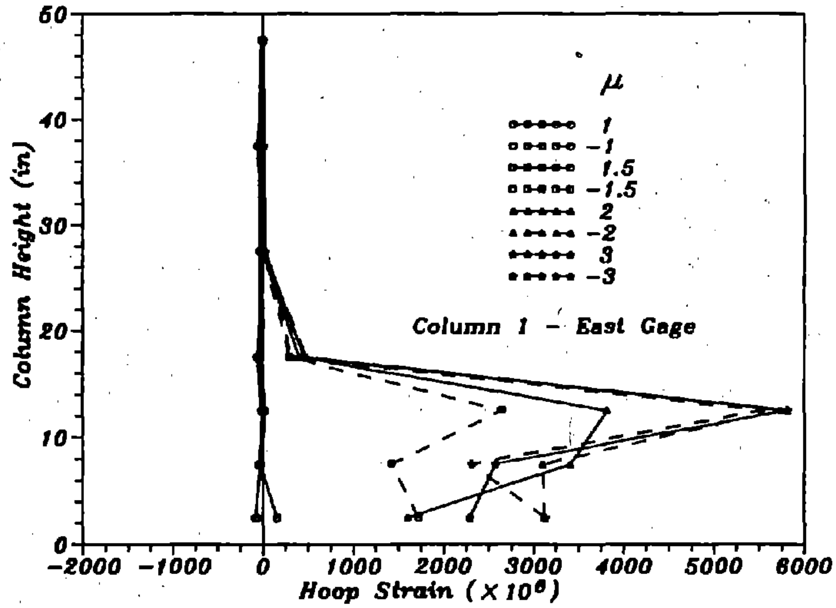

(a) East Generator

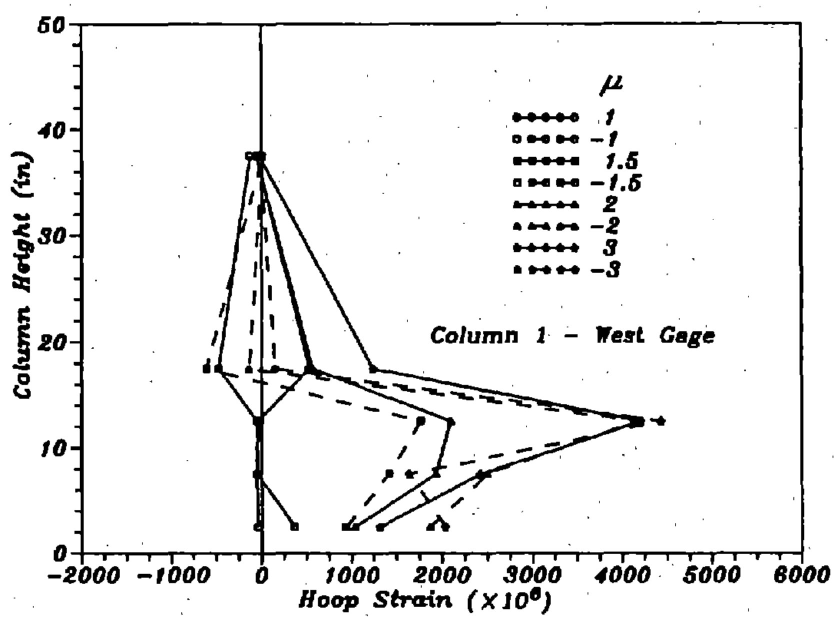

(b) West Generator

Figure 4.37: E-W Hoop Reinforcement Strains - Column 1 'As-Built'

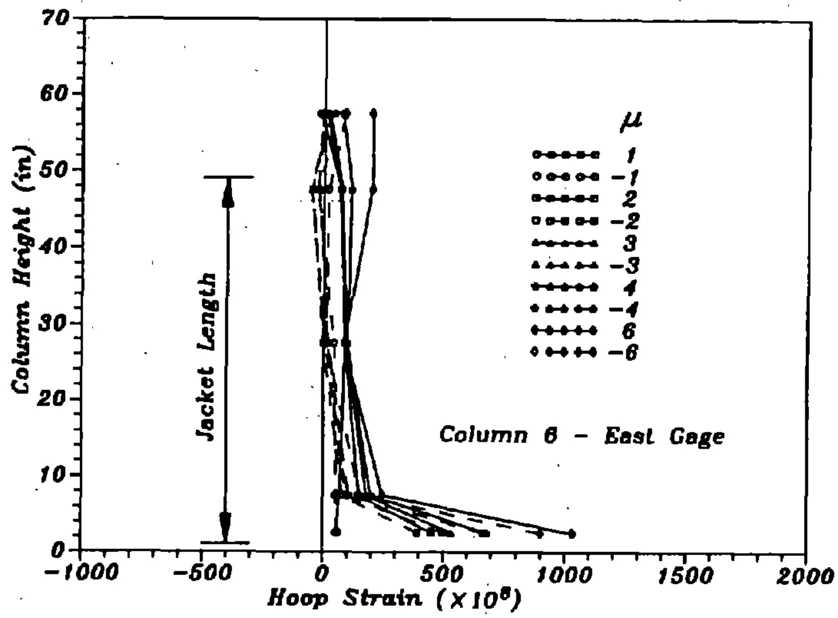

(a) East Generator

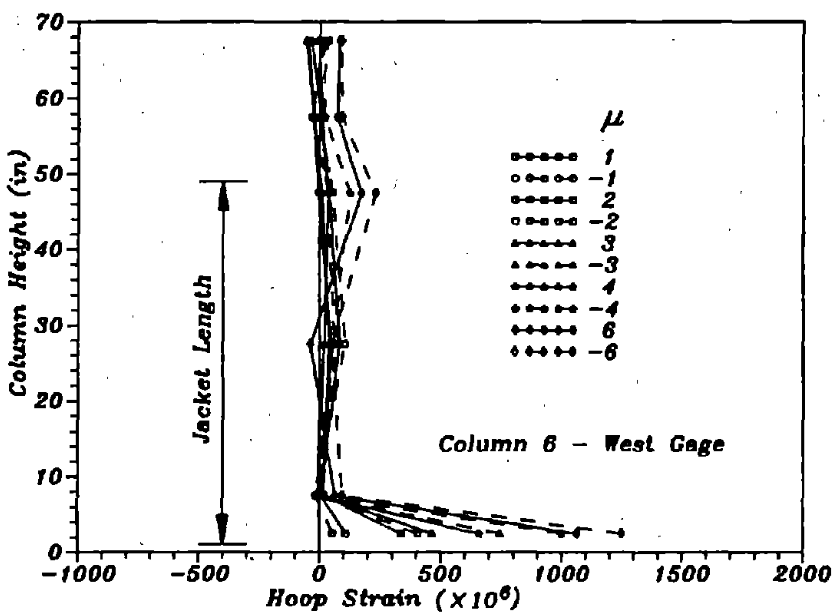

(b) West Generator

Figure 4.38: E-W Hoop Reinforcement Strains - Column 6 'Retrofitted'

(b) Column 6 'Retrofitted'

The hoop reinforcement strains on the east generator of column 6 are shown in Figure 4.38(a). Compare to those of 'as-built' column 1, a very effective suppression of reinforcement hoop strains by the steel jacket was evident, as can be seen by comparing Figure 4.37 and Figure 4.38. The largest hoop reinforcement strain recorded on the east generator of column 6 was 1050×10^{-6}, occurring in the first hoop at $\mu = 6$. The magnitude was below the yield strain of the hoop steel, and represented only 20% of the largest strain observed for the east generator of column 1.

The dramatic suppression of hoop reinforcement strains by the steel jacket was repeated on the west generator, as can be seen in Figure 4.38(b). The largest hoop reinforcement strain recorded on the west generator was 1250×10^{-6}; only slightly larger than those measured on the east generator.

4.5.2.2 Columns with Continuous Reinforcement

(a) Column 3 'As-Built'

The hoop reinforcement strains on the east generator of column 3 are shown in Figure 4.39(a). The strains were smaller than that on the corresponding generator of column 1, as can be seen by comparing Figure 4.39(a) with Figure 4.37(a). The third and fourth hoops were the only instrumented hoops on the east generator to show any significant strains. The largest strain recorded was 1100×10^{-6} occurring in the fourth hoop at $\mu = 4$, but was below yield of the hoop steel and was only 18% of the largest strain recorded on the same generator for column 1. Compression buckling of the longitudinal reinforcement at $\mu = 4$

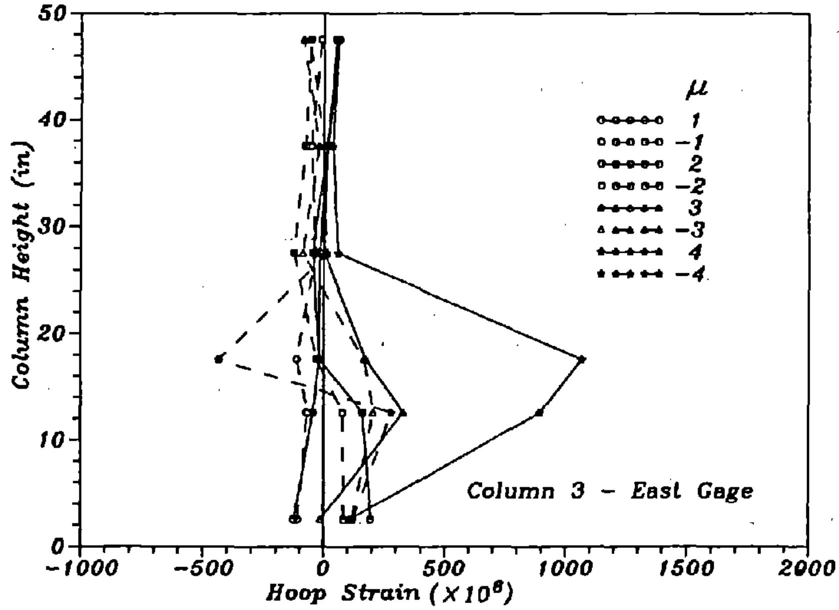

(a) East Generator

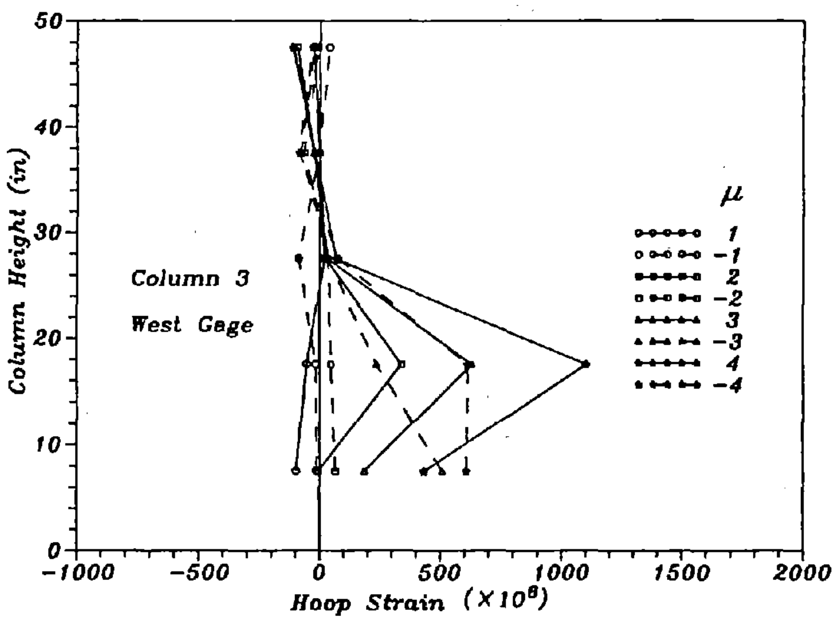

(b) West Generator

Figure 4.39: E-W Hoop Reinforcement Strains - Column 3 'As-Built'

induced significant tension in the hoops even on the east-west generators.

The distribution of hoop reinforcement strains recorded on the west generator of column 3 was similar to that on the east generator, as can be seen in Figure 4.39(b). The largest hoop reinforcement strain occurred in the fourth hoop, with about the same magnitude (1100×10^{-6}) as the east generator. The strain gage on the west generator of the first hoop was damaged during the construction of the test unit.

<u>(b) Column 4 'Retrofitted'</u>

The suppression of hoop reinforcement strains by the steel jacket was equally pronounced in column 4, as shown in Figure 4.40. The hoop reinforcement strains on the east and west generators of column 4 were slightly smaller than those on the corresponding generators of column 6, as can be seen by comparing Figure 4.38 and 4.40. The largest strain recorded on the east generator of column 4 occurred in the second hoop, with a magnitude of about 450×10^{-6}, whereas the largest strain for column 6 occurred in the first hoop with a magnitude of 1050×10^{-6}. On the west generator, the first and second hoops were the only hoops in column 4 to register any appreciable strains. The largest strain occurred in the second hoop with magnitude of about 850×10^{-6} at $\mu = 6$.

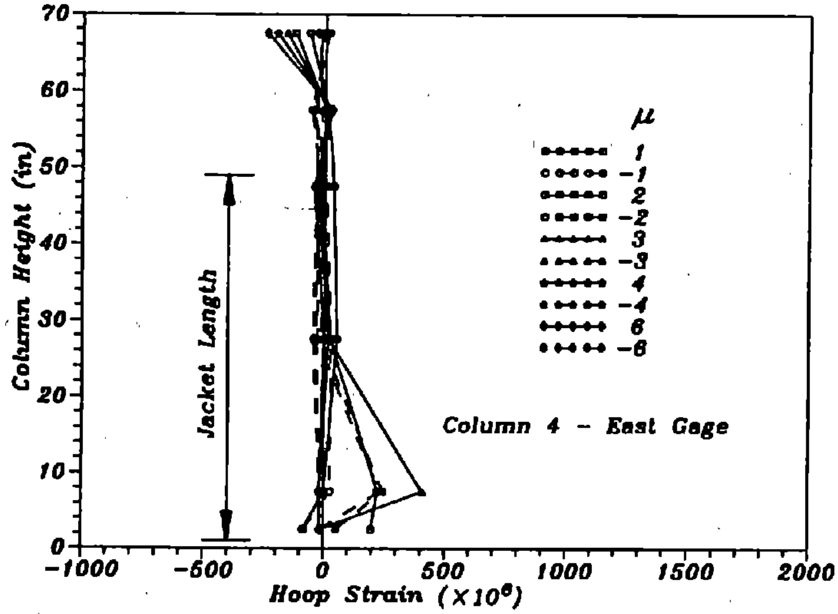

(a) East Generator

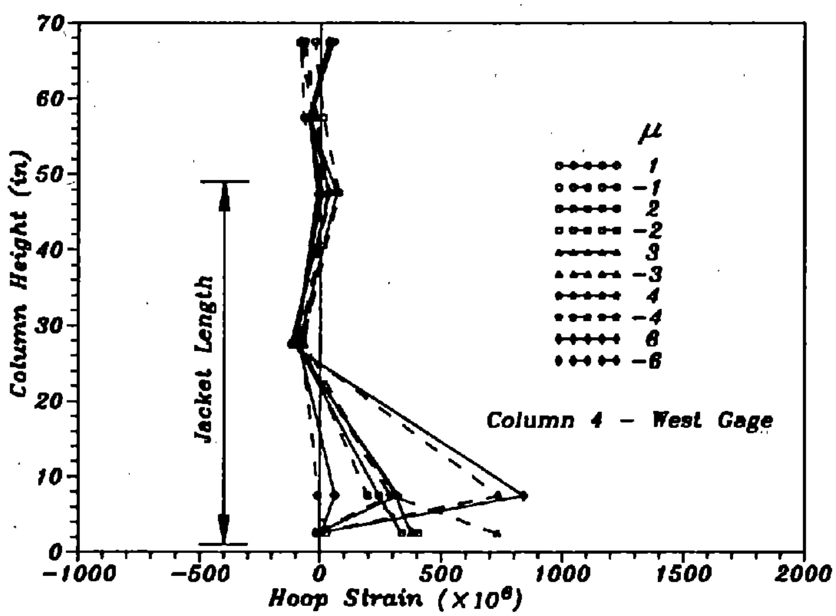

(b) West Generator

Figure 4.40: E-W Hoop Reinforcement Strains - Column 4 'Retrofitted'

Chapter 5

Discussion of Results

5.1 Summary of Results

A summary of the test results is presented in Table 5.1. Note that the parameter μ_f denotes the displacement ductility factor at failure of the column. The experimental yield displacement for repaired column 1-R was taken to be the same as in the initial test.

Table 5.1: **Test Results**

Col	Δ_y	V_i or V_p	Max Force	K^e_{col}	μ_f	Failure Mode
1	1.297"	52.0 kips	49.0 kips	40.1 kip/in	1.5	Bond Failure at Lap
2	1.200"	58.4 ..	58.5 ..	48.7 ..	3	Footing Failure
3	1.082"	49.3 ..	55.0 ..	45.6 ..	4	Confinement Failure
4	1.084"	55.9 ..	73.0 ..	51.6 ..	8	Low-Cycle Fatigue
5	1.160"	50.3 ..	46.0 ..	43.4 ..	1.5	Bond Failure at Lap
6	1.090"	55.4 ..	77.0 ..	50.8 ..	7	Low-Cycle Fatigue
1-R	1.297"	52.0 ..	54.0 ..	40.1 ..	3	Bond Failure at Lap

The largest yield displacement was for column 1 with $\Delta_y = 1.297$ inches. Two factors contributed to the relatively large yield displacement, namely, the additional lateral displacement as a result of incipient bond failure at the lap-splice, and compliance of the flexibly supported footing. The additional displacement from footing support on pile-blocks may be estimated from comparison of the yield displacements between column 1 and 5. The difference of concrete compressive strengths between these two columns must, however, be accounted for. It is assumed that the yield displacement, Δ_y, is inversely proportional to the elastic modulus of concrete, E_c, which in turn is assumed to be proportional to $\sqrt{f'_{co}}$. The yield displacement for column 5, if it were constructed with the same concrete as for column 1, would be 1.160" $\times \sqrt{5540/5094}$ = 1.209" (see Table A.1 in Appendix A for concrete compressive strengths). The difference between the yield displacement for column 1 and the adjusted yield displacement for column 5 i.e. 1.297" - 1.209" = 0.088" represented the additional displacement due to rotation of column 1 footing being supported on pile-blocks. The difference is equivalent to a footing rotation of 0.088"/(144"+9") = 5.75×10^{-4} radians. Figure 5.1 shows that a comparable footing rotation was measured for column 1. At $\mu = 1$, the measured rotations was 5.2×10^{-4} radians, averaged for the two load directions.

The lateral displacement contribution from bond failure may be estimated by comparing the yield displacements of column 1 with that of column 3 after accounting for the difference in concrete compressive strengths between the two columns and the additional displacement due to footing rotation. The yield displacement of column 3, after adjusting for the difference of concrete compressive strengths, is 1.082" $\times \sqrt{5540/4725}$ = 1.172". Thus the lateral displacement contribution from bond failure is 1.297" − 0.088" − 1.172" = 0.037". The contribution from incipient bond failure is therefore smaller than that contributed by footing rotation at $\mu = 1$.

The largest lateral force measured was for column 6 at 77 kips; 39% larger than the predicted plastic lateral force V_p of 55.4 kips. The difference was primarily due to strain-hardening of the longitudinal steel. The maximum lateral force predicted by moment-curvature analysis, using the actual measured ultimate tensile strength of the longitudinal steel i.e. $f_{su} = 1.58 f_y$ (see Appendix

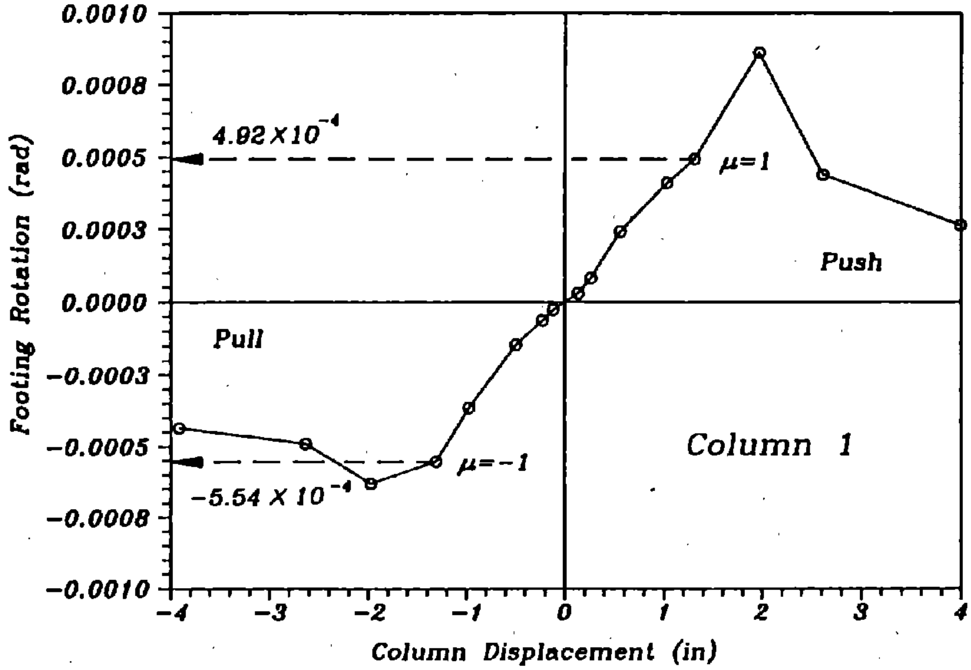

Figure 5.1: **Measured Rotation of Footing for Column 1**

A for steel properties), is 72 kips. When the measured lateral load is corrected for the horizontal component of the applied vertical load, estimated to be about 5%, agreement between predicted and observed strength is very close.

The potential shear strength contribution from the steel jacket is large compared to the applied lateral force. By substituting f_{yj} = 54 ksi, t_j = 3/16 inch and D_j = 24.875 inches into Eqn. 1.17, the shear force capable of being resisted by the steel jacket is V_{sj} = 386 kips. The critical region for shear thus comprises the upper region of the column outside the steel jacket. The shear strength can be assessed in the conventional manner as the sum of resistances by concrete and internal hoops. The concrete contribution V_c may be taken from the ACI expression [38]:

$$V_c = 2(1 + \frac{P}{2000A_g})\sqrt{f'_{co}}A_e \tag{5.1}$$

where A_e is the effective shear area, and is taken as $0.8A_g$ [35]. The shear force resisted by the internal hoops may be given by [6]:

$$V_{sh} = \frac{\pi}{2} A_{sh} f_{yh} \frac{d_s}{s} \tag{5.2}$$

Using $P = 400$ kips, $A_g = 452$ in^2 and $f'_{co} = 5425$ psi for column 6 in Eqn. 5.1 gives $V_c = 76.9$ kips. The substitution of $A_{sh} = 0.05$ in^2, $f_{yh} = 51$ ksi, $d_s = 22.2$ inches and $s = 5$ inches into Eqn. 5.2 gives V_{sh} of 17.7 kips. Thus the ideal shear capacity of the column excluding the steel jacket contribution is 94.6 kips, about 22% larger the maximum shear force noted in column 6.

The comparison between the lateral stiffnesses of column 3 and 4 offers the best estimate of the stiffness increase as a result of a fully grouted steel jacket, since no bond failure or footing rotation were involved. It can be seen from Table 5.1 that the stiffness increase due to steel jacketing was about 13%. However, since the concrete for column 4 had a compressive strength approximately 15% higher than for column 3, some of the stiffening effect will be due to the increased compressive strength.

The lateral strength envelopes for all columns with lapped starter bars and continuous reinforcement are shown in Figures 5.2(a) and (b), respectively. The dramatic improvement of flexural ductility provided by fully grouted steel jackets is apparent in these plots. Also the more gradual degradation of lateral strength in column 5 as a result of partial retrofit when compared to 'as-built' column 1 is obvious in Figure 5.2(a).

5.2 Asymptotic Strength of 'As-Built' Lapped Columns

The lateral strength envelope of Figure 5.2(a) shows that, at large column

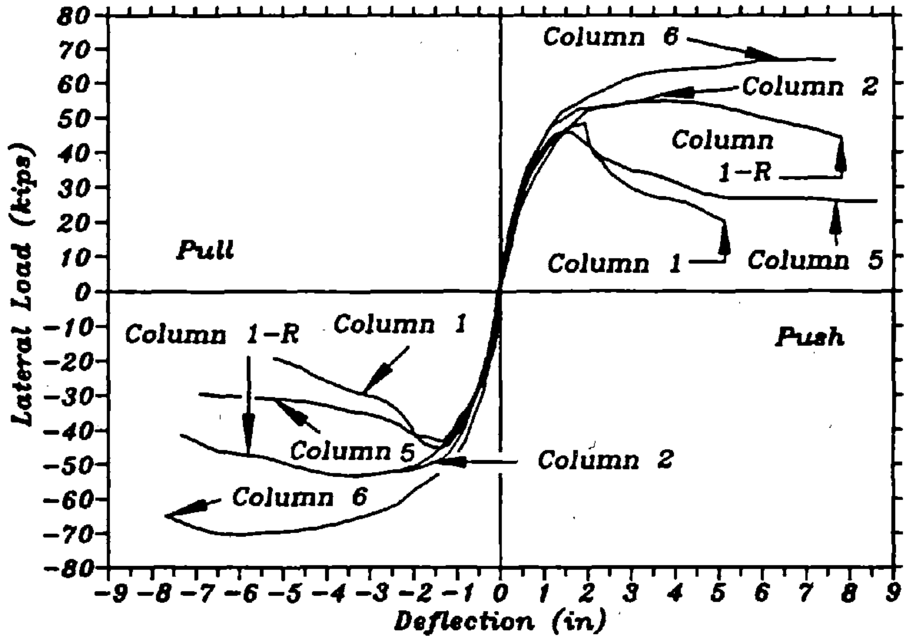

(a) Columns With Lapped Starter Bars

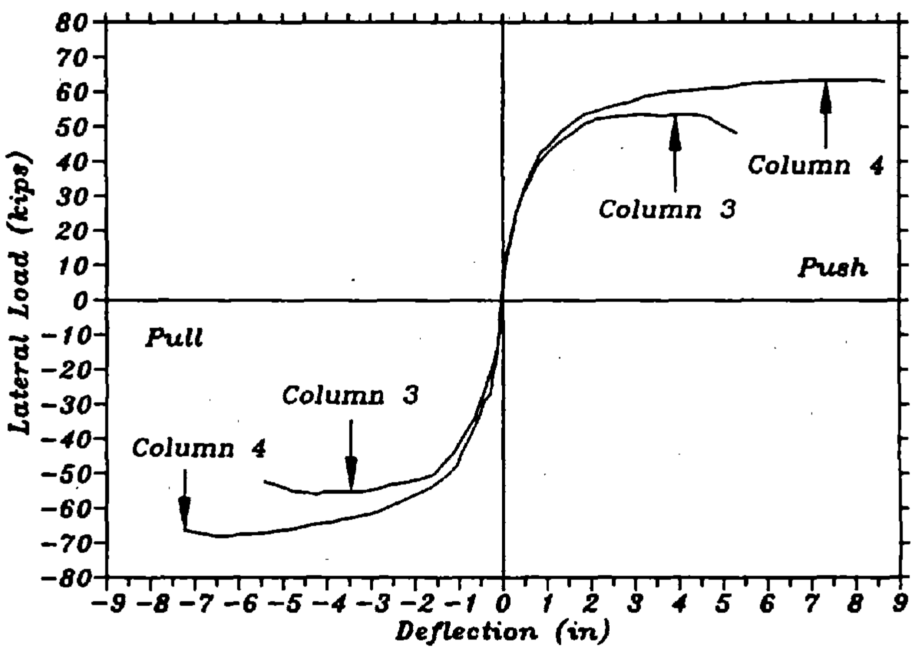

(b) Columns With Continuous Reinforcement

Figure 5.2: Lateral Strength Envelopes of Test Columns

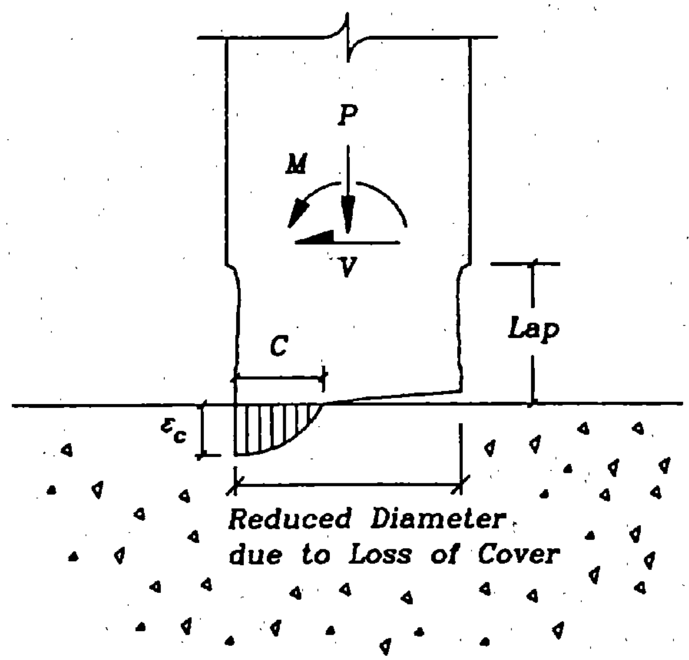

(a) Column Base Section After Complete Bond Failure

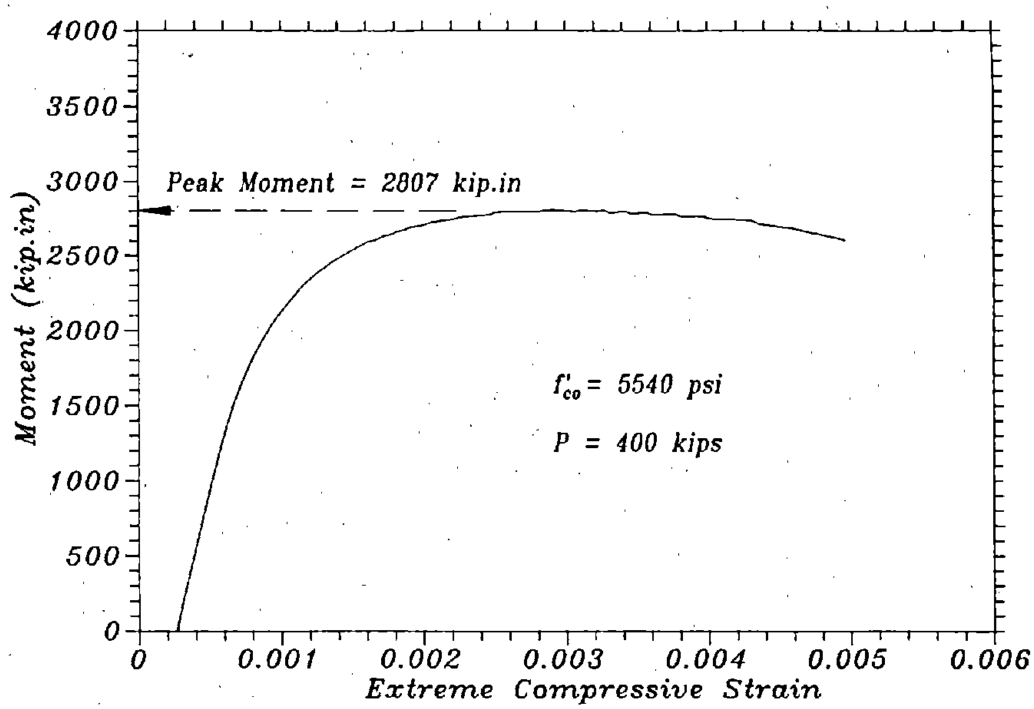

(b) Variation Of Moment With Compressive Strain

Figure 5.3: Moment Resisted By The Axial Load

displacements, the lateral strength of column 1 degraded asymptotically to about 20 kips. The following analysis is carried out to compare the asymptotic strength with the lateral load resisted by the applied axial load.

Figure 5.3(a) shows the base section of the column when a complete bond failure in the lap-splice region has occurred. The effective diameter of the section has been reduced to the inside of the longitudinal steel. To obtain the moment resisted by the axial load, an iterative process is employed in which the section is divided into a number of strips similar to that used by King [36] and using a linear strain profile across the section. For a given extreme fiber compressive strain, ϵ_c, the depth of compression zone is determined from the equilibrium of vertical forces. The non-linear stress-strain curve for unconfined concrete proposed by Mander et al [21] was used for the concrete compressive stress. A unique moment can be computed once the compression zone depth is known. Note that since the loadstub rotation is small and the bar forces almost passes through the center of column, the vertical force at the base section may be taken as P. Figure 5.3(b) shows the variation of moment as ϵ_c was increased from the uniform compression strain to the spalling strain of unconfined concrete. A peak moment of 2807 kip.in was obtained at about $\epsilon_c = 0.003$ which translates into a lateral force of 19.5 kips, and approximately corresponds to the degraded lateral strength of column 1 at $\mu = 4$.

5.3 Weak Footing Failure Mechanism

The brittle failure of the weak footing in column 2 is disturbing and the cause for the failure warrants further discussion. A moment-curvature analysis carried out at the base section of column 2 shows that a resultant compressive force of $C_c + C_s = 739.8$ kips and tensile force of $T_s \doteq 339.8$ kips are required for developing the maximum lateral force noted during testing of column 2. The resultant forces are shown in Figure 5.4(a) and (b). The compressive force is mainly resisted by a major diagonal strut C_1 connecting the compression zone of the column to the nearest pile block. The tensile force T_s is transferred to the footing by bond and is equilibrated by a tension fan T_1 and two minor compressive fans i.e. C_2 radiating from the compression zone in the column and C_3 which fans from the other pile-block. A horizontal tie force of T_2 is required in the bottom reinforcement of the footing to maintain overall equilibrium.

Figure 5.4(b) shows an equivalent strut and tie model for the footing. It is assumed that the tension force T_s diminishes to zero by bond at depth of 14 inches. The node for application of T_s is taken as 7 inches i.e. half the bond length, below the critical column section. The equilibrium of forces in the truss requires significant tie force to be developed in the column-footing joint. For the chosen truss geometry, a tie force of $T_1 = 420$ kips is required. The horizontal component of T_1 is 398 kips. Note that the magnitude of the tie force T_1 increases with the angle of the tie. Failure occurred within the joint region under the column perpendicular to the tension force T_1, as a consequence of inadequate joint shear reinforcement. The column/footing joint is analogous to an exterior beam-column joint in a reinforced concrete building frame. However, the practice of bending the column bars radially outwards at the bottom of the footing (see reinforcement details in Figure 2.1(a)) to provide stability to the reinforcement cage and for ease of bar placement, results in an unfavorable situation where any joint shear failure is immediately accompanied by total footing collapse. Since the tension force in the longitudinal reinforcement is transferred to the 90^0 hook,

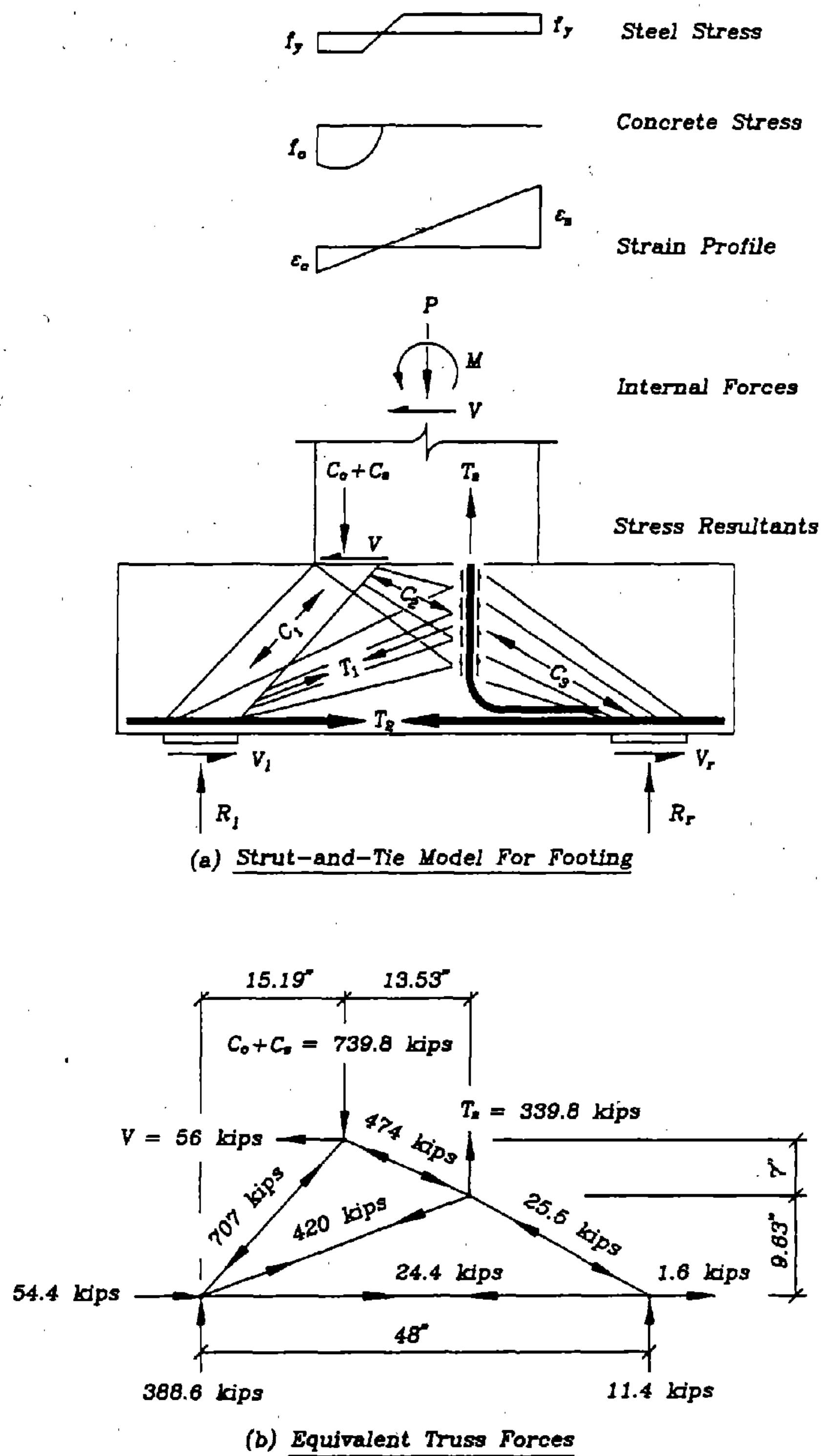

Figure 5.4: Load Resisting Mechanism in Weak Footing

the outward bending of these bars provided no restraint against the propagation of the diagonal joint crack to the base of the footing. Good practice in reinforced concrete frame design would require the beam reinforcement to be bent into the joint to provide a reaction to the compressive force C_2 (Figure 5.4(a)) at the bend, should the tension capacity of the tie T_1 be exceeded.

As pointed out earlier, footings for the remaining columns were designed to carry the entire tie force T_1 by diagonal reinforcement, as shown in Figure 2.1(b). The diagonal reinforcement in footing of column 4 was instrumented with strain gages. Figure 5.5 shows the variation of strains in the diagonal reinforcement with displacement. Tensile strain corresponding to a stress of 26 ksi (or $T_1 = 123$ kips) was developed in the diagonal reinforcement at $\mu = 7$. It should be noted that the tie force T_1 had been relieved by placing the footing in uniform bearing instead of pile-block support.

5.4 Equivalent Plastic Hinge Length

The measurement of curvatures allowed an equivalent plastic hinge length to be defined. By assuming that the post-yield deformation of column is achieved by the formation of a plastic hinge of length L_p at the base within which curvatures are equal to the base curvatures, the lateral displacement Δ of the column may be written as:

$$\Delta = \Delta_y + \theta_p(L' - 0.5L_p) \tag{5.3}$$

where L' is the column height, and $\theta_p = (\phi - \phi_y)L_p$ denotes the plastic rotation when curvature ϕ exceeds the yield curvature ϕ_y. Eqn. 5.3 can be rewritten as:

$$L_p = L' - \sqrt{(L')^2 - 2(\mu - 1)\frac{\Delta_y}{\phi - \phi_y}} \tag{5.4}$$

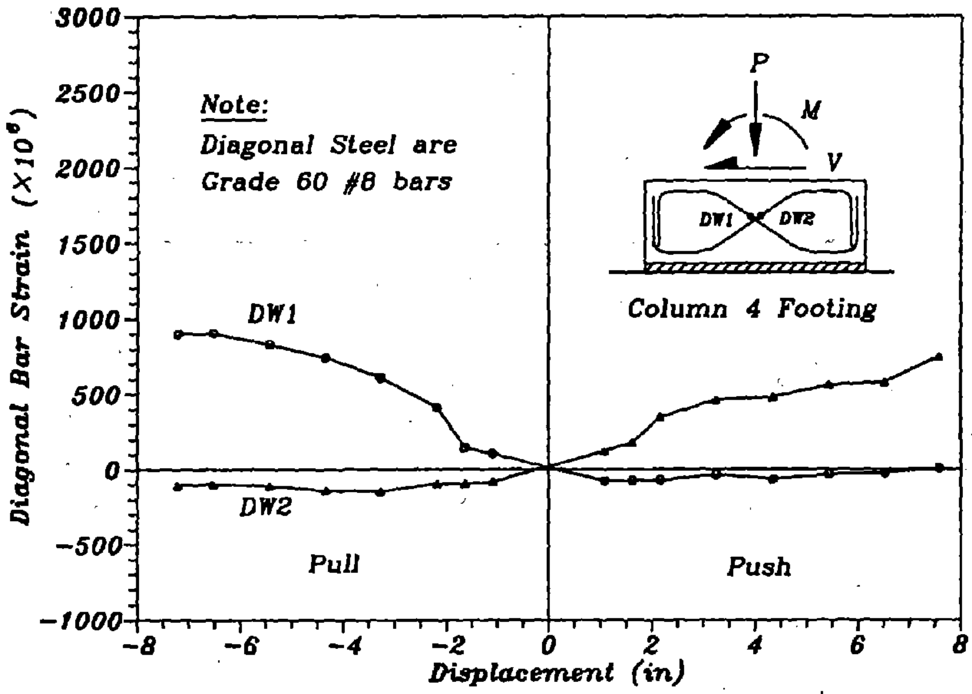

Figure 5.5: **Strain Envelope in Footing Diagonal Reinforcement**

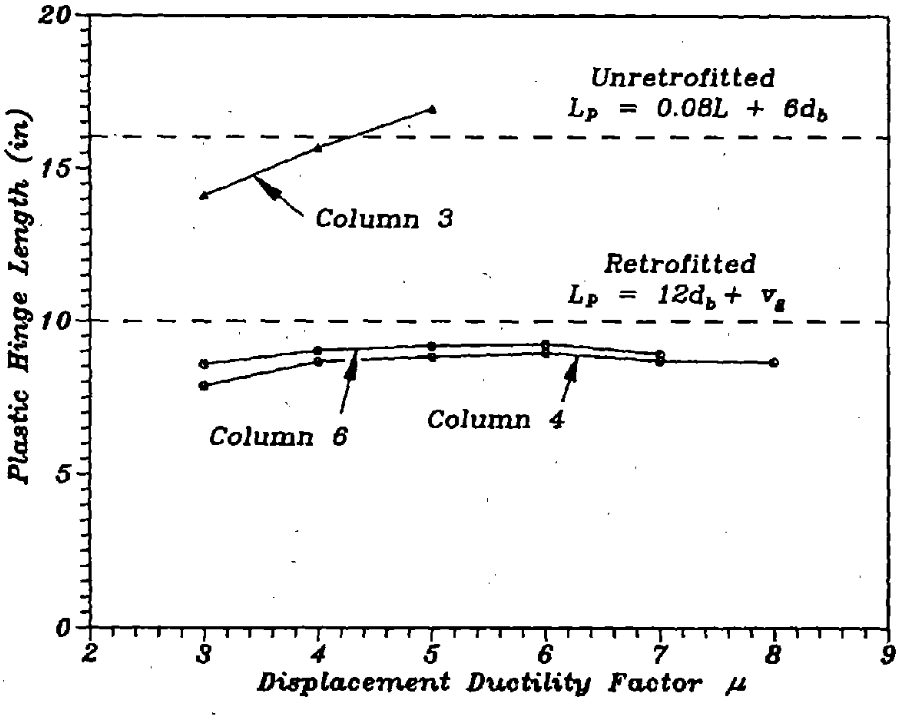

Figure 5.6: **Equivalent Plastic Hinge Length for Test Columns**

Thus an experimental definition of the equivalent plastic hinge length L_p can be made when the measured curvatures and experimental yield displacement Δ_y are used. It should be noted that ϕ_y is the measured curvature at $\mu = 1$.

Figure 5.6 shows the relationship between equivalent plastic hinge length and displacement ductility factor for columns 3, 4 and 6. It can be seen that the plastic hinge length increases more rapidly with displacement ductility factor for the 'as-built' column than for retrofitted columns. It has been proposed [39] that for 'as-built' columns, the equivalent plastic hinge length may be approximated by:

$$L_p = 0.08L' + 6d_b \tag{5.5}$$

where d_b denotes the longitudinal bar diameter. In Eqn. 5.5, the second term reflects the increase in effective plastic hinge length with strain penetration into the base, which is proportional to bar diameter. It can be seen from Figure 5.6 that the experimental plastic hinge length compares well with prediction of Eqn. 5.5 for $\mu \geq 3$. Since the presence of the steel jacket restricted the spread of curvatures up the column, it appeared reasonable to expect strain penetration into the jacketed region to equal that into the footing, given as $6d_b$ above. Hence the equivalent plastic hinge length for retrofitted column is expected to be:

$$L_p' = 12d_b + v_g \tag{5.6}$$

where v_g denotes the vertical gap provided between the toe of steel jacket and top of footing. It is seen from Figure 5.6 that Eqn. 5.6 slightly overestimates the plastic hinge length.

5.5 Neutral Axis Depths

In this section the neutral axis depth predicted by the moment-curvature analysis carried out for the base section are compared with that measured by the strain gages on the longitudinal reinforcement. The experimental neutral axis depth was estimated by a best-fit line through the strain profiles presented in Section 4.4.2. The moment-curvature analysis used the Mander's model for confined concrete [21] and adapted here for retrofit with a steel jacket.

Figure 5.7(a) and (b) show the comparison of theoretical and measured neutral depths for 'as-built' column 1 and retrofitted column 6. It can be seen that the measured neutral axis depths were slightly larger than the predicted neutral axis depths at small lateral loads but otherwise agreement is good. The measured neutral axis depth for column 1 decreased rapidly from about 20 inches at a lateral load of 15 kips to 9.5 inches at a lateral load of 45 kips. The neutral axis depths at peak lateral load of 49 kips (i.e. $\mu = 1.5$) for column 1 was not included in the plot since it was difficult to estimate the neutral axis depth from the strain profile at that stage. The prediction of the neutral axis depth was better for retrofitted column 6.

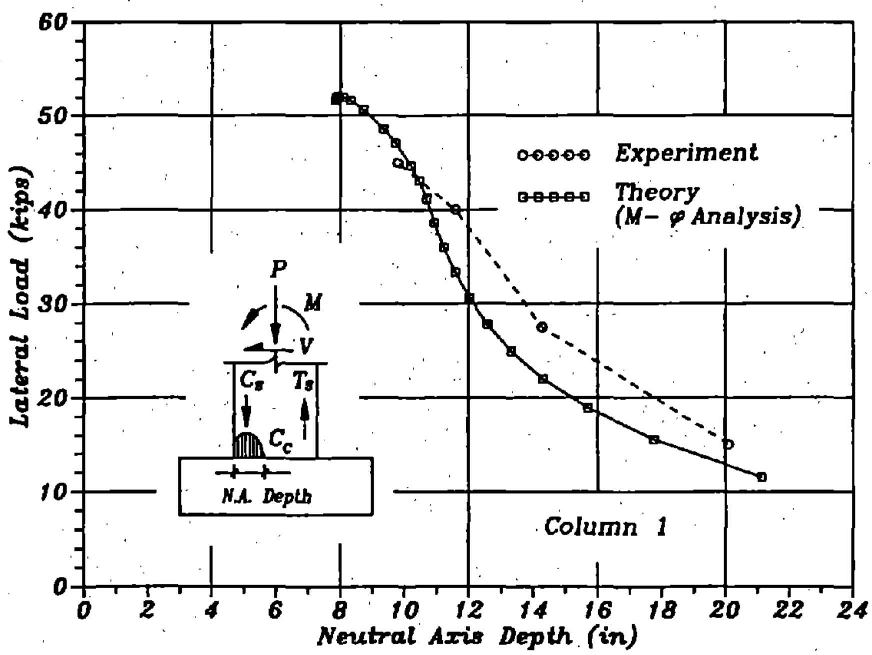

(a) 'As- Built' Column 1

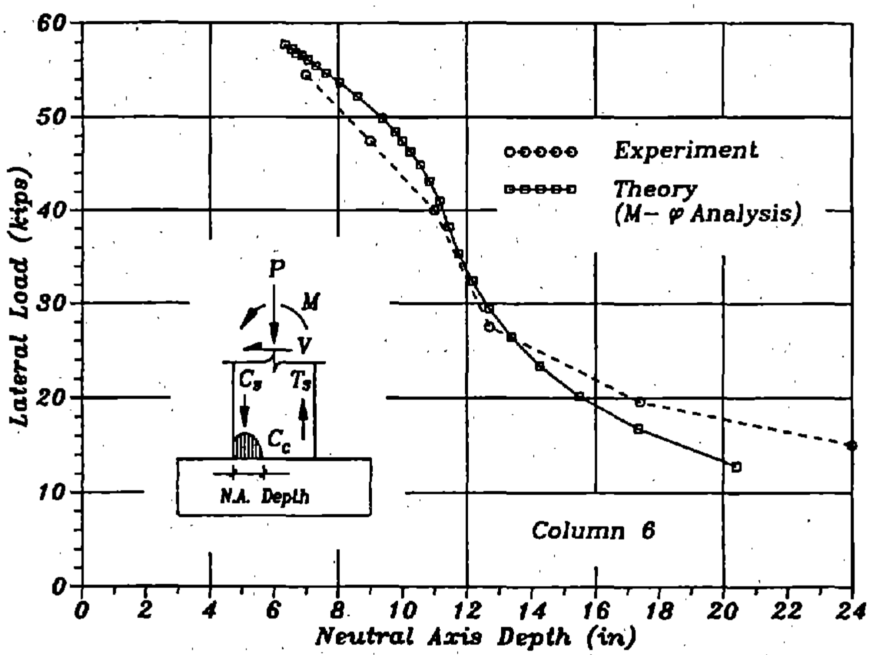

(b) Retrofitted Column 6

Figure 5.7: Comparisons of Neutral Axis Depths

Chapter 6

Conclusions

The flexural retrofit program indicated that cylindrical steel jackets are effective in enhancing flexural ductility capacity of the circular bridge columns. The following conclusions are made:

<u>'As-built' Columns</u>

1. Under seismic conditions, pre-1971 circular bridge columns with lapped starter bars in the potential plastic hinge region are likely to suffer bond failure at less than their nominal flexural strength. The use of 20 times the bar diameter as lap length resulted in rapid degradation of flexural strength for column 1 after displacement ductility of $\mu = 1.5$ or a drift ratio of 1.3%. The strength degrades asymptotically to the value resisted by the axial load.

2. For column 3 with continuous reinforcement through the potential plastic hinge region, the nominal flexural strength of the column was developed. The displacement ductility factor corresponding to first spalling of cover concrete was $\mu = 3$. Final failure of the column occurred at $\mu = 5$ due to inadequate confinement of the concrete core and the loss of transverse restraint against compression buckling of the longitudinal steel. The degradation of flexural strength after spalling of cover concrete was less rapid compared to columns with lapped starter bars.

3. Failure mode observed for test column 2 constructed with a footing reinforced with only a bottom layer of reinforcement indicated that the pre-1970 design may be susceptible to joint shear failure in the region immediately under the column. Due consideration must therefore be made to ensure comparable footing strength before implementation of column retrofit by steel jacket.

Retrofitted Columns

1. Columns provided with a steel jacket at a volumetric confinement ratio of 3.1% in the potential plastic hinge region developed stable hysteresis loops up to displacement ductility factor of $\mu = 7$, or a drift ratio of about 5.3 %. Final failure of the columns was precipitated by low-cycle fatigue fracture of the longitudinal reinforcement resulting from alternating buckling and straightening. Bond failure at the lap-splices was eliminated.

2. The use of styrofoam wrap as cushion in grouted jacket to absorb the lateral expansion of cover concrete did not inhibit bond failure at the lap-splice at $\mu = 1.5$. The presence of the steel jacket however prevented a complete loss of cover concrete, resulting in slightly less rapid degradation of strength when compared to the 'as-built' lapped column, especially at large displacements. Significant circumferential strains were observed in the jacket at $\mu \geq 4$. Vertical load carrying capacity of the column was maintained up to a drift ratio of 6%.

3. Fully grouted steel jackets increase the lateral stiffness of the column. The stiffness increase would depend on the thickness and length of the jacket and the bond stress at the jacket/grout interface. The increase in lateral stiffness obtained in this study was in the range of 10 to 15 %.

4. Steel jacketing can be effective in post-earthquake repair of columns which have suffered bond failure at the lap-splices of the longitudinal reinforcement. Although the hysteresis response of the repaired column indicated less energy absorption than that of retrofitted but undamaged columns, the flexural strength of the column can be restored. A drift ratios of more than 4% was obtained before a significant degradation of lateral strength was observed.

5. The calibration of curvature measurement supports the expression for an equivalent plastic hinge length of $L_p = 0.08L' + 6d_b$ for 'as-built' columns with continuous reinforcement. In retrofitted columns, large inelastic rotations occurred over a smaller region and the reduction in equivalent plastic hinge length to $L_p = 12d_b + v_g$, where v_g = the vertical gap between the toe of jacket and footing, appears appropriate at this stage.

6. The steel jacket need not be extended to full height of the column when only flexural retrofit is required. The criterion that the moment demand immediately above the jacket is less than 75% of the original flexural capacity for the determination of jacket length was successful in ensuring the formation of plastic hinge at the base of the column.

References

[1] G.G. Fung, R.J. Lebeau, E.D. Klein, J. Belvedere, and A.F. Goldschmidt. *Field Investigation of Bridge Damage in the San Fernando Earthquake.* Technical Report, Bridge Department, Division of Highways California Department of Transportation, Sacramento, California, 1971. 209 pp.

[2] P.C. Jenning. *Engineering Features of the San Fernando Earthquake of Feb. 9, 1971.* Report EERL 71-02, Earthquake Engineering Research Laboratory, California Institute of Technology, Pasadena, California, June 1971.

[3] A.L. Elliott. The San Fernando Earthquake: A lesson in highway and bridge design. *Civil Engineering-ASCE*, 95–97, September 1972.

[4] J.H. Gates. California's seismic design criteria for bridges. *Jour. Struct. Div., ASCE*, 114, ST12:2301–2313, Dec. 1988.

[5] *Guide Specifications For Seismic Design of Highway Bridges.* American Association Of State Highway Transportation Officials, Washington D.C., 1983.

[6] M.J.N. Priestley and R. Park. *Strength and Ductility of Bridge Substructures.* Road Research Unit Bulletin 71, New Zealand National Roads Board, Wellington, New Zealand, 1984. 120 pp.

[7] W.C. Stone and G.S. Cheok. *Inelastic Behavior of Full-Scale Bridge Columns Subjected to Cyclic Loading.* Report No. NIST/BSS-166, Na-

tional Institute of Standards and Technology, U.S. Department of Commerce, Gaithersburg, MD 20899, Jan 1989.

[8] L.G. Selna, L.J. Malvar, and R.J. Zelinski. Box girder bar and bracket seismic retrofit devices. *ACI Struct. Jour.*, 86(5):532–540, Sept/Oct 1989.

[9] L.G. Selna, L.J. Malvar, and R.J. Zelinski. Bridge retrofit testing: hinge cable restrainers. *Jour. Struct. Div., ASCE*, 115(4):920–934, April 1989.

[10] O.H. Degenkolb. *Concrete Box Girder Bridges.* American Concrete Institute Monograph No. 10, Detroit, Michigan, 1977.

[11] R. Zelinski. California highway bridge retrofit strategy and details. In *Final Proceeding - Second Workshop on Bridge Engineering Research in Progress*, National Science Foundation and Civil Engineering Department, University of Nevada, Reno, October 29-30 1990.

[12] M.J.N. Priestley. Damage of the I-5/I-605 Separator in the Whittier Earthquake of October 1987. *Earthquake Spectra*, 4(2):389–405, 1988.

[13] J.H. Gates, S. Mellon, and G. Klein. The Whittier Narrows, California Earthquake of October 1, 1987 - Damage to State Highway Bridges. *Earthquake Spectra*, 4(2):377–388, 1988.

[14] H.S. Lew, editor. *Performance of Structures During the Loma Prieta Earthquake of October 17, 1989*, National Institute of Standards and Technology, U.S. Department of Commerce, Gaithersburg, MD 20899, 1990. NIST Special Publication 778.

[15] J.A. Blume, N.M. Newmark, and L.H. Corning. *Design of Multistory Reinforced Concrete Building for Earthquake Motions.* Portland Cement Association, 33 West Grand Avenue, Chicago 10, Illinois, 1961.

[16] R. Park and R.W.G Blakeley. *Seismic Design of Bridges.* Road Research Unit Bulletin 43 Vol. 3, New Zealand National Roads Board, Wellington, New Zealand, 1979.

[17] *Seismic Retrofitting Guidelines For Highway Bridges Report No. ATC-6-2.* Applied Technology Council, Palo Alto, California, Aug 1983.

[18] R.J.T. Park, M.J.N. Priestley, and W.R. Walpole. The seismic performance of steel encased reinforced concrete piles. *Bulletin of the New Zealand National Society for Earthquake Engineering*, 16(2):123–140, June 1983.

[19] R.J.T. Park, M.J.N. Priestley, and W.R. Walpole. *The Seismic Performance of Steel Encased Concrete Piles.* research report 82-12, Department of Civil Engineering, University of Canterbury, Christchurch, New Zealand, Feb. 1982.

[20] R.J.T. Park, M.J.N. Priestley, and J.B. Berrill. *Seismic Performance of Steel-Encased Concrete Piles.* research report 87-5, Department of Civil Engineering, University of Canterbury, Christchurch, New Zealand, May 1987.

[21] J.B. Mander, M.J.N. Priestley, and R. Park. Theoretical stress-strain model for confined concrete. *Jour. Struct. Div., ASCE*, 114(8):1804–1826, Aug. 1988.

[22] J.B. Mander, M.J.N. Priestley, and R. Park. Observed stress-strain behavior of confined concrete. *Jour. Struct. Div., ASCE*, 114(8):1827–1849, Aug. 1988.

[23] T. Paulay. Lapped splices in earthquake-resisting columns. *ACI Jour.*, 79(6):46–50, Nov/Dec 1982.

[24] *Code of Practice for the Design of Concrete Structures, NZ 3101*. Standards Association of New Zealand, Wellington, New Zeal, 1982 (Amended 1989).

[25] *Bridge Design Specifications Manual*. California Department of Transportation, Sacramento, California, 1986.

[26] B. Sivakumar, P. Gergely, and R.N. White. Suggestions for the design of R/C lapped splices for seismic loading. *Concrete International*, 46–50, Feb 1983.

[27] M.J.N. Priestley and F. Seible. *Seismic Assessment and Retrofit of Bridges.* research report SSPR-91/03, Department of Applied Mechanics and Engineering Sciences, University of California, San Diego, La Jolla, CA 92093, July 1991.

[28] T. Akimoto, H. Nakajima, and F. Kogure. Seismic strengthening of reinforced concrete bridge piers on Metropolitan Expressway. In *U.S. - Japan Workshop on Seismic Retrofit of Bridges*, Public Works Research Institute, Ministry of Construction, Tsukuba Science City, Japan, December 17-18 1990.

[29] Y. Matsuura, I. Nakamura, and H. Sekimoto. Seismic strengthening method for reinforced concrete bridge piers on Hanshin Expressway. In *U.S. - Japan Workshop on Seismic Retrofit of Bridges*, Public Works Research Institute, Ministry of Construction, Tsukuba Science City, Japan, December 17-18 1990.

[30] R.W. Furlong. Strength of steel-encased concrete beam columns. *Jour. Struct. Div., ASCE*, 93(5):113–124, Oct. 1967.

[31] R.B. Knowles and R. Park. Strength of concrete filled steel tubular columns. *Jour. Struct. Div., ASCE*, 95(12):2565–2587, Dec. 1969.

[32] M. Tomii, K. Yoshimura, K. Sakino, Y. Morishita, and F. Esaki. *Investigations on Transversely Super Reinforced Concrete Structures and Concrete Filled Steel Tube Structures.* research report, Kyushu University, Japan, Department of Architecture, Faculty of Engineering, May 1988.

[33] K. Kawashima, S. Unjoh, and H. Iida. Seismic inspection and seismic strengthening of reinforced concrete bridge piers with termination of main reinforcement at mid-height. In *U.S. - Japan Workshop on Seismic Retrofit of Bridges*, Public Works Research Institute, Ministry of Construction, Tsukuba Science City, Japan, December 17-18 1990.

[34] Y.H. Chai, M.J.N. Priestley, and F. Seible. Flexural retrofit of circular reinforced concrete bridge columns by steel jacketing - COLRET - a computer program for strength and ductility calculation. Research Report - University of California, San Diego.

[35] Ang Beng Ghee, M.J.N. Priestley, and T. Paulay. Seismic shear strength of circular reinforced concrete columns. *ACI Struct. Jour.*, 86(1):45–59, Jan/Feb 1989.

[36] D.J. King and M.J.N. Priestley. *Computer Program For Concrete Column Design.* research report 86-12, Department of Civil Engineering, University of Canterbury, Christchurch, New Zealand, May 1986.

[37] R. Park and T. Paulay. *Reinforced Concrete Structures.* A Wiley-Interscience Publication, New York, 1975.

[38] *Building Code Requirements For Reinforced Concrete (ACI 318-83 Revised 1986).* American Concrete Institute, Detroit, Michigan, 1987.

[39] M.J.N. Priestley and R. Park. Strength and ductility of concrete bridge columns under seismic loading. *ACI Struct. Jour.*, 84(1):61–76, Jan/Feb 1987.

[40] J.S. Przemieniecki. *Theory of Matrix Structural Analysis.* Dover Publications, Inc., New York, 1985.

[41] W.F. Chen and D.J. Han. *Plasticity For Structural Engineers.* Springer-Verlag, New York, 1988.

[42] D.R.J. Owen and E. Hinton. *Finite Elements In Plasticity: Theory and Practice.* Pineridge Press Limited, Swansea, U.K., 1980.

Appendix A

Materials and Construction

A.1 Summary of Material Strengths

A summary of the material strengths is given in Table A.1. The concrete compressive strengths shown were an average of three 6" diameter cylinders tested at the time of column testing.

Table A.1: **Table of Material Strengths**

Col	Concrete	Longitudinal Steel		Hoop Steel	Steel Jacket
	f'_{co}	f_y	f_{su}	f_{yh}	f_{yj}
1	5540 psi	45.7 ksi	72.2 ksi	51 ksi	45 ksi (1-R)
2	5600 psi	45.7 ksi	72.2 ksi	51 ksi	42 ksi
3	4725 psi	45.7 ksi	72.2 ksi	51 ksi	—
4	5520 psi	45.7 ksi	72.2 ksi	51 ksi	47 ksi
5	5094 psi	45.7 ksi	72.2 ksi	51 ksi	54 ksi
6	5425 psi	45.7 ksi	72.2 ksi	51 ksi	54 ksi

A.2 Concrete

The test columns were constructed using ready-mix concrete supplied by a local company in San Diego. Table A.2 summarizes the mix design for the concrete. It should be noted that a water-reducing admixture was added during batching to achieve the slump needed for vertical casting of the columns. Typical slump values were between 4 and 6 inches at the laboratory.

Table A.2: **Concrete Mix Design**

Constituents	**Weight (lb/yd^3)**
Cement (Type II)	658
Coarse Aggregate (1/2" Max)	1651
Fine Aggregate (Sand)	1302
Water	350

A.3 Reinforcement

The stress-strain characteristics of the reinforcing steel for the columns were determined from tensile tests. Strain data were acquired using a calibrated extensiometer over a nominal gage length of 4 inches.

The stress-strain curves for the main steel (#6 deformed bars) are shown in Figure A.1(a). The yield and ultimate tensile strength, averaged over three bars, were 45.7 and 72.2 ksi, respectively, and the modulus of elasticity was 28707 ksi. The ratio of ultimate to yield strength was $f_{su}/f_y = 1.58$. Strain-hardening occurred between 1.14 and 1.73% strain, with an average value of $\epsilon_{sh} = 1.45\%$.

The yield strength for the transverse hoops was slightly higher than that of the longitudinal steel, at 51 ksi and the steel possessed a relatively small ultimate tensile strength i.e. 61 ksi. The ratio of ultimate to yield strength, f_{su}/f_y, was only 1.20. The onset of strain-hardening was also less distinct when compared to that of the #6 bars. The modulus of elasticity for the hoops averaged 28088 ksi. The stress-strain curves for the #2 hoop are shown in Figure A.1(b).

A.4 Steel Jacket

The half shells for the steel jackets were fabricated from A36 hot-rolled steel and welded together by a certified welder using structural steel electrodes. Test

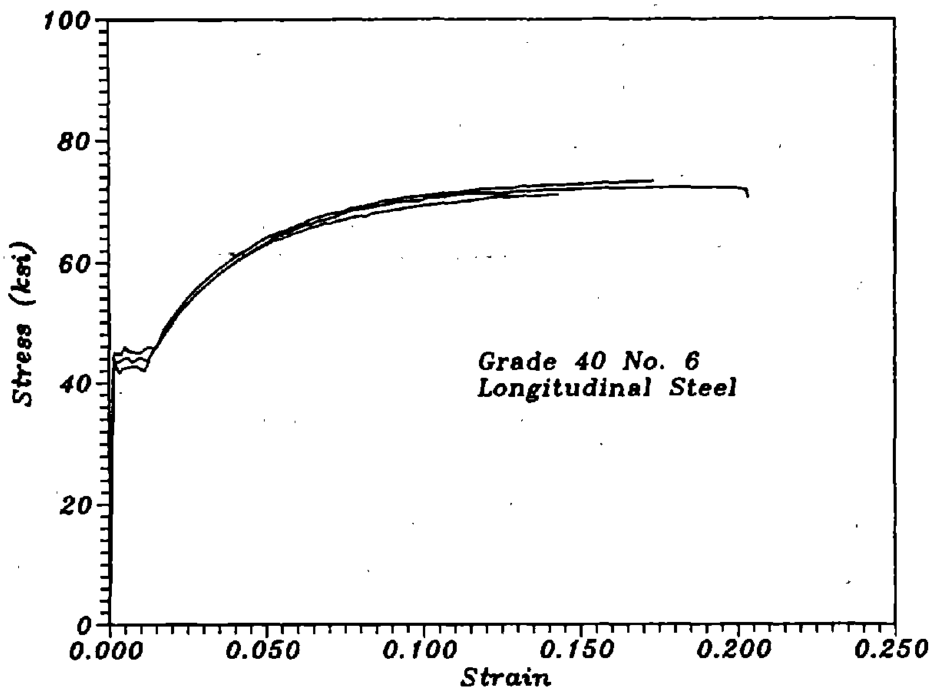

(a) Longitudinal Steel

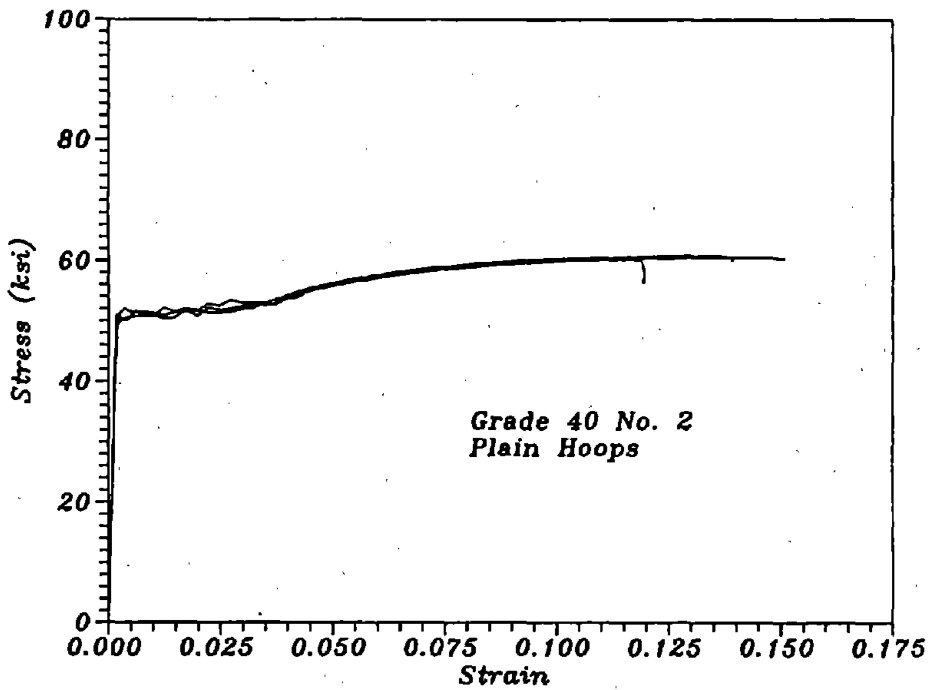

(b) Transverse Steel

Figure A.1: Stress-Strain Curves for Reinforcing Steel

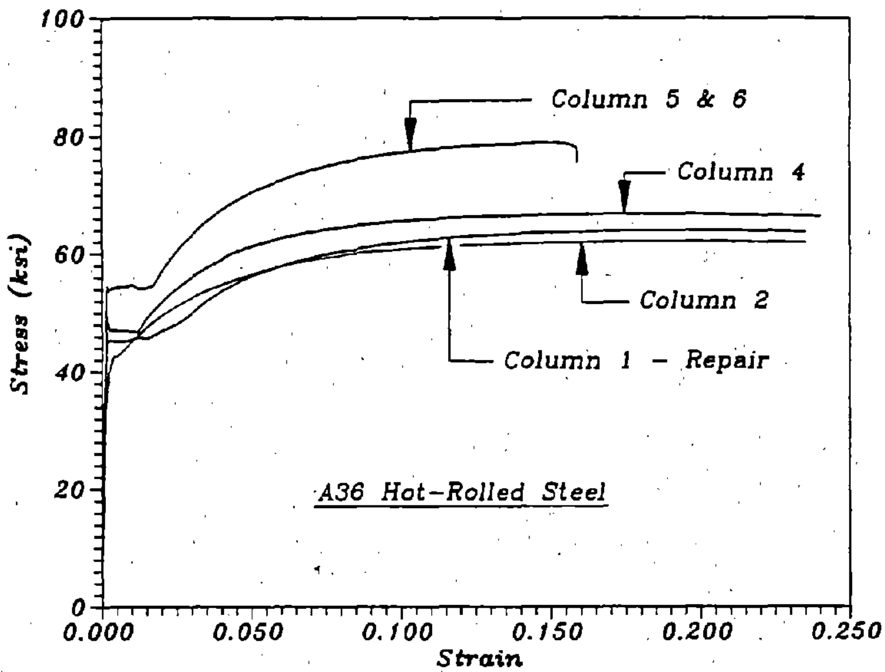

Figure A.2: **Stress-Strain Curves for Steel Jackets**

pieces in the form of flat strips (2 inches wide) were ordered for tensile tests. The stress-strain curves for all the jackets are shown in Figure A.2. Note that there was considerable variation in the stress-strain curves for the jacket. The highest yield strength of 54 ksi was noted for column 5 and 6. It should be pointed out that the steel jackets for column 5 and 6 were fabricated from the same batch of steel, and are therefore represented by only one line in Figure A.2.

A.5 Grout

The steel jackets were bonded to columns using a cement-based grout having a water/cement weight ratio of 0.42. A water-reducing, expansive admixture (Intraplast N) was added at a dosage of 1% cement by weight to compensate for the possible shrinkage. Compression cylinders (2" diameter × 4" height), sampled from each mix of grout and showed an average compressive strength of 2200 psi at 14 days when restrained against expansion caused by the additive. If the cylinders were left unrestrained, compressive strengths as low as 1000 psi were obtained.

A.6 Construction of Test Columns

The test units were constructed in pairs over a period of about twelve months. Each unit was cast in two phases; the footings being cast first, followed by the column portion. Plywood forms were used for the footing. Six vertical hold-down sleeves were cast in the footing using $1\frac{1}{2}$ inch PVC pipes. In addition, two 8 inch diameter sleeves were formed in the footing to accommodate the lateral displacement of the high-strength bars which passed through the footing and were used for axial load application. Reinforcement for the weak footing was assembled into one mat unit before being placed in the form. For the strong footing, it was more convenient to tie the reinforcement cage in the form. The completed reinforcement cage for the strong footing is shown in Figure A.3(a). All reinforcement for the footing was provided with a minimum of one inch cover. A start-up curb of one inch height, as seen in Figure A.3(b), was constructed together with the footing to receive the cardboard form for the circular column.

For columns with lapped starter bars, the reinforcement was fabricated independent of the footing construction. The longitudinal bars were assembled into a stable cage, as shown in Figure A.4(a), before being lifted and lap-spliced with the starter bars. In the case of continuous reinforcement, the column bars were securely tied to the bottom reinforcing mat of the footing prior to casting of footing.

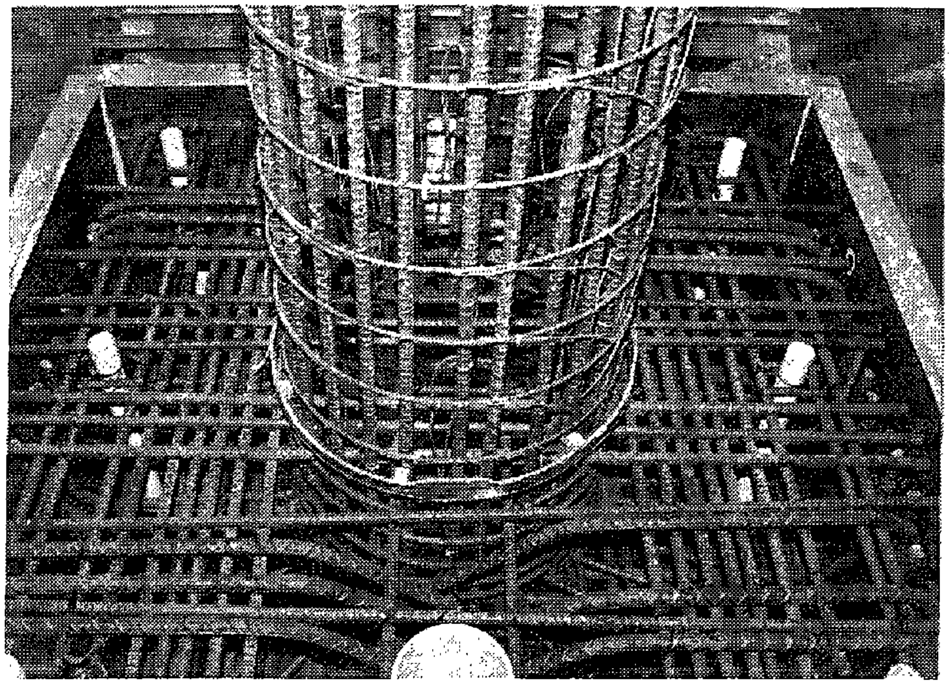

(a) Strong Footing Reinforcement

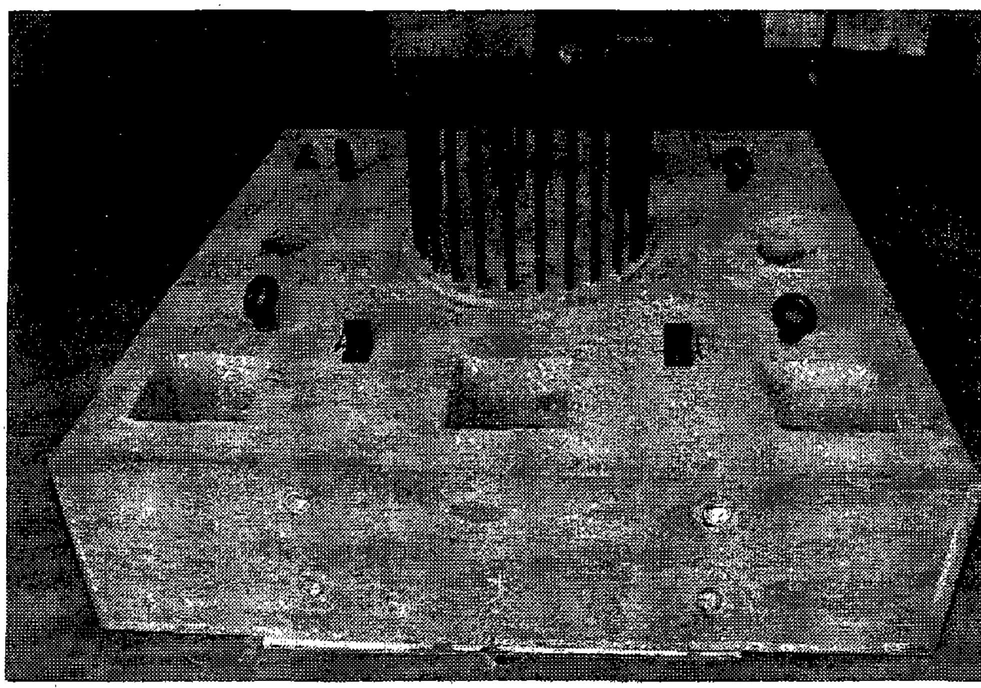

(b) Completed Footing with Starter Bars

Figure A.3: Construction of Footing

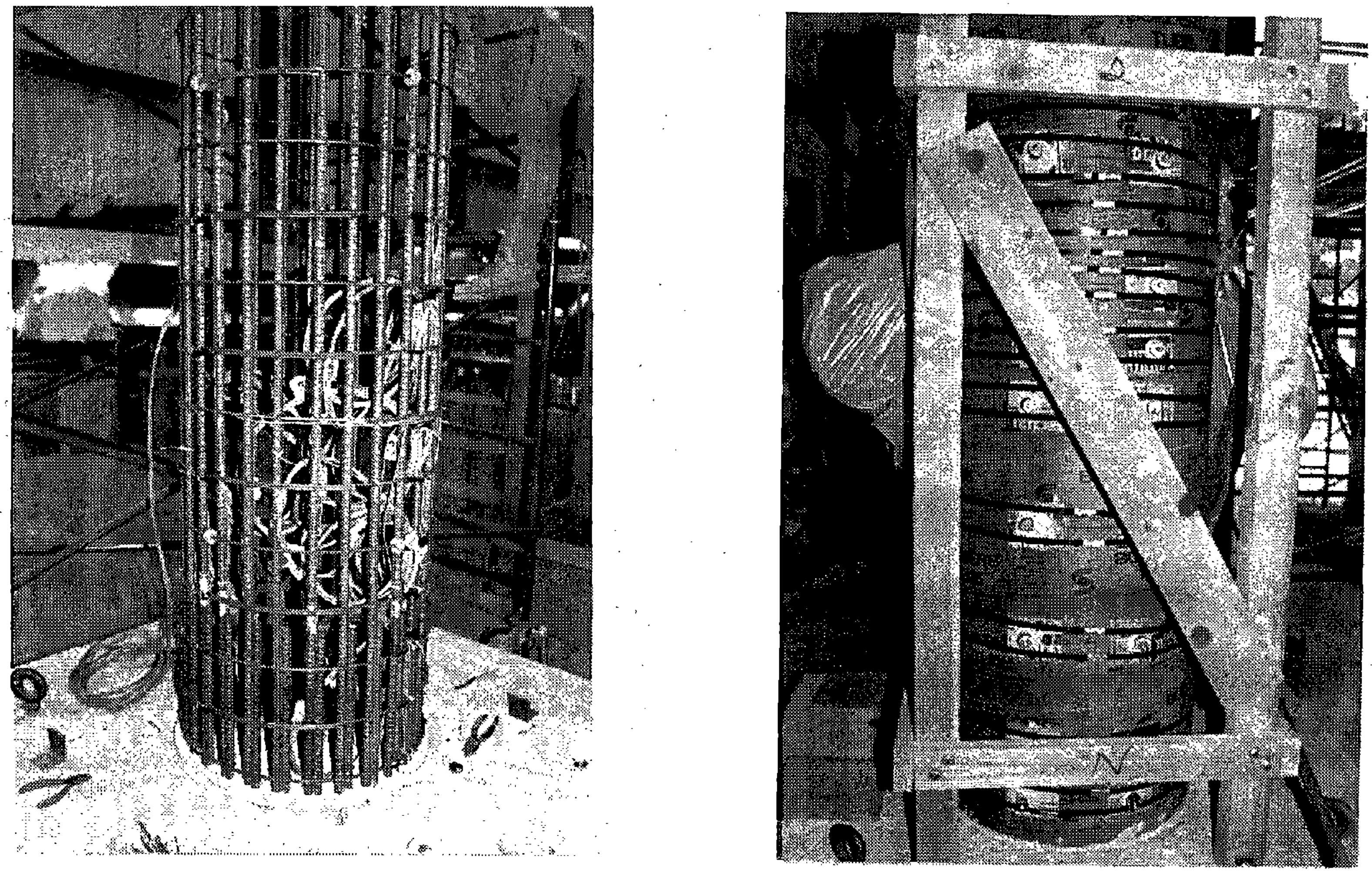

(a) Lap-Splicing of Column Reinforcement

(b) Forming of Column Portion

Figure A.4: Construction of Test Units

Figure A.4(b) shows the forming work for the column. The cardboard tubes for the column were provided with wax-lining to produce a good surface finish and for ease of striping after curing. Square patches were cut in the tube to allow curvature rods to be inserted and tied to the column bars. The cut-outs were then steel banded back to the form and tightly sealed against the concreting pressure. Plywood forms were used for the loadstub and were supported by 4" × 4" timber posts at four corners. Four $1\frac{1}{2}$ inch PVC pipes were cast in the loadstub for subsequent attachment of the horizontal actuator.

The concrete for the column was placed in three equal lifts from one batch of concrete. Weep-holes (3/16" in diameter) were drilled at 12" spacing on four sides of the tube to allow visual confirmation that thorough compaction of the concrete was achieved. All concrete was covered with wet burlap and left for at least 24 hours before removal of forms.

The grout for the jacket was mixed at the laboratory using carefully sieved cement. The grout mix was injected using two hand-operated commercial garden spray containers with a capacity of 3 gallons each and capable of delivering a pressure up to 70 psi. The concrete surface was first wet with water before grout injection. Four inlets symmetrically distributed along the bottom of the jacket were used. A complete fill of the gap was guaranteed by the grout exiting from the air vents placed near the top of the jacket. Actual effective grouting pressure was expected to be less than 20 psi.

Appendix B

Jacket Stress-Strain Conversion

B.1 Theoretical Background

The procedure of converting the strains on the steel jacket into stress requires the use of the incremental theory of plasticity since some of the measured strains indicate deformation beyond yielding of the material. The orientations of strain gages are assumed to coincide with the directions of principal strains. Since the lateral confining pressure f'_{lj} is small when $D_j/t_j \gg 0$, the steel jacket is regarded as in the state of plane stress. It is also assumed that no hardening occurs in the steel jacket which then allows the yield function to be written as:

$$\mathcal{F}(\tilde{\sigma}) = 0 \tag{B.1}$$

where $\tilde{\sigma}$ is the stress vector. Upon differentiating

$$\begin{aligned} d\mathcal{F} &= \left(\frac{\partial \mathcal{F}}{\partial \tilde{\sigma}}\right)^T d\tilde{\sigma} && \text{(B.2)} \\ &= \tilde{\mathbf{a}}^T d\tilde{\sigma} && \text{(B.3)} \\ &= 0 && \text{(B.4)} \end{aligned}$$

where $\tilde{\mathbf{a}} \equiv \frac{\partial \mathcal{F}}{\partial \tilde{\sigma}}$ is called a flow vector.

For small deformation, the total strain increment can be decomposed into the elastic and plastic components i.e.

$$d\tilde{\epsilon} = d\tilde{\epsilon}^e + d\tilde{\epsilon}^p \tag{B.5}$$

where $d\tilde{\epsilon}, d\tilde{\epsilon}^e$, and $d\tilde{\epsilon}^p$ are the total, elastic and plastic strain increments respectively.

The elastic strain increment is related to the stress increment via Hooke's Law:

$$d\tilde{\epsilon}^e = \tilde{\mathbf{D}}^{-1} d\tilde{\sigma} \tag{B.6}$$

where $\tilde{\mathbf{D}}^{-1}$ is the elastic compliance matrix.

For an isotropic material [40], the matrix $\tilde{\mathbf{D}}^{-1}$ under plane-stress condition is given by:

$$\tilde{\mathbf{D}}^{-1} = \frac{1}{E}\begin{bmatrix} 1 & -\nu & 0 \\ -\nu & 1 & 0 \\ 0 & 0 & 2(1+\nu) \end{bmatrix} \tag{B.7}$$

where E, ν are the elastic modulus and Poisson's ratio.

The plastic strain increment $d\tilde{\epsilon}^p$ is given by the associated flow rule [41] which states:

$$d\tilde{\epsilon}^p = d\lambda \frac{\partial \mathcal{F}}{\partial \tilde{\sigma}} \tag{B.8}$$

where $d\lambda$ is a non-negative proportionality factor called the plastic multiplier.

Substituting the expressions for $d\tilde{\epsilon}^e$ and $d\tilde{\epsilon}^p$ into Eqn. B.5 gives the incremental relation between stress and strain as:

$$d\tilde{\epsilon} = \tilde{\mathbf{D}}^{-1} d\tilde{\sigma} + d\lambda \frac{\partial \mathcal{F}}{\partial \tilde{\sigma}} \tag{B.9}$$

$$= \tilde{\mathbf{D}}^{-1} d\tilde{\sigma} + d\lambda \tilde{\mathbf{a}} \tag{B.10}$$

Premultiplying both sides of the above equation by $\tilde{\mathbf{a}}^T \tilde{\mathbf{D}}$ gives:

$$\tilde{\mathbf{a}}^T \tilde{\mathbf{D}} d\tilde{\epsilon} = \underbrace{\tilde{\mathbf{a}} d\tilde{\sigma}}_{0} + d\lambda \tilde{\mathbf{a}}^T \tilde{\mathbf{D}} \tilde{\mathbf{a}} \tag{B.11}$$

which allows the plastic multiplier to be written as:

$$d\lambda = \frac{\tilde{\mathbf{a}}^T \tilde{\mathbf{D}} d\tilde{\epsilon}}{\tilde{\mathbf{a}}^T \tilde{\mathbf{D}} \tilde{\mathbf{a}}} \tag{B.12}$$

Substituting the plastic multiplier back into Eqn. B.10:

$$d\tilde{\epsilon} = \tilde{\mathbf{D}}^{-1}d\tilde{\sigma} + \frac{\tilde{\mathbf{a}}\tilde{\mathbf{a}}^T\tilde{\mathbf{D}}}{\tilde{\mathbf{a}}^T\tilde{\mathbf{D}}\tilde{\mathbf{a}}}d\tilde{\epsilon} \tag{B.13}$$

which can be rearranged into:

$$d\tilde{\sigma} = \tilde{\mathbf{D}}\left[1 - \frac{\tilde{\mathbf{a}}\tilde{\mathbf{a}}^T\tilde{\mathbf{D}}}{\tilde{\mathbf{a}}^T\tilde{\mathbf{D}}\tilde{\mathbf{a}}}\right]d\tilde{\epsilon} \tag{B.14}$$

$$= \tilde{\mathbf{D}}^{ep}d\tilde{\epsilon} \tag{B.15}$$

where

$$\tilde{\mathbf{D}}^{ep} \equiv \tilde{\mathbf{D}}\left[1 - \frac{\tilde{\mathbf{a}}\tilde{\mathbf{a}}^T\tilde{\mathbf{D}}}{\tilde{\mathbf{a}}^T\tilde{\mathbf{D}}\tilde{\mathbf{a}}}\right] \tag{B.16}$$

is the elasto-perfectly plastic material stiffness matrix.

The yield function adopted for the steel jacket is the Von Mises yield criterion which is given by:

$$\mathcal{F}(\tilde{\sigma}) = \sigma_L^2 + \sigma_H^2 - \sigma_L\sigma_H - \sigma_y^2 = 0 \tag{B.17}$$

B.2 Program Implementation

The incremental nature of the plasticity theory can best be implemented on a digital computer. Basic steps in the numerical procedure are summarized in Figure B.1.

For any load increase beyond yield of material, it is necessary to determine the portion of the increment that is elastic and the portion that produces plastic deformation and then adjust the stress and strain terms until the yield criterion and the constitutive laws are satisfied. To achieve this, the stress increment is first assumed to be entirely elastic i.e.

$$d\tilde{\sigma}_e^r = \tilde{\mathbf{D}}d\tilde{\epsilon}^r \tag{B.18}$$

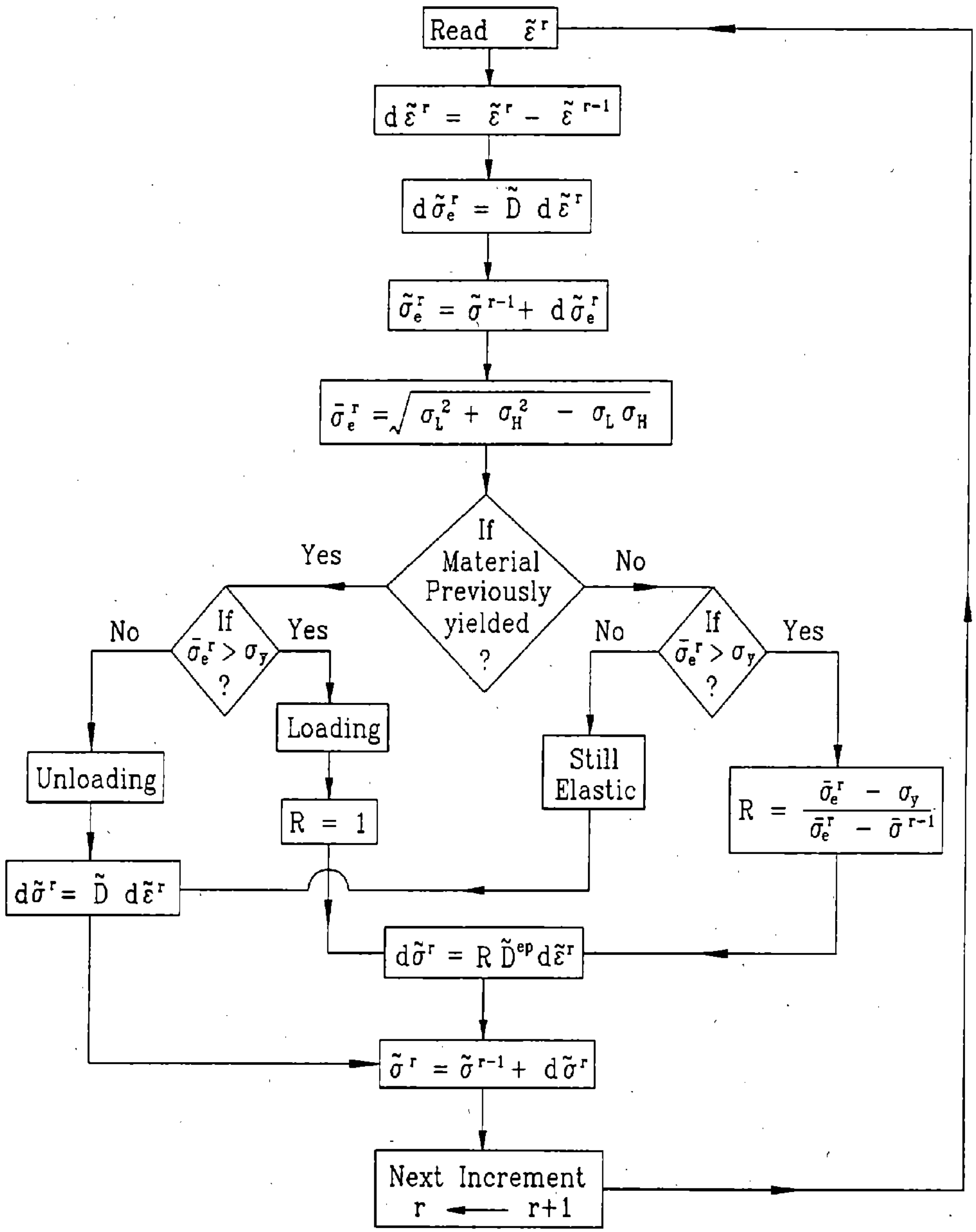

Figure B.1: **Flow Chart For Elasto-plastic Analysis** where the subscript denotes elastic behavior. The total stress at iteration r is given by:

$$\tilde{\sigma}_e^r = \tilde{\sigma}^{r-1} + d\tilde{\sigma}_e^r \tag{B.19}$$

where $\tilde{\sigma}^{r-1}$ is the converged stress for iteration $r-1$. An effective stress can be defined in terms of the components of the stress vector and be used to check against the uniaxial yield stress σ_y to see if yielding will occur. The effective stress for iteration r is defined as:

$$\bar{\sigma}^r = \sqrt{\sigma_L^2 + \sigma_H^2 - \sigma_L \sigma_H} \tag{B.20}$$

When components of the elastic stress vector $\tilde{\sigma}_e^r$ is used, the effective stress is denoted with a subscript e i.e. $\bar{\sigma}_e^r$.

If the effective stress $\bar{\sigma}_e^r$ exceeds the material yield stress σ_y, plastic redistribution of stress will occur. If yielding has previously occurred for iteration $r-1$, the entire stress increment $d\tilde{\sigma}_e^r$ must be redistributed i.e. $R = 1$. If however yielding did not occur in the previous iteration, only a portion of the stress increment need to be redistributed (see Figure B.2). The redistribution factor R in this case is taken as:

$$R = \frac{AB}{AC} = \frac{\bar{\sigma}_e^r - \sigma_y}{\bar{\sigma}_e^r - \bar{\sigma}^{r-1}} \tag{B.21}$$

where $\bar{\sigma}^{r-1}$ is the previously converged effective stress.

The redistribution of excess stress $Rd\tilde{\sigma}_e^r$ can be carried using the constitutive equation below:

$$d\tilde{\sigma}^r = R\tilde{\mathbf{D}}^{ep} d\tilde{\epsilon}^r \tag{B.22}$$

where $\tilde{\mathbf{D}}^{ep}$ is the elasto-perfectly plastic material stiffness matrix derived in the last section.

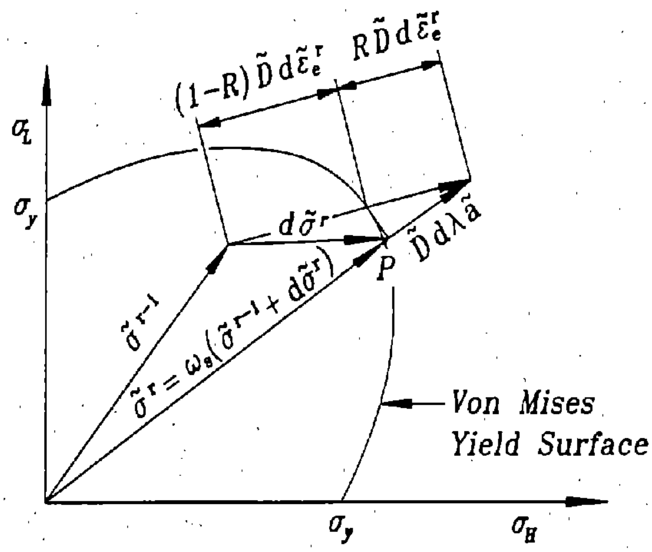

Figure B.2: **Incremental Stress Changes at Initial Yield**

The stress state at iteration r obtained by adding the stress increment $d\tilde{\sigma}^r$ to the previous stress state $\tilde{\sigma}^{r-1}$ may however depart from the yield surface depending on the magnitude of the strain increment $d\tilde{\epsilon}^r$. In order to remain on the yield surface it is necessary to scale back the stresses by a factor ω_s:

$$\omega_s = \frac{\sigma_y}{\bar{\sigma}^r} \tag{B.23}$$

where $\bar{\sigma}^r$ is the effective stress computed in Eqn. B.20 using the redistributed stress $\tilde{\sigma}^r$.

If relatively large load increment sizes are used, the procedure described above can lead to inaccurate prediction of the final point P on the yield surface if the stress point is in the vicinity of a region of large curvature of the yield surface [42]. Greater accuracy can be achieved by relaxing the excess stress $Rd\tilde{\sigma}_e^r$ in smaller steps. The number of steps m chosen is the nearest integer less than $(\bar{\sigma}_e^r/\sigma_y - 1)8 + 1$. The scaling back of redistributed stress is carried out for each step.